GEORGIA INSTITUTE OF TECHNOLOGY
OFFICE OF CONTRACT ADMINISTRATION
SPONSORED PROJECT INITIATION

Date: October 10, 1979

Project Title: A New Numberical Approach for Compressible Viscous Flows

Project No: E-16-651

Project Director: Dr. J. C. Wu

Sponsor: NASA - Lewis Research Center

Agreement Period: From 9/10/79 Until ~~9/9/80~~ 9/8

Type Agreement: Grant No. NSG 3307

Amount: $45,678 NASA
2,500 GIT (E-16-340)
$48,178 TOTAL

Reports Required: Semi-Annual Status Reports; Final Technical Report

Sponsor Contact Person (s):

Technical Matters

(NASA Technical Officer)
Eric P. McFarland
Computational Fluid Mechanics Branch
Fluid System Components Division MS5-9
NASA - Lewis Research Center
21000 Brookpark Road
Cleveland, OH 44135
216/433-4000, Ext. 6838

Contractual Matters
(thru OCA)

John E. Dilley
Grants Officer
NASA - Lewis Research Center
21000 Brookpark Road
Cleveland, OH 44135

Defense Priority Rating: None

Assigned to: Aerospace Engineering (School/Laboratory)

COPIES TO:

Project Director
Division Chief (EES)
School/Laboratory Director
Dean/Director-EES
Accounting Office
Procurement Office
Security Coordinator (OCA)
Reports Coordinator (OCA)
Library, Technical Reports Section
EES Information Office
EES Reports & Procedures
Project File (OCA)
Project Code (GTRI)
Other C. E. Smith

CA-3 (3/76)

GEORGIA INSTITUTE OF TECHNOLOGY OFFICE OF CONTRACT ADMINISTRATION

SPONSORED PROJECT TERMINATION SHEET

Date 5/7/82

Project Title: A New Numerical Approach for Compressible Viscous Flows

Project No: E-16-651

Project Director: Dr. J. C. Wu

Sponsor: NASA - Lewis Research Center

Effective Termination Date: 12/8/81

Clearance of Accounting Charges: _____

Grant/Contract Closeout Actions Remaining:

none

- ☐ Final Invoice and Closing Documents
- ☐ Final Fiscal Report
- ☐ Final Report of Inventions
- ☐ Govt. Property Inventory & Related Certificate
- ☐ Classified Material Certificate
- ☐ Other _____

Assigned to: AE (School/Laboratory)

COPIES TO:

Administrative Coordinator	Research Security Services	EES Public Relations (2)
Research Property Management	Reports Coordinator (OCA) ✓	Computer Input
Accounting	Legal Services (OCA)	Project File
Procurement/EES Supply Services	Library	Other _____

Semi-Annual Progress Report

for the period September 10, 1979 to March 9, 1980

on NASA-Lewis Research Center

Grant No. NSG 3307

A NEW NUMERICAL APPROACH FOR COMPRESSIBLE VISCOUS FLOWS

Prepared by

J. C. Wu, Professor

and

S. G. Lekoudis, Assistant Professor

School of Aerospace Engineering

Georgia Institute of Technology

1. INTRODUCTION

The main objective of the research being conducted under NASA Lewis Research Center grant no. NSG 3307 is the development of a new numerical technique for solving the compressible Navier-Stokes equations. This new technique utilizes an integral representation of the kinematics of the flowfield. In the case of a steady flow, an integral representation of the kinetics of the flowfield can also be utilized.

In the case of an incompressible flow, both the kinetics and the kinematics of the flowfield have been expressed as integral representations (Reference 1 and 2). Compressibility introduces two additional unknowns into the problem. In the present work, the dependent variables selected to represent the new unknowns are the dilitation and the enthalpy. The main advantage of the integral representation is that it permits the computation to be confined to the viscous region of the flow. In the case of an incompressible flow, the viscous region is the region of non-negligible vorticity. In the case of compressible flow, the viscous region is the region of non-negligible vorticity and dilitation.

Progress that has been made towards the attainment of the objectives of this research, both in the analytical formulation and in the numerical procedures, is outlined in the following.

2. PROGRESS IN THE ANALYTICAL FORMULATION

As stated in the introduction, the main objective of this research is the development of a new numerical technique for solving the compressible Navier-Stokes equations. The present research utilizes the experience gained in solving incompressible Navier-Stokes equations. For incompressible flows, both the kinetics and the kinematics of the flow can be represented in terms of integrals relating the velocity and the vorticity (References

1, 3, 4). If the flow is steady, the integral representation for the kinematics is somewhat simplified (Reference 1).

In the case of steady compressible flow, integral-representation describing both the kinetics and the kinematics of the problem have been derived and were presented in the research proposal (Reference 5) leading to the present project. The development of an integral-differential formulation for the case of unsteady two dimensional compressible viscous flow has been completed and is outlined below.

The vorticity ω and the dilitation β are defined by:

$$\vec{\nabla} \times \vec{v} = \vec{\omega} \tag{1}$$

$$\vec{\nabla} \cdot \vec{v} = \beta \tag{2}$$

where $\vec{v}$ is the velocity vector. Substituting (1) and (2) into the Navier-Stokes equations, one obtains after some lengthy algebra, the following governing equations:

$$\frac{\partial \omega}{\partial t} = - \vec{v} \cdot \vec{\nabla} \vec{\omega} + \left(\frac{\mu}{\rho R_e}\right) \nabla^2 \omega + \phi \ (\rho, \beta, \vec{\omega}, h) \tag{3a}$$

$$\frac{\partial \beta}{\partial t} = - \vec{v} \ \nabla \beta + \left(\frac{4/3 \mu}{\rho R_e}\right) \nabla^2 \beta + \psi \ (\rho, \beta, \vec{\omega}, h) \tag{3b}$$

$$\frac{\partial \ln \rho}{\partial t} = - \vec{v} \cdot \vec{\nabla} \ln \rho - \beta \tag{3c}$$

$$\frac{\partial h}{\partial t} = - \vec{v} \cdot \nabla h + \left(\frac{\gamma k}{\rho R_e P_r}\right) \nabla^2 h + \Theta \ (\rho, \beta, h, \vec{\omega}) \tag{3d}$$

where ρ is the density and h is the enthalpy of the fluid

$$R_e = \frac{\rho_\infty u_\infty L}{\mu_\infty} \tag{4a}$$

$$P_r = \frac{c_p \mu}{k} \tag{4b}$$

$$\gamma = c_p / c_v \tag{4c}$$

are the usual definition of the Reynolds number, the Prandtl number, the ratio of specific heats, and L, u_∞, ρ_∞ and T_∞ have been used in the nondimensionalization. The terms ϕ, ψ, and Θ, are "source-like" terms, are identically zero in the incompressible case, and are

$$\phi = -\omega\beta + \frac{\mu}{\rho^2 R_e} \left(4/3 \left|\vec{\nabla}\beta \times \vec{\nabla}\rho\right| - \vec{\nabla}\rho \cdot \vec{\nabla}\omega\right) + \frac{\gamma - 1}{\gamma} \vec{\nabla} \ln\rho \times \vec{\nabla} h + \frac{c_1}{R_e} \tag{5}$$

$$c_1 = \frac{1}{\rho}(u_y + v_x)(\mu_{xx} - \mu_{yy}) + \frac{2}{\rho}(v_y - u_x)\mu_{xy} + \mu_x \left\{\frac{2}{\rho} \nabla^2 v + \frac{2}{\rho} u_{xy} - \frac{1}{\rho^2}(\rho_x u_y - v_x \rho_x - 2\rho_y u_x + \frac{2}{3}\rho_y \beta)\right\} + \mu_y \left\{-\frac{2}{\rho} \nabla^2 u + \frac{2}{\rho} v_{xy} - \frac{1}{\rho^2}(2\rho_x v_y - u_y \rho_y - v_x \rho_y - \frac{2}{3}\beta\rho_x)\right\} \tag{5a}$$

$$\psi = -(u_x^2 + v_y^2 + 2u_y v_x) + \frac{\mu}{\rho^2 R_e} \left\{-\frac{4}{3} \nabla\rho \cdot \nabla\beta + \left|\nabla\rho \times \nabla\omega\right|\right\} - \frac{\gamma - 1}{\gamma}(\nabla^2 h + h \nabla^2 \ln\rho + \nabla h \cdot \nabla \ln\rho) + \frac{c_2}{R_e} \tag{6}$$

$$c_2 = \frac{8}{3\rho} \nabla\beta \cdot \nabla\mu + \frac{2}{3}\left|\nabla\omega \times \nabla\mu\right| - \frac{2}{3\rho} \beta \nabla^2 \mu + \frac{2}{\rho}(u_x \mu_{xx}$$

$$+ v_y \mu_{yy}) + (v_x + u_y)\mu_{xy} - \frac{1}{\rho^2}(v_x + \mu_y) + \rho_y \mu_x$$

$$+ \frac{2}{3}\frac{\beta}{\rho^2}\nabla\rho\nabla\mu - \frac{2}{\rho^2}(\rho_x u_x \mu_x + \rho_y v_y \mu_y) \qquad (6a)$$

$$\Theta = -(\gamma - 1)\beta h + \frac{\gamma\mu}{\rho R_e}\left[\frac{\beta^2}{3} + (2u_x - \beta^2) + (2v_x - \omega)^2\right] + \frac{\gamma}{\rho R_e P_r}\vec{\nabla} h . \vec{\nabla} k \qquad (7)$$

In the above expression the vector product terms denote the magnitude of the resulting vector.

The equations (3) are four equations with six scalar unknowns e, h, β, ω and $\vec{v}$. The needed relation to close the system is obtained from the kinematics of the problem. From (1) and (2) we obtain

$$\vec{v}(\vec{r}_o, t) = -\frac{1}{2\pi}\int_R \frac{\vec{\omega} \times (\vec{r} - \vec{r}_o) + \beta(\vec{r} - \vec{r}_o)}{|\vec{r} - \vec{r}_o|^2} dR + \vec{v}_\infty \qquad (8)$$

In (8) R is the domain of the flowfield where ω and β are non-negligible.

The analytical formulation for two-dimensional unsteady compressible Navier-Stokes equations in terms of vorticity and dilitation, as described above, has been applied to two test problems.

2. PROGRESS IN THE COMPUTATIONAL ALGORITHMS

2.1 Flow over a flat plate

The compressible flow at a zero angle of attack over a flat plate of length L, at Mach number $M_\infty = 0.5$ and Prandtl number 1, was investigated using the approach described in Section 2. The relatively coarse grid had uniform $\Delta x = 0.1L$ and $\Delta y = .04L$. The computational domain was extended 0.5L ahead of the leading edge of the plate, 1.5L behind the trailing edge of the plate and .8L above the plate.

Figures 1 and 2 show the distribution of the streamwise velocity u and the enthalpy h, at midplate, after steady state convergence was obtained, at a nondimensional time level $t = \frac{L}{u_\infty} = 2$. The numerical calculations predict an overshoot at the u profile when compared with the boundary layer theory. This overshoot is due to the boundary-layer displacement effect and is expected. Figure 3 shows the vorticity distribution at midplate from the present method, from boundary layer theory, and from a finite-difference solution of the Navier-Stokes equations. Considering that the Navier-Stokes calculations were done with different grids, the results are in reasonable agreement.

2.2 Flow around a circular cylinder

The second test problem solved using the present method is the flow over a circular cylinder, at $R_e = 40$, $M_\infty = 0.4$ and $P_r = 1$. The computational field is subdivided into three-regions bounded by concentric circles with their center at the center of the cylinder, and with radii 0.35R, 2.525R and 17.916R, where R is the cylinder radius. Inside the first circle the integral representation for the kinematics was used. In the other two regions, a Poisson type equation for the kinematics was solved. However the velocity at the boundaries of the regions was obtained from the integral representation for the kinematics. This segmentation technique was found to accelerate the convergence rates and also reduce the required CPU time.

In the polar grid used, the spacing in the Θ direction was $\pi/20$, and the spacing in the radial direction was exponential with

$$dr = e^z dz \text{ and } dz = .06$$

The computations were stopped at a time level $t = R/U_\infty = 15.1$ when a steady state solution has been achieved. The time step was varied gradually from .05 to .15. Small time steps were used at the beginning of the calculation (impulsive start) because the flowfield was varying rapidly.

Figure 4 shows the pressure distribution at the cylinder surface computed from the present method and a finite-difference technique. Considering the difference in grids used, the results are in reasonable agreement. Figure 5 shows again the surface pressure distribution obtained from the present method in the incompressible limit, together with experimental data and from applying the Karman-Tsien (K.T.) rule to the incompressible results. Although the K.T. rule applies strictly to slender bodies, it seems to underestimate the compressibility effects on the pressure distribution.

Figures 6 and 7 are computer generated plots of the streamlines and equal vorticity lines for the flow around the cylinder, both for the incompressible and the compressible flow case.

In summary, the integral-differential method has been found capable of accurately predicting the compressible flowfield around the circular cylinder.

4. WORK IN PROGRESS

At the time of the writing of this report, the steady state compressible flow solution of the Navier-Stokes equations has been programmed using integral representations for both the kinematics and the kinetics of the flowfield. The program is at the debugging stage. The method uses triangular elements for the flow in a channel.

PUBLICATIONS

This research project was initiated only six months ago. The following documents, however, have been prepared under partial support by NASA-Lewis Research Center. It is expected that much of the information reported in these documents will become available in the open literature in the near future.

1. J. C. Wu, "Accomodation of Diverse Length-Scales in General Viscous Flows," an invited paper to be presented in June, 1980, at the Second International Symposium on Innovative Numerical Analysis in Applied Engineering Science and to be published in the Symposium Proceeding by the University of Virginia Press.
2. Y. M. Rizk, "A Integral-Representation Approach for Time-Dependent Viscous Flows," a Ph.D. Thesis, Georgia Institute of Technology, March 1980 (in print).
3. M. M. ElRefaee, "A Numerical Study of Laminar Unsteady Compressible Flow over Airfoils," a Ph.D. thesis proposal, Georgia Institute of Technology, February 1980.

REFERENCES

1. J. C. Wu, and M. Wahbah, "Numerical Solution of Viscous Flow Equations Using Integral Representations," Proceedings of the Fifth International Conference on Numerical Methods in Fluid Dynamics, Lecture Series in Physics, Springer-Verlag, Vol. 59, pp. 448-453, 1976.
2. M. M. Wahbah, "Computation of Internal Flows with Arbitrary Boundaries Using the Integral Representation Method," Georgia Institute of Technology Report, March, 1978.

3. J. C. Wu, and Y. M. Rizk, "Integral-Representation Approach for Time-Dependent Viscous Flows," Proceedings of the Sixth International Conference on Numerical Methods in Fluid Dynamics, Lecture Notes in Physics, Springer-Verlag, Vol. 90, 1978, pp. 558-564.

4. Y. M. Rizk, "A Integral-Representation Approach for Time-Dependent Viscous Flows," a Ph.D. Thesis, Georgia Institute of Technology, March 1980 (in print).

5. J. C. Wu, "A New Numerical Approach for Compressible Viscous Flows," A Research Proposal submitted to NASA-Lewis Research center, Georgia Institute of Technology, April 1979.

6. M. M. ElRefaee, "A Numerical Study of Laminar Unsteady Compressible Flow over Airfoils," a Ph.D. thesis proposal, Georgia Institute of Technology, February 1980.

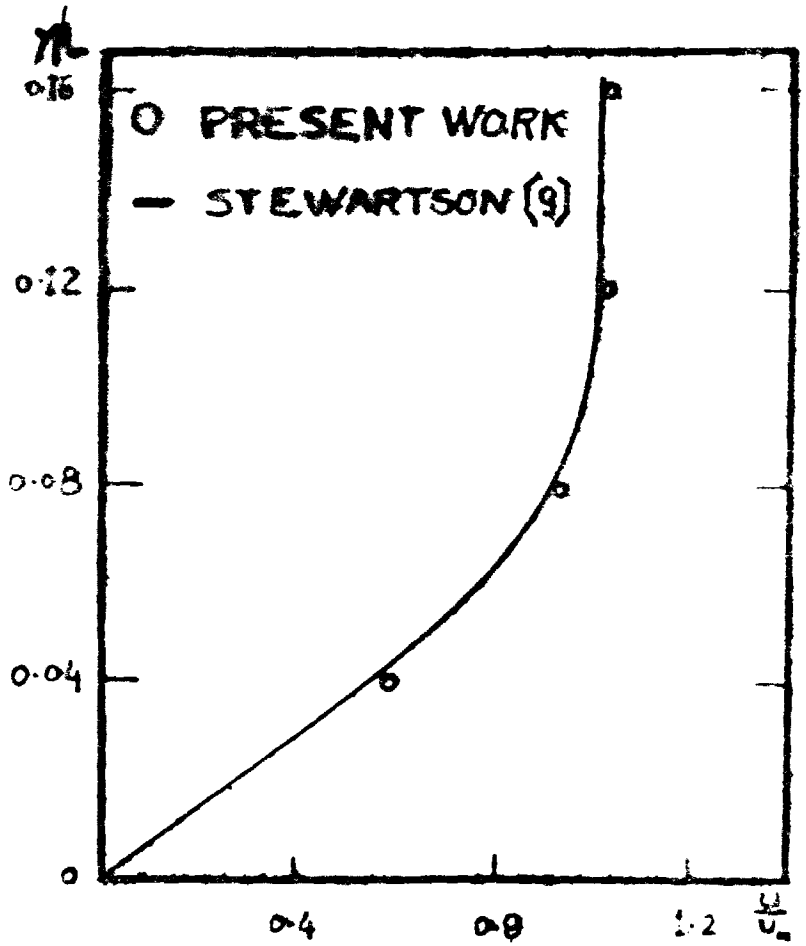

F.1 VELOCITY PROFILE

RE = 1000
M∞ = 0·5
PR = 1·0

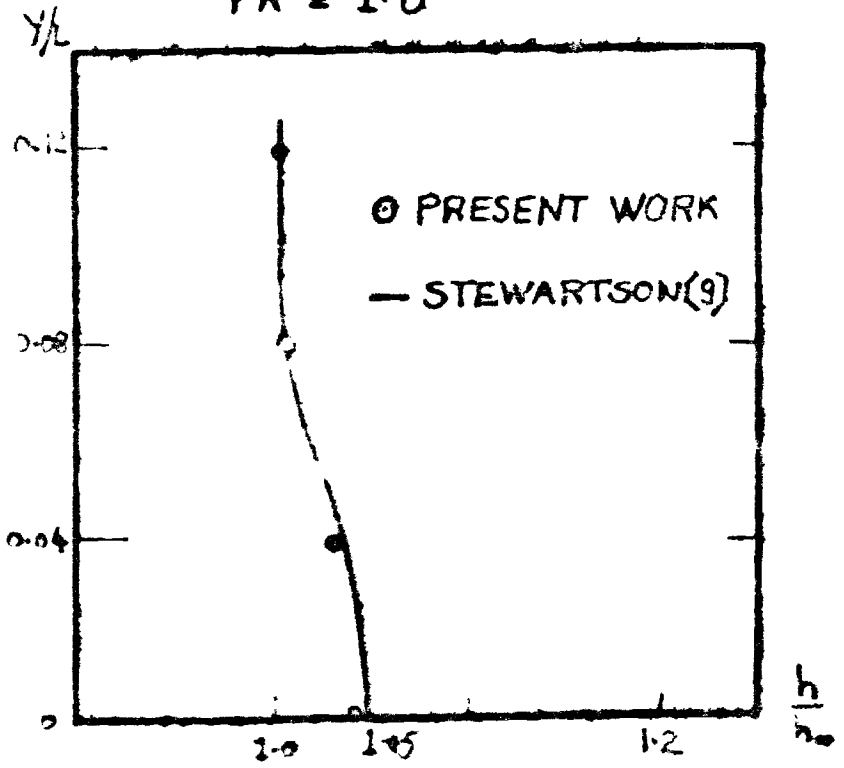

F.2 ENTHALPY PROFILE

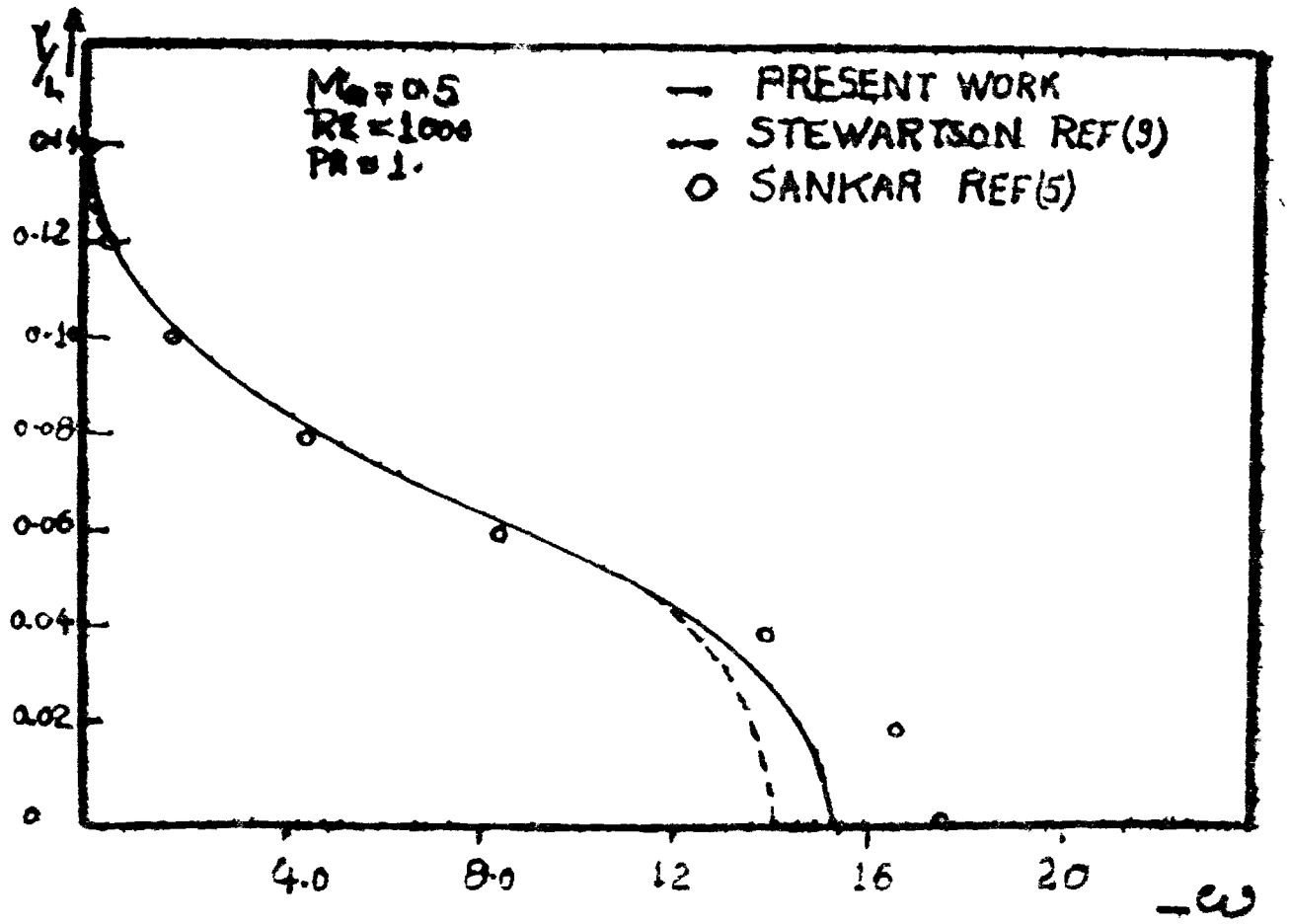

F.3 VORTICITY PROFILE AT MID PLATE

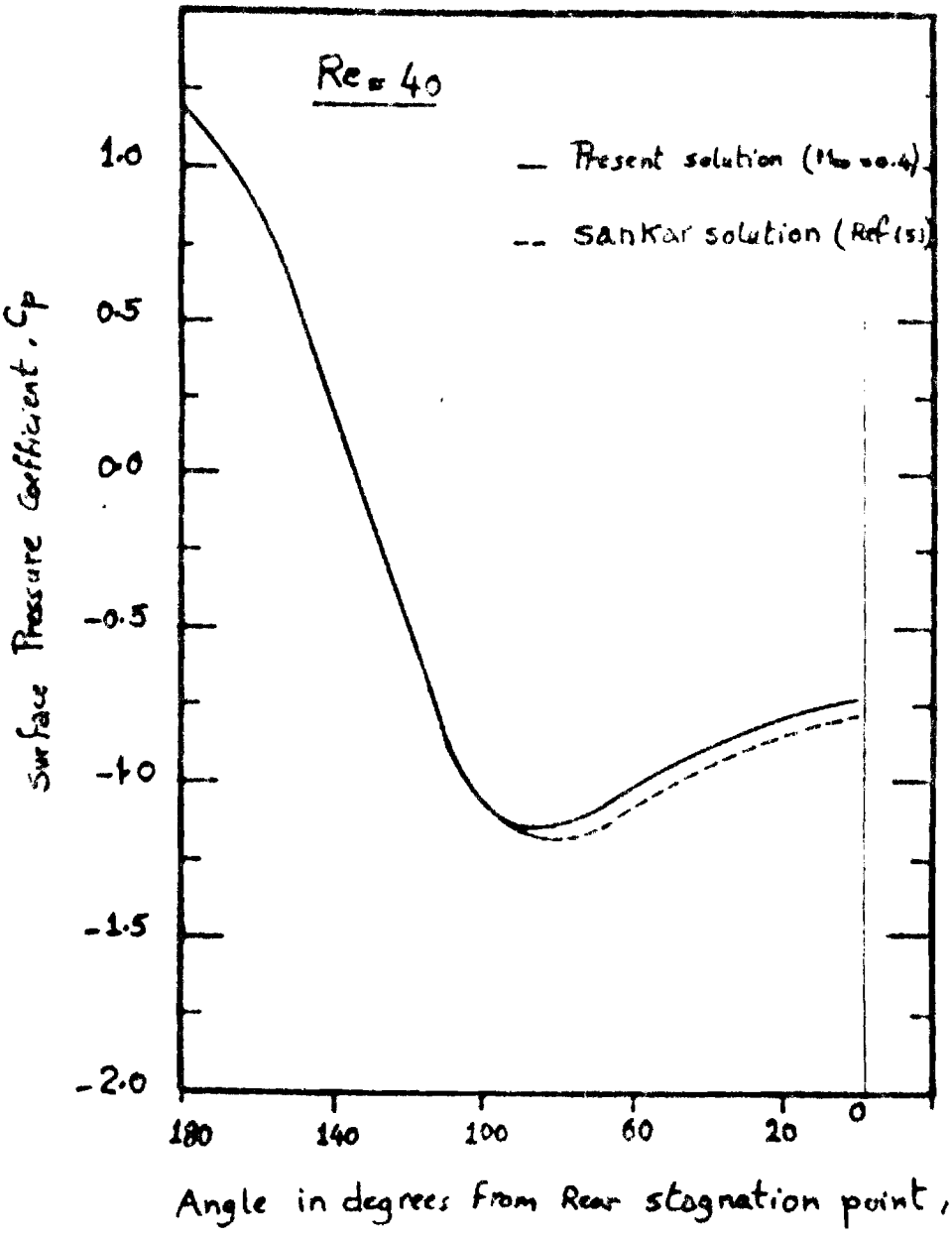

Figure 4. Circular cylinder Surface Pressure Distribution

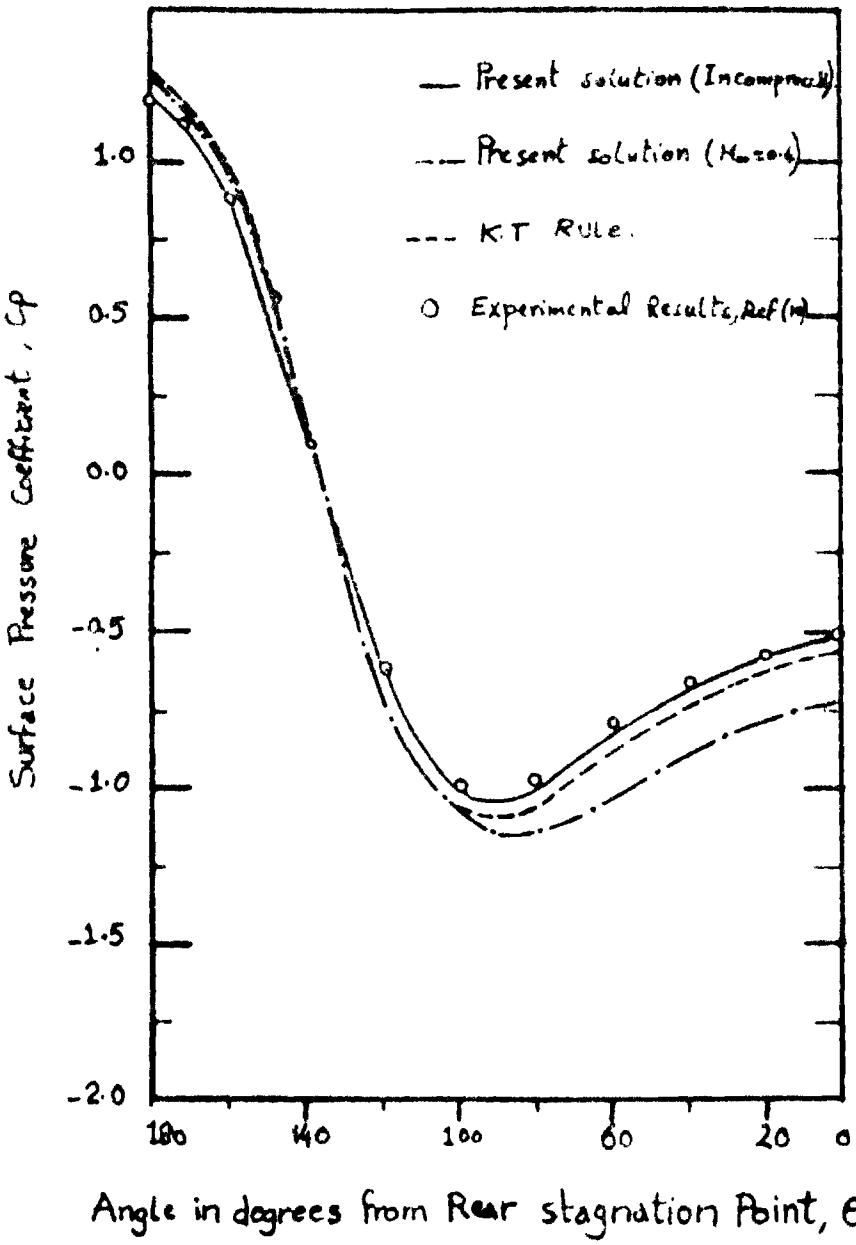

Figure 5. Circular Cylinder Surface Pressure Distribution at Later Time Levels

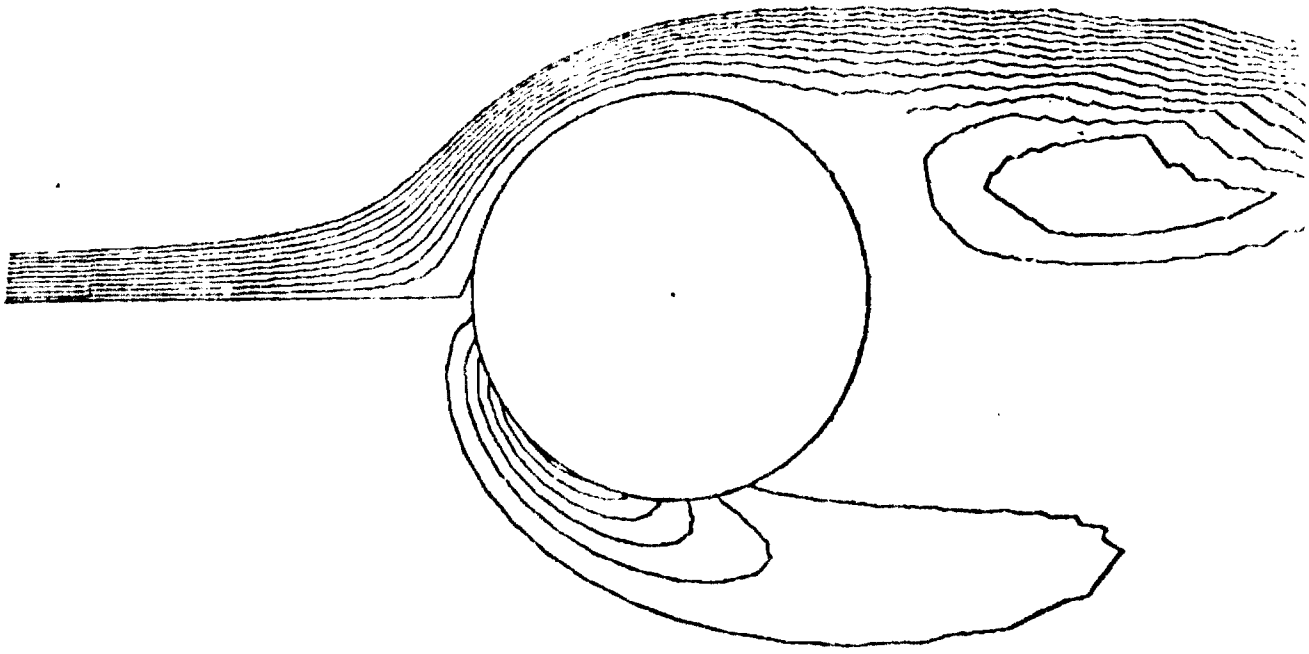

Figure 6 Streamlines and Constant Vorticity Contours For Viscous Incompressible Flow Past a circular cylinder (Re=40)

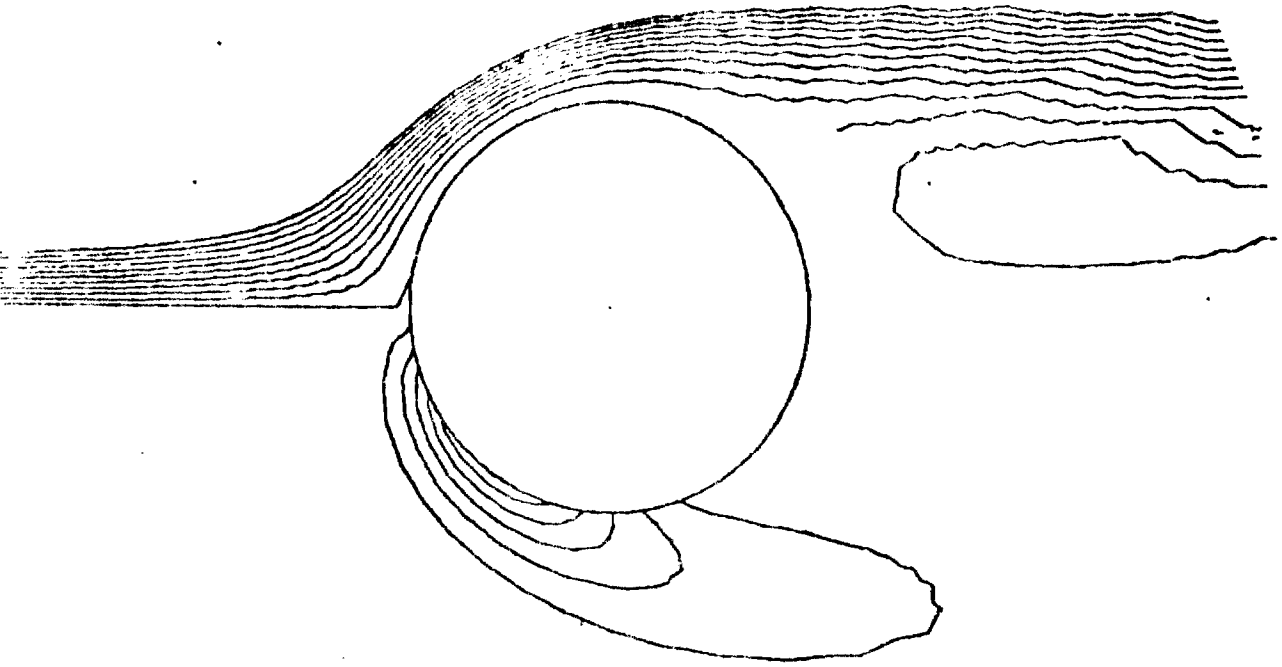

Figure 7: Streamlines and constant Vorticity Contoures For Viscous Flow Past a circular cylinde $\{ Re = 40 , M_\infty = 0.4, Pr = 1. \}$.

Semi-Annual Progress Report

for the period September 9, 1980 to March 9, 1981

on NASA Lewis Research Center

Grant No. NSG 3307

A NEW NUMERICAL APPROACH FOR COMPRESSIBLE VISCOUS FLOWS

Prepared by

J. C. Wu, Professor

and

S. G. Lekoudis, Assistant Professor

School of Aerospace Engineering

Georgia Institute of Technology

1. INTRODUCTION

The main objective of the research being conducted under the NASA Lewis Research Center Grant NSG-3307 is the development of a new numerical technique for solving the compressible Navier-Stokes equations. This new technique uses an integral representation of the kinematics of the flowfield. For steady flow, an integral representation of the kinetics can also be used. Progress that has been made towards the attainment of the objectives of this research is outlined in the following.

2. THE STATIC STALL OF AN AIRFOIL IN COMPRESSIBLE FLOW

A full cycle of events, observed before in the incompressible flow case, has been successfully computed for the static stall of a Joukowski airfoil at $M = 0.4$. Details of the work are in Publications 1 and 2. Publication 1 has been attached as Appendix A to this progress report. The two main conclusions from the study are the following: 1) The developed numerical technique is capable of predicting the complicated flowfield around a stalled airfoil. The scheme has been tested by comparing with results obtained from conventional finite-difference techniques. 2) Compressibility delays the occurence of events, such as formation of the primary bubble and its subsequent bursting.

Several observations were made during the present study. The results described below are for a Reynolds number, based on the airfoil chord, of 1,000, and, for the compressible case, for a freestream Mach number 0.4 and a Prandtl number unity. The airfoil, a 9% thick modified Joukowski airfoil, was at a 15^{o} angle of attack. The dimensionless time T is based on the cylinder radius to which the airfoil is transformed and on the freestream velocity.

Several checks were performed, with compressibility "switched off". Figure 1 shows the history of loads after the impulsive start at $T = 0$, for two different grid spacings in the azimouthal direction. Although the figure indicates that the truncation errors are small, they are significant enough to warrant special attention when compressi-

bility effects are examined. Also, to the authors knowledge, this is the first computation of a "second cycle" of events for the static stall case. This second cycle starts around T = 30, and the amplitude of the oscillating force coefficients is reduced. Figure 2 shows a comparison of the history of loads obtained from the present method and from a finite-difference technique[1]. The results of Reference 1 were obtained with a second order (in time) accurate scheme and with twice more grid points than the ones used in the present study. Figures 3, 4, 5 and 6 show comparisons between incompressible and compressible results. The compressiblity effects are small because of the low subsonic Mach number, which means that in a practical situation of static stall, incompressible theory could accurately predict the amplitudes of the load variation. The results were obtained with the same grid for both the incompressible and the compressible cases so as to make the effects of the grid error comparable for the two cases.

Figures 7 and 8 show load histories obtained by a finite-difference technique[2]. The results for M = 0.2 are virtually the same as in the incompressible case. Although the initial conditions used in Reference 2 (uniform flow with the freestream velocity) are different than those used in the present study (potential flow solution), the compressibility effects observed are very similar to those computed using the integral technique. This difference in the initial conditions precludes a detailed quantitative comparison. However, comparing Figures 4 and 5 with Figures 7 and 8 shows that the maximum and minimum lift and drag computed from the two techniques are in good agreement.

PUBLICATIONS

The following documents have been prepared under support by NASA-Lewis Research Center:

1. J. C. Wu, M. El-Refaee and S. G. Lekoudis, "Solutions of the Unsteady Two-Dimensional Compressible Navier-Stokes Equations Using the Integral Representation Method," AIAA Paper 81-0046, presented at the AIAA 19th Aerospace Sciences Meeting in St. Louis, Missouri, Jan. 12-15, 1981.

2. M. El-Refaee, "A Numerical Study of Laminar Unsteady Compressible Flow over Airfoils," Ph.D. Thesis School of Aerospace Engineering, Georgia Institute of Technology, 1981 (in preparation).

REFERENCES

1. Mehta, U. B. and Lavan, Z., "Starting Vortex, Separation Bubbles and Stall - A Numerical Study of Laminar Unsteady Flow Around an Airfoil," J. Fluid Mech., Vol. 67, pp. 227-256, 1975.

2. Sankar, N. L. and Tassa, Y., "Reynolds Number and Compressibility Effects on Dynamic Stall of a NACA 0012 Airfoil," AIAA Paper 80-0010.

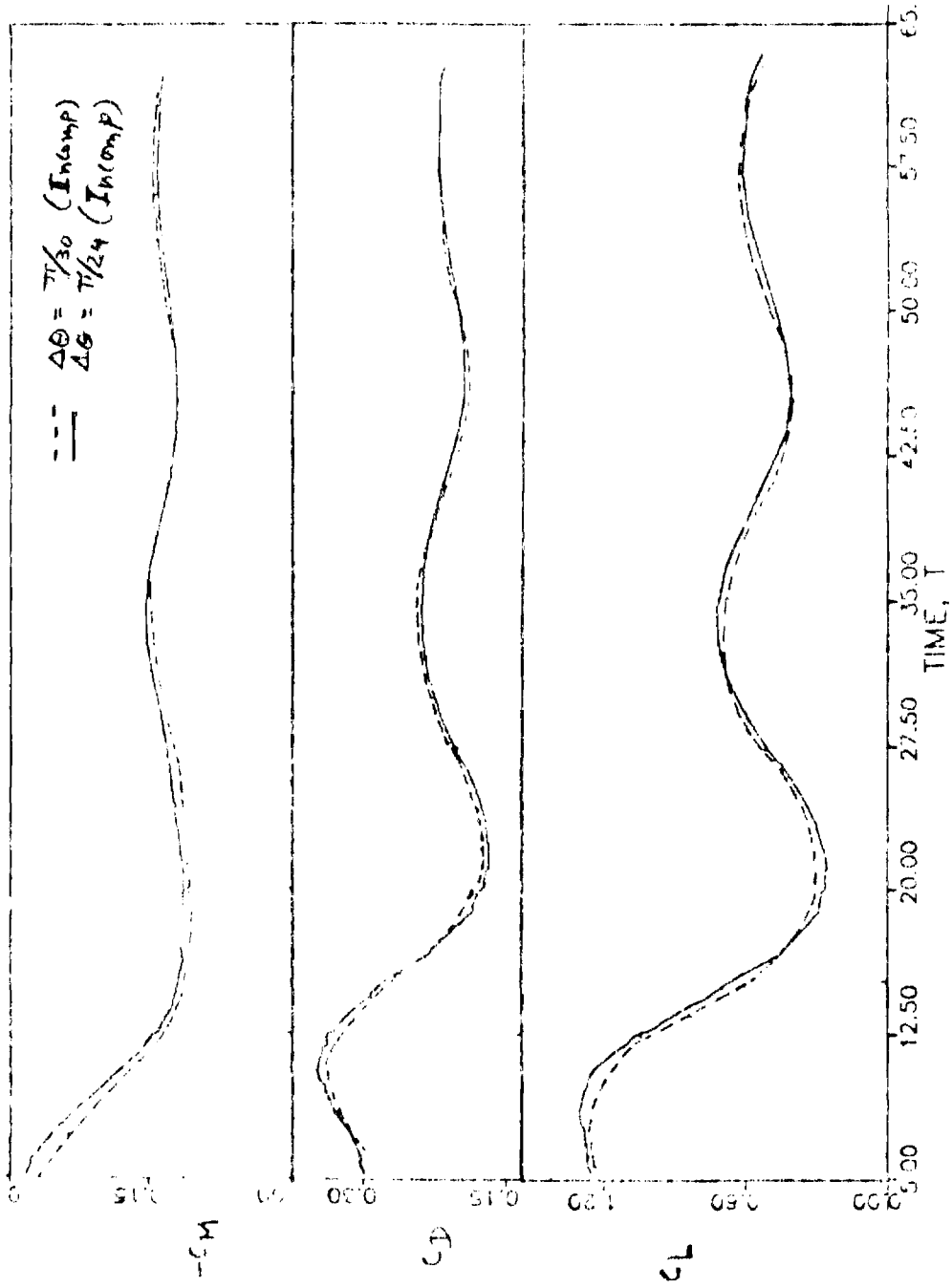

FIGURE (1) TIME HISTORIES OF LOADS FOR INCOMPRESSIBLE FLOW

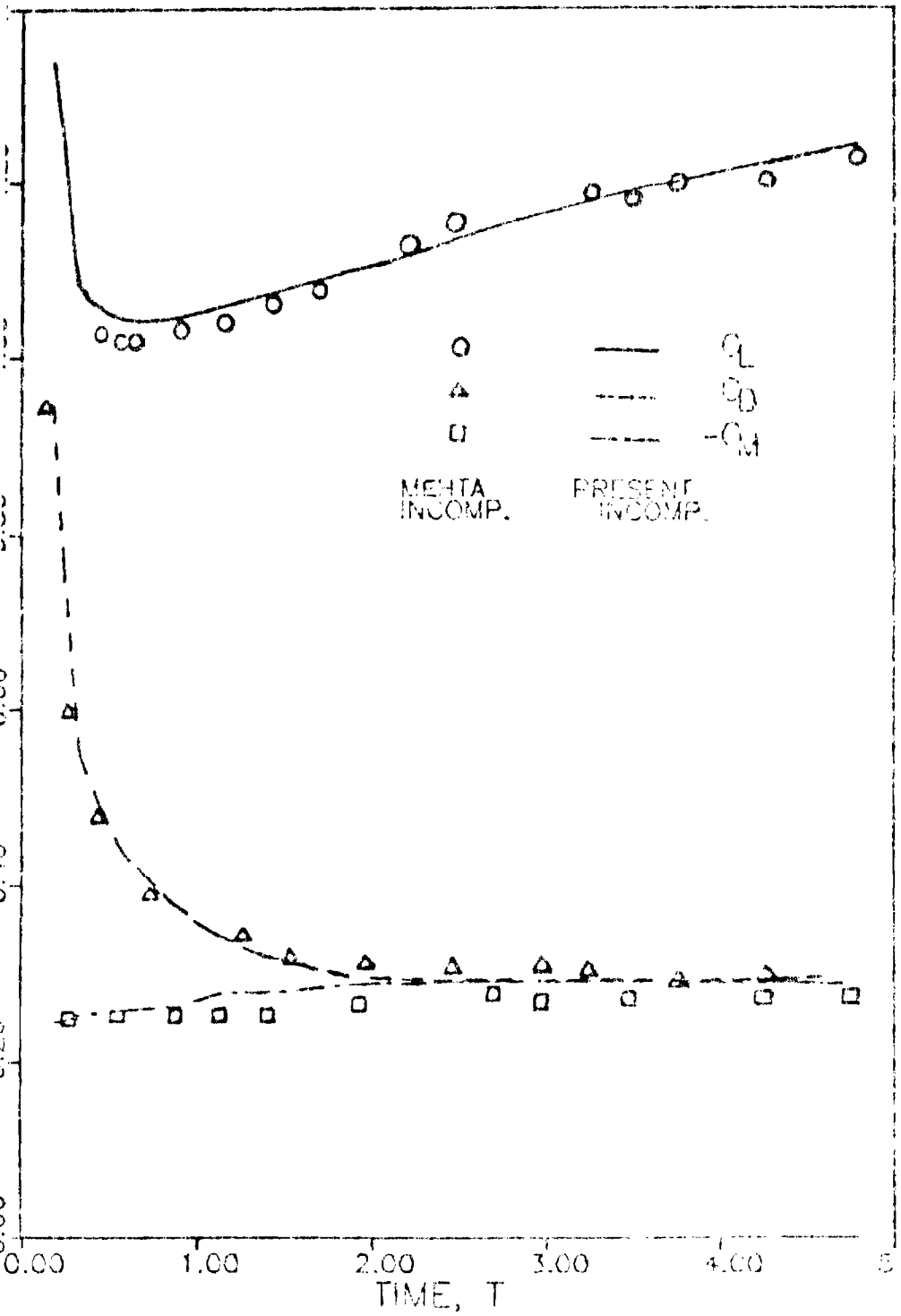

FIGURE(2) COMPARISON OF TIME HISTORY OF LOADS BETWEEN THE PRESENT INCOMP. RESULTS AND MEHTA'S RESULTS

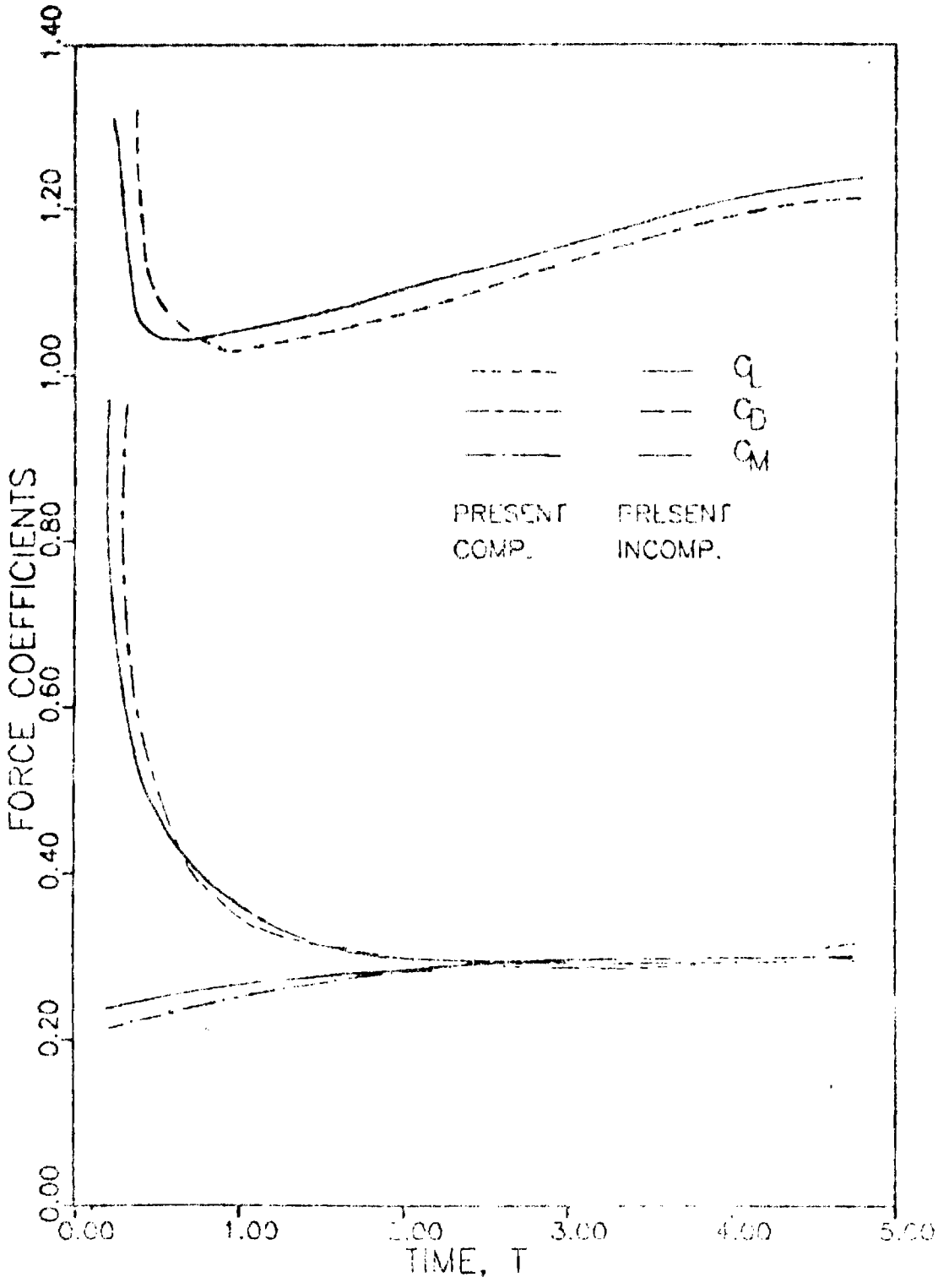

FIGURE(13). TIME HISTORIES OF LOADS , T=0. TO T=5.0

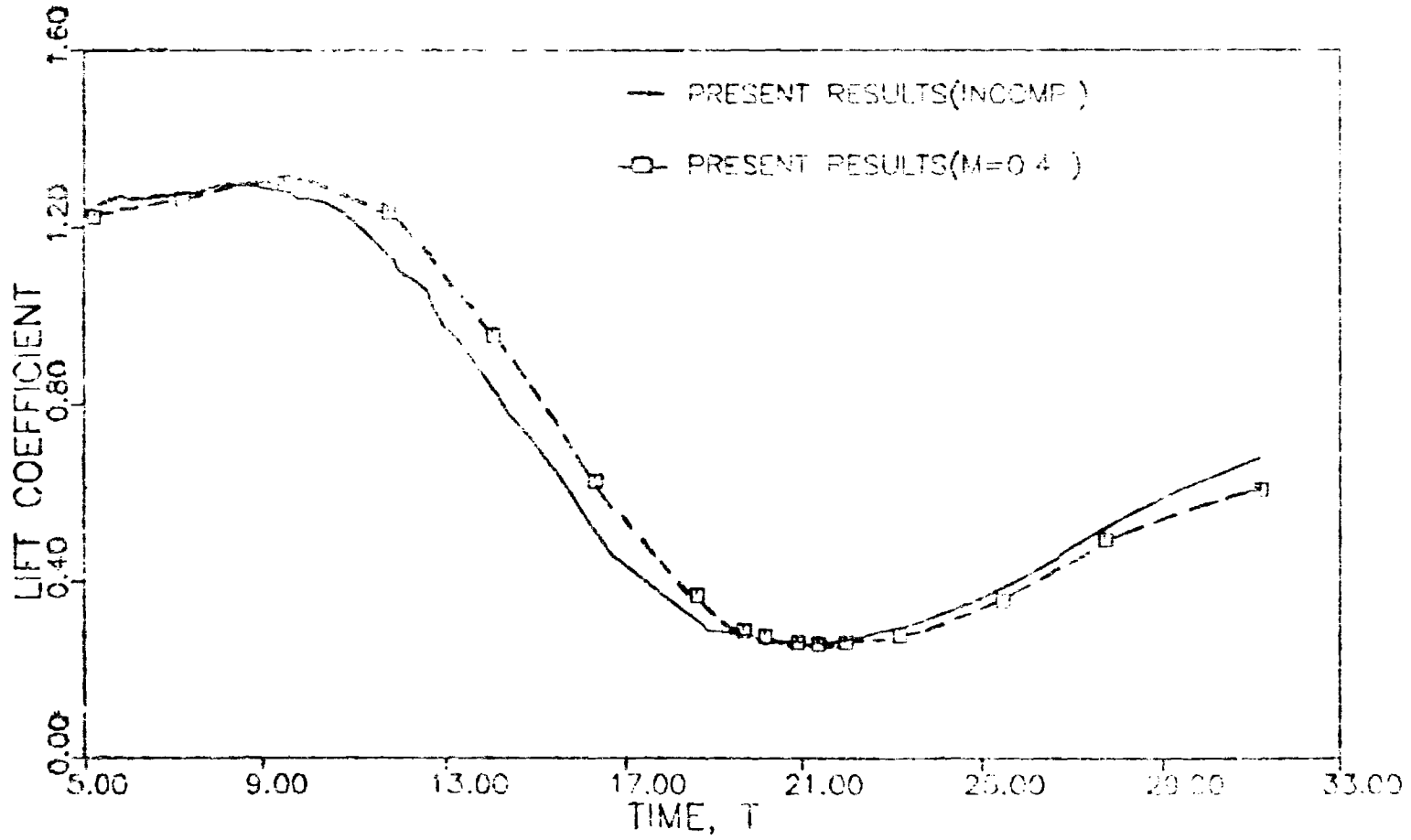

FIGURE(4). TIME HISTORIES OF LOADS

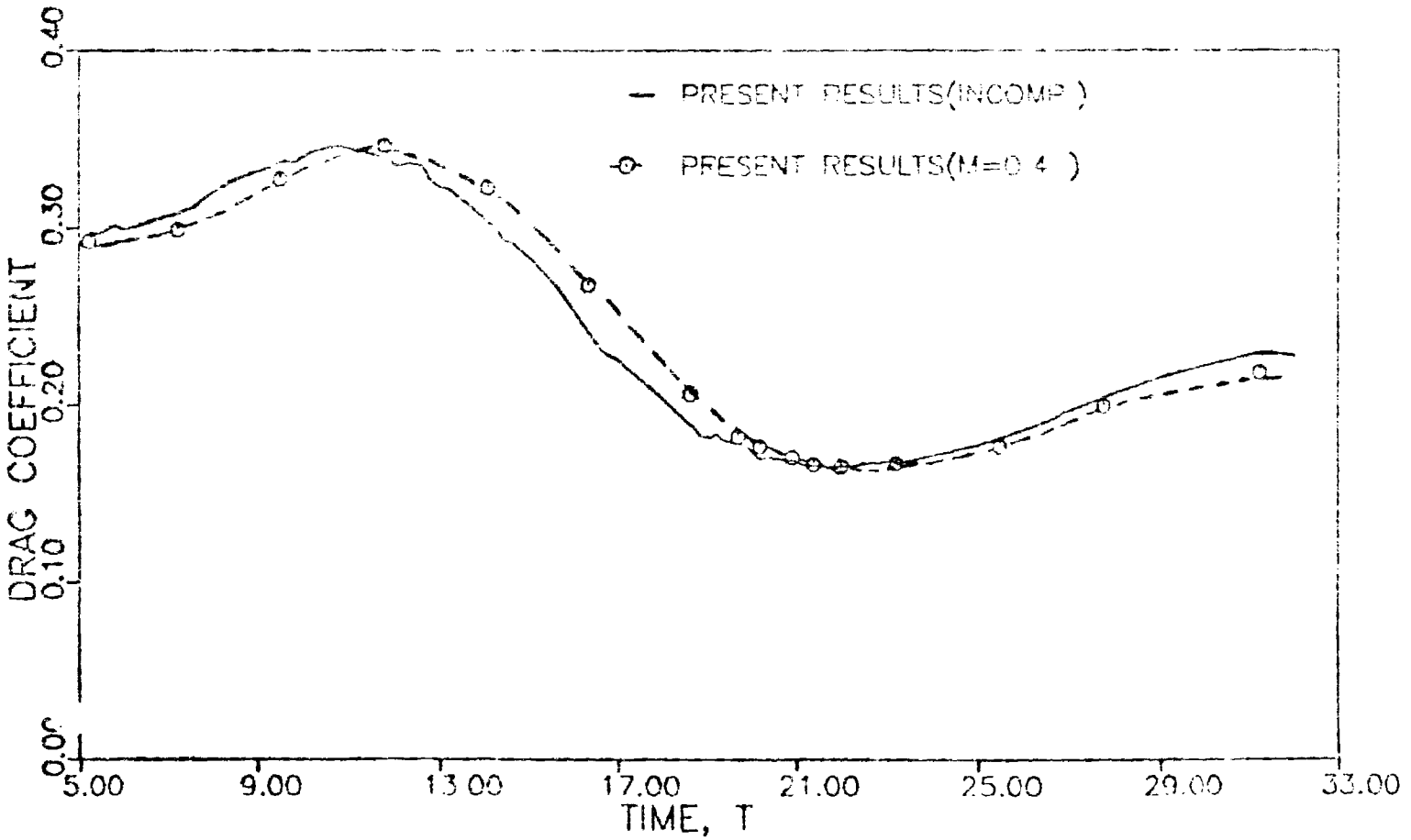

FIGURE(5). TIME HISTORIES OF LOADS

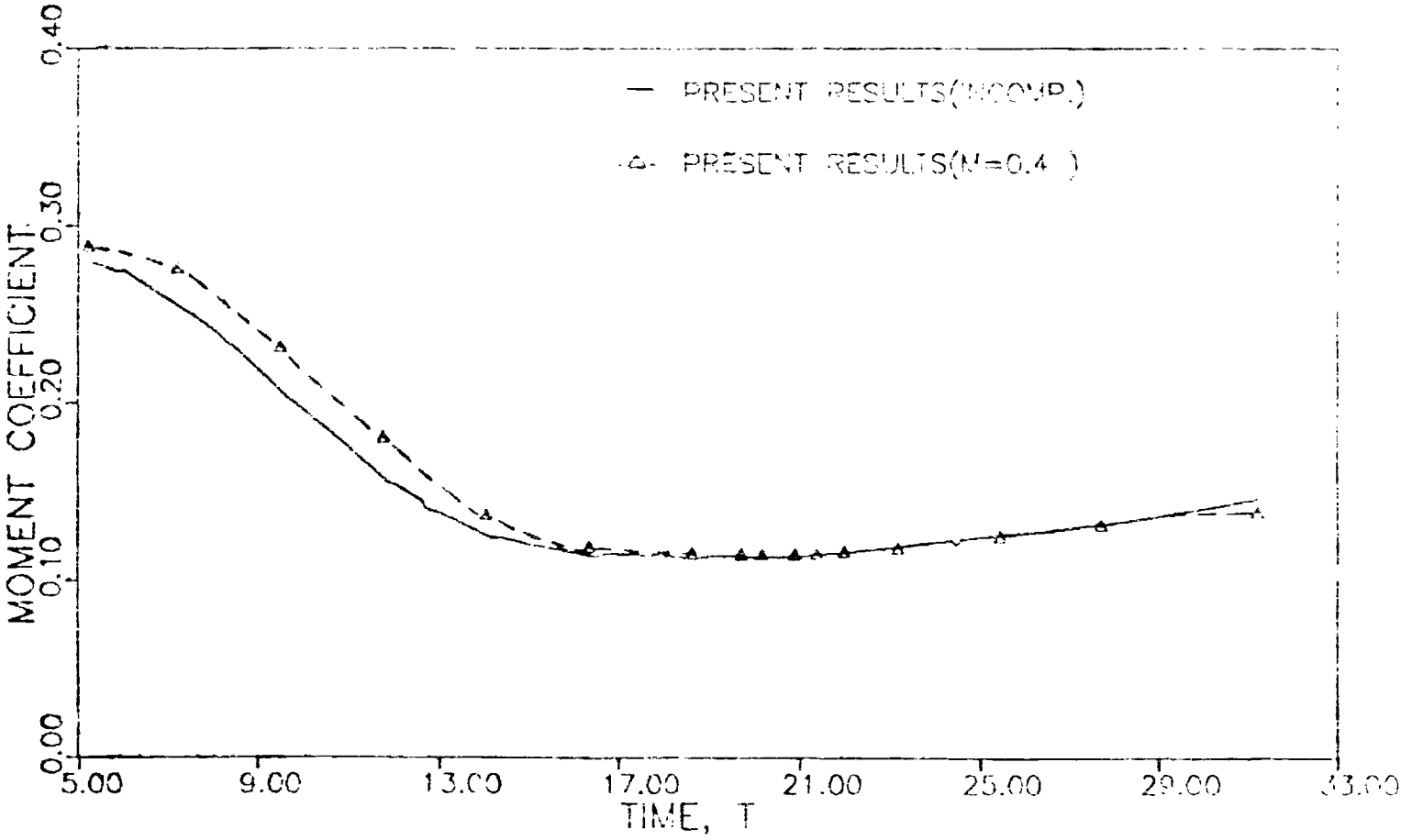

FIGURE(6). TIME HISTORIES OF LOADS

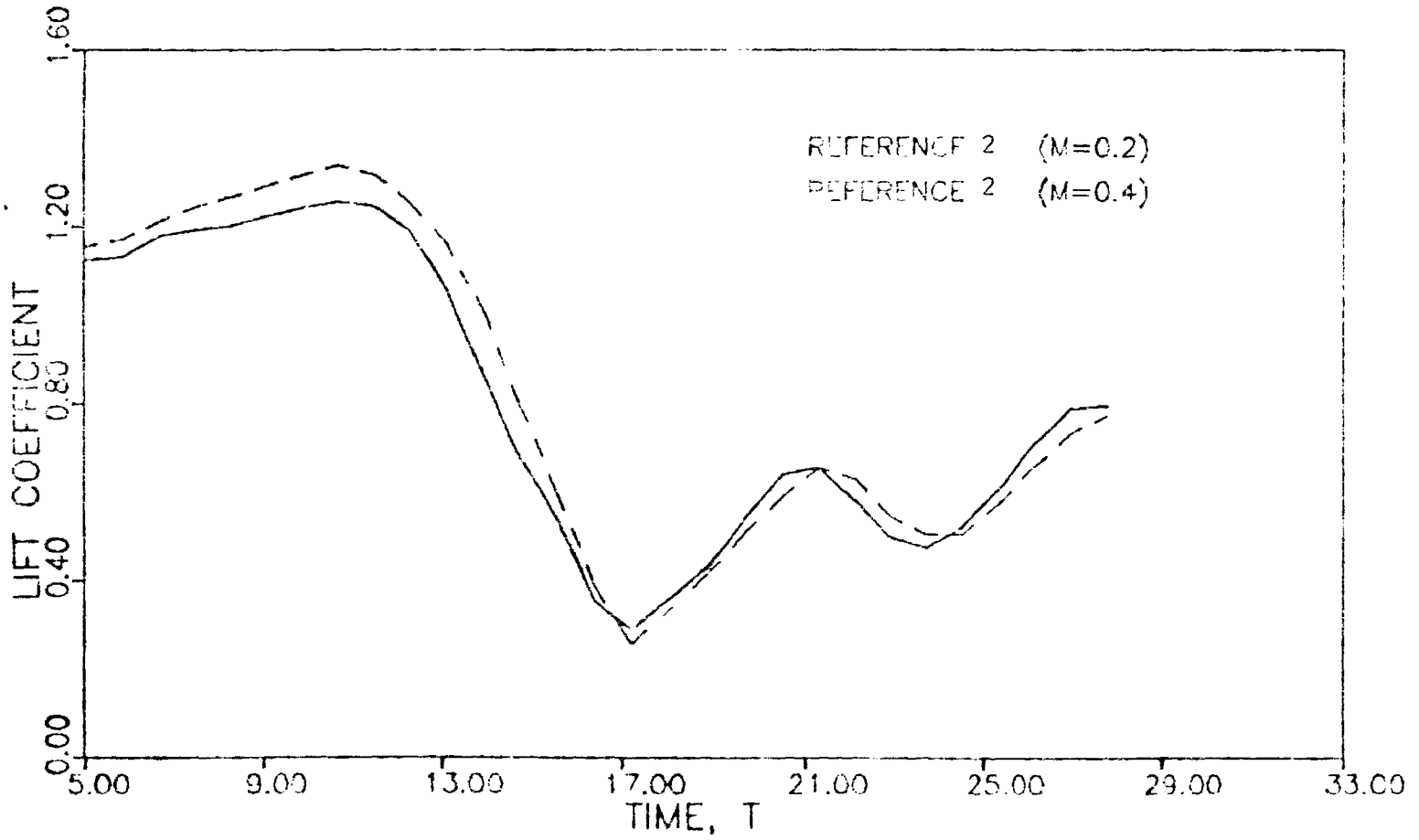

FIGURE(7). TIME HISTORIES OF LOADS

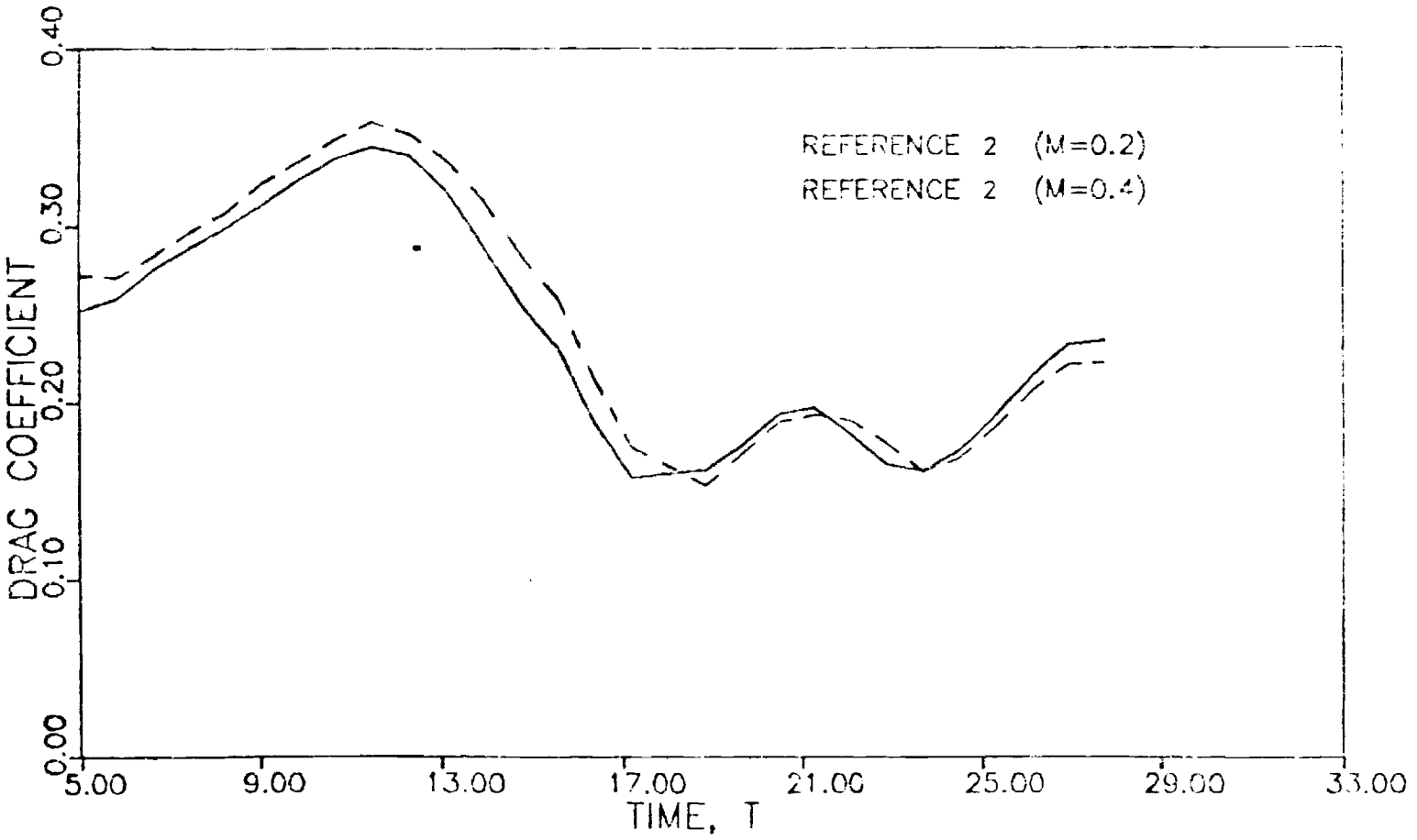

FIGURE(8). TIME HISTORIES OF LOADS

APPENDIX A

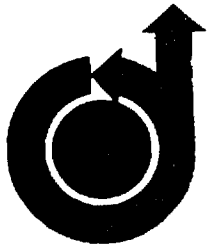

AIAA-81-0046

Solutions of the Unsteady Two-Dimensional Compressible Navier-Stokes Equations Using the Integral Representation Method

J.C. Wu, M. El-Refaee and S.G. Lekoudis, Georgia Institute of Technology, Atlanta, Ga.

AIAA 19th AEROSPACE SCIENCES MEETING

January 12-15, 1981/St. Louis, Missouri

SOLUTIONS OF THE UNSTEADY TWO-DIMENSIONAL COMPRESSIBLE NAVIER-STOKES EQUATION USING THE INTEGRAL REPRESENTATION METHOD

J. C. Wu*, M. M. ElRefaee+ and S. G. Lekoudis•
School of Aerospace Engineering
Georgia Institute of Technology
Atlanta, Georgia 30332

Abstract

The integral representation method was used to obtain numerical solutions of the compressible, unsteady, two-dimensional Navier-Stokes equations for subsonic flows. The equations were written with the vorticity, the dilatation, the density and the enthalpy as the dependent variables. The method was tested by solving the following problems: the flows over a flat plate, around a circular cylinder and around a Joukowski airfoil. The last two problems involved massive flow separation. The approach offers the capability of confining the domain of computations to the region where two quantities are non-negligible, the vorticity and the difference in dilatation between the real flow and the potential flow around the body.

1. Introduction

The equations that govern most of the flows of interest in aerodynamic applications are the Navier-Stokes equations. Because of their complexity, analytical solutions are available only for an extremely small number of problems. Hence, numerical solutions are being sought. For flowfields with certain characteristics, simplifications of the Navier-Stokes equations, compatible with the characteristics, have been used to predict these flowfields. However, there are cases of importance in applications where simplifications of the equations are not allowed because of the nature of the flowfield. Examples of such cases are the static and dynamic stalls of airfoils and the complicated flows inside turbomachinery devices.

The computation of the flowfield around airfoils undergoing static or dynamic stall has already been performed by several investigators. References 1 through 5 describe different methods for solving the problem in incompressible flow. The compressible flow problem has been examined in References 7 and 8. These calculations require considerable resources, especially for the case of high Reynolds number flows. Some of the reasons for the requirements will be explained below.

Most of the methods used to obtain numerical solutions to the Navier-Stokes equations have common characteristics. They use finite-difference techniques and they apply the infinity boundary conditions at some finite distance from the body. They compute the surface vorticity, a quantity of importance in the accuracy of the calculations, using essentially interpolation procedures. One reason that is costly to obtain these solutions is that a large number of grid points must be used. That is so because the grid must capture the details of the flow where the gradients are large and also extend far enough so that the infinity boundary conditions can be used with some confidence.

A different approach for computing unsteady viscous flowfields was presented in References 9 and 10. The main advantage of this approach, called the integral representation method, are the following: First, the computations are confined to regions of non-negligible vorticity, which is quite small for high Reynolds number flows. Hence, the number of points in the computational grid is smaller than the number required by more conventional approaches for comparable accuracy. Second, the surface vorticity is computed directly and not through interpolation. Moreover, the infinity boundary conditions are satisfied exactly. For the case of incompressible flows, the flowfield around airfoils with massive separation was computed using this approach in References 2 through 6.

In the present study, the integral approach is extended to compressible flows. This has been achieved by using the dilatation as a dependent variable. The resulting system of equations needs to be solved only where the vorticity and the dilatation are non-negligible. Because the dilatation is significant at distances from the body where the vorticity is already negligible, at high Reynolds numbers, the approach does not seem as advantageous, as in the incompressible case. However the problem has been reformulated so that solutions are needed only in regions where the vorticity is non-negligible and the dilatation difference between the viscous flow and the potential flow around the same configuration is also non-negligible.

The developed formulation has been applied to the following problems: The problem of the flow over a flat plate, around a circular cylinder, and around an airfoil. The last two problems involve massive flow separation. The formulation is described in section 2 of this paper. The numerical procedure used is described in section 3, the results and discussion are in section 4, and the conclusions are in section 5.

* Professor, Associate Fellow, AIAA.
+ Research Assistant, Student Member AIAA.
• Assistant Professor, Member AIAA.

2. The Analytical Formulation

2.1 The governing equations

In an unbounded two-dimensional region R, the conservation of mass for compressible flow can be expressed as[13]

$$\vec{V}(\vec{r},t) = \frac{1}{2\pi} \int_R \frac{\vec{\omega}(\vec{r}_o,t)\times(\vec{r}-\vec{r}_o)+\beta(\vec{r}_o,t)(\vec{r}-\vec{r}_o)}{|\vec{r}-\vec{r}_o|^2} dR + \vec{V}_\infty \qquad (1)$$

where

$$\vec{\omega}(\vec{r},t) = \nabla \times \vec{V}(\vec{r},t) \qquad (2a)$$

$$\beta(\vec{r},t) = \nabla \cdot \vec{V}(\vec{r},t) \qquad (2b)$$

are the definitions of vorticity $\vec{\omega}$ and dilatation β, and $\vec{V}_\infty$ is the assumed uniform velocity at infinity. The equations (1) and (2) describe the kinematics of the flow because, once $\vec{\omega}$ and β are known, the instantaneous velocity field is known everywhere through the integral (1). In the incompressible flow case, the vorticity $\vec{\omega}$ is governed by the vorticity transport equation, obtained by applying the curl operator on the momentum equation (Navier-Stokes equation) and using (2a). In the compressible case, $\beta \neq 0$, an equation governing the transport of the dilatation β is needed. Using the definitions (2) and applying the curl and the divergence operators on the compressible momentum equation for two-dimensional flow, we obtain:

$$\frac{\partial \omega}{\partial t} = - v.\nabla\omega + \left(\frac{\mu}{\rho R_e}\right) \nabla^2\omega + \phi\,(\rho,\beta,\omega,h) \qquad (3)$$

$$\frac{\partial \beta}{\partial t} = - v.\nabla\beta + \left(\frac{4/3\mu}{\rho R_e}\right) \nabla^2\beta + \psi\,(\rho,\beta,\omega,h) \qquad (4)$$

where ω denotes the magnitude of vorticity vector. The terms ϕ and ψ are given in the appendix, look like "source" terms, and are identically zero in the incompressible case. In (3) and (4) R_e is the Reynolds number, ρ the density, μ the (variable) viscosity and h is the enthalpy. All the quantities in (3) and (4) are nondimensional. Hence, it seems necessary, in order to solve the system (1), (2), (3) and (4) and obtain answers to the problem of compressible flow, to have ρ and h available. They can be obtained by solving the following equations for ρ and h:

$$\frac{\partial \ln\rho}{\partial t} = - \vec{v}.\nabla \ln\rho - \beta \qquad (5)$$

$$\frac{\partial h}{\partial t} = - \vec{v}.\nabla h + \left(\frac{\gamma k}{\rho R_e Pr}\right) \nabla^2 h + \theta\,(\rho,\beta,h,\vec{\omega}) \qquad (6)$$

The expression (5) is the conservation of mass and (6) is the energy equation. θ are "source" terms and are given in the appendix. In (6), the perfect gas equation of state is used, Pr is the Prandtl number, k is the thermal conductivity, γ the ratio of specific heats. The system of equations (1) to (6) is closed and completely equivalent to the familiar Navier-Stokes equations written in primitive variables, provided that the dependence of Pr, μ, k, and γ on the state properties ρ and h are known. The following observation can be made about this system.

Because (1) and (2) completely define the flowfield (the instantaneous pressure can be easily obtained through a numerical integration of the momentum equation once the velocities are known) we need only to solve for the part of the flowfield where ω and β are non-negligible. For high Reynolds number flows, ω is substantial only in a region close to the body and in the wake. Hence this approach offers a reduction of the computational region, compared with more conventional formulations. This has already been demonstrated in calculations of problems involving incompressible flows[2-6]. In the compressible flow problem examined here, the computational domain must extend far enough from the body to include the region where β is substantial, at least in the computational sense. For the case of the subsonic flow around an airfoil, potential flow theory indicates that this region has a length scale comparable with the airfoil chord. Hence, it seems that the developed formulation does not offer any substantial advantage over the more conventional approaches. However, by using potential flow solutions around the body, it will be shown in section 2.2 that the domain of computations can be further reduced.

2.2 Use of the potential flow solution to further reduce the domain of computations.

The equation (1) can be written in the following form:

$$\vec{V}(\vec{r},t) = \frac{1}{2\pi} \int_{R_1} \frac{\vec{\omega}(\vec{r}_o,t)\times(\vec{r}-\vec{r}_o)+\beta(\vec{r}_o,t)(\vec{r}-\vec{r}_o)}{|\vec{r}-\vec{r}_o|^2} dR + \frac{1}{2\pi} \int_{R_2} \frac{\beta(\vec{r}_o,t)(\vec{r}-\vec{r}_o)}{|\vec{r}-\vec{r}_o|^2} dR + \vec{V}_\infty \qquad (7)$$

where R_1 is the region of the flow where vorticity is non-negligible and R_2 is the rest of the domain, extending to infinity for exterior flow problems. This expression can be written for potential flows around the same body:

$$\vec{V}_p(\vec{r},t) = \frac{1}{2\pi} \int_{R_1} \frac{\beta_p(\vec{r}_o,t)(\vec{r}-\vec{r}_o)}{|\vec{r}-\vec{r}_o|^2} dR + \frac{1}{2\pi} \int_{R_2} \frac{\beta_p(\vec{r}_o,t)(\vec{r}-\vec{r}_o)}{|\vec{r}-\vec{r}_o|^2} dR + \frac{1}{2\pi} \int_S \frac{\gamma_p x(\vec{r}-\vec{r}_o)}{|\vec{r}-\vec{r}_o|^2} dS + \vec{V}_\infty \qquad (8)$$

where the subscript p indicates potential flow and γ_p is the vortex sheet strength on the surface S of the body, due to the potential flow. Then, if R_1 extends far enough from the body, the combination of (7) and (8) gives:

$$\vec{V}(\vec{r},t) = \frac{1}{2\pi}\int_{R_1}\frac{\vec{\omega}\times(\vec{r}-\vec{r}_o)+(\beta-\beta_p)(\vec{r}-\vec{r}_o)}{|\vec{r}-\vec{r}_o|^2}\,dR$$

$$-\frac{1}{2\pi}\int_{S}\frac{\gamma_p \times (\vec{r}-\vec{r}_o)}{|\vec{r}-\vec{r}_o|^2}\,dS + \vec{V}_p \qquad (9)$$

The relation (9) implies the following. First $\beta-\beta_p$ in R_2 is small enough so that its effect on the velocity in R_1 is negligible. Second, one needs to solve only in R_1, which is a smaller region than the region where β is significant. Thus, the approach does offer a reduction of the computational domain, compared with conventional approaches. Detailed discussion of this advantage is given in Reference 11.

2.3 The surface vorticity

Imposing the no-slip condition on the body surface overspecifies the boundary condition for the vorticity transport equation. This statement has already been discussed in detail in other publications dealing with the integral representation approach, and a detailed description can be found in Reference 10. It can be shown[10], that the surface vorticity can be uniquelly determined by applying the no-slip condition on the integral expression for the kinematics of the problem. For the case of the compressible flow problem examined here, the application of the no-slip condition on (9) gives:

$$\int_S \frac{(\vec{\gamma}-\vec{\gamma}_p)\times(\vec{r}_s-\vec{r}_o)}{|\vec{r}_s-\vec{r}_o|^2}dS + \int_{R_1}\frac{\vec{\omega}\times(\vec{r}_s-\vec{r}_o)+(\beta-\beta_p)(\vec{r}_s-\vec{r}_o)}{|\vec{r}_s-\vec{r}_o|^2}dR = 0 \qquad (10)$$

where the subscript S denotes the solid boundary and γ is the unknown surface vorticity, to be obtained by solving the integral equation (10) for $\vec{\gamma}$.

Equation (10) is a vector equation. An efficient method to solve (10) for γ has been developed and applied to the incompressible flow case. To describe the method briefly, the dot product of (10) with the vector $\vec{t}$, tangential to the body surface, is taken and the principle of conservation of total vorticity is used to transfer $\vec{\gamma}$ outside the first integral. The area integrals involving $\vec{\omega}$ are evaluated using Fourier series expansion because the flow is periodic in θ, in a polar coordinate system (r,θ). This applies both to the cylinder and to airfoil problems because the computational domain for the airfoil is the outside of the cylinder, to which the airfoil is transformed. The same technique has been used in the present study with the extra complication of evaluating the area integrals involving the dilatation using Fourier series. Details can be found in Reference 11.

3. The Numerical Procedures

Because the computation of the flow around the airfoil is the most complicated of the problem that have been attacked, using the formulation described in section 2, the subsequent discussion will be confined to this case.

The region around the Joukowski airfoil was transformed onto the region outside a circular cylinder through e conformal transformation[11]. Hence, for both the cylinder and the airfoil problems, the computational domain was the same. In this domain a polar coordinate system (r,θ) was used. For the case of the airfoil, the governing equations are the same as in the case of the circular cylinder, the only difference being the appearance of the scale factor of the transformation. This procedure, used several times before in the solution of incompressible flow problems, can be found in References 4, 5, and 11.

For reasons of computational efficiency, the integral representation for the kinematics was used only in a part of the computational domain. This part included the outer boundary, the first eight grid lines around the airfoil, and a region between the airfoil and the downstream boundary. This region was bounded by two grid lines in the radial direction and included the trailing edge of the airfoil. In the rest of the computational domain, a Poisson equation for the velocity in the θ - direction was solved. Then, the definition of the dilatation β was used to obtain the velocity in the r-direction.

The transport equations for ω, β, ρ and h, equations (3), (4), (5) and (6) respectively, have the same form. Hence, the numerical scheme used to solve them is kept identical. The equations were solved in the computational domain using a polar grid with equal spacing in θ, $\pi/24$, and increasing spacing in the radial direction according to

$$r_j = 1 + \exp\left[z_o + (j-1)\Delta z\right] \qquad (11)$$

with the cylinder radius having a length of unity and j increasing away from the cylinder. An implicit finite-difference scheme was used for the solution of the transport equations. The time derivative was approximated using first order backward differencing and the diffusion and source terms were approximated using second order central differencing at the solution time level. The convection terms were approximated, in their conservation form, by second order[14] upwind differencing. The finite-difference equations were linearized by delaying the velocities at the convection terms by one time step, and by delaying some quantities in the source terms. The resulting algebraic equations were solved using a successive "point under-relaxation" scheme. The relaxation sweeps were alternating in the θ-direction because that was found to accelarate convergence. The sequence of the calculations was as follows:

1) With all the dependent variables known at the previous time level, the vorticity transport equation is solved to obtain the values of the interior vorticity.

2) New values of the boundary vorticity are obtained using the integral representation, as described in section 2.3. The steps 1 and 2 are repeated until a prescribed convergence criterion is satisfied.

3) The rest of the transport equations are solved to determine the values of β, ρ and h at the new time level.

4) Using the new ω and β, the velocities are computed in the θ-direction. As mentioned before, the integral relationship is used for the first eight grid lines next to the body, at the outer boundary, and at a region that includes the trailing edge of the airfoil and is bounded by two grid lines in the radial direction. In the rest of the domain, a Poisson equation is solved for the velocity in the θ-direction using finite-differences. Then the velocities in the r-direction are obtained using the definition of the dilatation. The time is advanced and the procedure is repeated from step 1.

The zero derivative of h and ρ normal to the wall was used as boundary condition (adiabatic wall). The value of β at the wall was obtained using three-point extrapolation at each iteration of the transport equation for β. The potential flow values used for all the field variables were used as upstream boundary conditions at the outer boundary. Zero second derivatives for h, ρ and β, and zero vorticity were used as downstream boundary conditions at the outer boundary. The wake never approached the outer boundary during the calculations.

4. Results and Discussion

The formulation presented in section 2 of this paper was tested by solving for the flow over a flat plate, around a circular cylinder and around a 9% thick Joukowski airfoil. A description of the results follows.

The flow over a flat plate was solved for the conditions: freestream Mach number 0.5, Prandtl number 1, Reynolds number based on plate length 1,000. A relatively coarse grid with uniform $\Delta x = 0.1L$, $\Delta y = .04L$ was used. The grid extended 0.5L ahead of the leading edge of the plate, 1.5L behind the trailing edge of the plate and 0.8L above the plate. Figure 1 shows the vorticity at the middle of the plate obtained using the present formulation and a purely finite-difference technique[7,12]. The differences are partly due to the different grids and partly due to the different numerical schemes used.

The second test problem solved was the flow over a circular cylinder. The conditions used were: free stream Mach number 0.4, Prandtl number 1, Reynolds number based on the cylinder radius 40. The computations were started by using the potential flow solution at the beginning and stopped at a time level of 7.5, based on the freestream velocity and the cylinder diameter, when numerically steady state was achieved. To test the program, the vorticity transport equation was solved alone by "switching off" the source terms. Thus, incompressible flow results were obtained. Figure 2 shows a comparison of the pressure coefficient obtained using the developed formulation, obtained for the incompressible flow case, and for experiments in incompressible flows[15]. The compressibility effect is small, as expected for the condition stated above. Figure 3 shows the compressible pressure coefficient obtained using the present approach and a purely finite-difference technique[7,12]. Table 1 shows some more comparisons.

The most complicated problem solved using the developed formulation, was the flow around a 9% thick Joukowski airfoil. The region outside the airfoil was mapped conformally onto the computational domain which was the region outside a circular cylinder. A grid with equal spacing in the circumferential direction and exponentially expanding in the radial direction was used. Figures 4 and 5 show the surface pressure distribution and vorticity of the airfoil, at zero angle of attack, for the following conditions: freestream Mach number 0.4, Prandtl number 1, Reynolds number, based on the airfoil chord, 1,000. The calculations were started by using the potential flow solution as the initial flowfield. Numerically steady state solution was obtained after a dimensionless time of 2.25, based on the freestream velocity and the airfoil chord. In Figures 4 and 5 the surface pressure and vorticity distributions are compared with results of a purely finite-difference technique[7,12]. Considering the differences in the grids and the techniques used, the results are close. Unfortunately, similar comparisons for the angle of attack case were not possible due to the different flowfields at the beginning of the calculations. Although the effect of the initial condition on the magnitude of the computed field variables decays rapidly, phase differences make further comparisons not possible. The airfoil exibited massive separation at 15° angle of attack. Figures 6, 7, 8 show the surface pressure distributions and 9, 10, 11 show the surface vorticity at three time levels after the beginning of the computations. Results for incompressible flow are also shown in these figures. The effect of compressibility, although small for the conditions stated above, is to delay the sequence of events, like the growing of the bubble and the bursting of the bubble from the airfoil surface. Figure 12 shows the streamline-like lines at the same three time levels. These streamline-like lines were obtained using the stream function corresponding to the calculated vorticity, and a stream function corresponding to the potential flow due to the computed dilatation β, in an additive fashion[11]. Because the compressibility effect is small, these lines are very close to the actual streamlines.

The grid was extended during the calculations due to the increasing viscous region of the flow. The average execution speed was .02 seconds per time step per grid point on a CDC 6600 computer.

Table 1

Quantity	Finite-Dif.[7,12]	Present Method
Angle of separation	127.5°	126.3°
Length of standing vortex over cylinder diameter	2.54	2.92
Drag coefficient due to pressure	1.32	1.23
Drag coefficient due to shear	0.561	0.520

5. Conclusions

The integral representation approach has been extended to the case of compressible flows, and has been used to solve the two-dimensional unsteady compressible Navier-Stokes equations for three subsonic test problems: the flow over a flat plate, around a circular cylinder and around an airfoil. The solution obtained compare favorably with existing finite-different solutions. More important, the method restricts the domain of computations to the viscous region of the flowfield. The viscous region is the region where the vorticity and the difference in dilatation between the real flow and the potential flow around the body are numerically significant.

Acknowledgement

The work was supported by the Computational Fluid Dynamics Branch of the NASA-Lewis Research Center through the Grant NSG 3307.

References

1. Metha, U. B. and Lavan, Z., "Starting Vortex, Separation Bubbles and Stall - A Numerical Study of Laminar Unsteady Flow Around an Airfoil," J. Fluid Mech. Vol. 67, pp. 227-256, 1975.

2. Wu, J. C. and Sampath, S., "A Numerical Study of Viscous Flow Around an Airfoil," AIAA Paper 76-337.

3. "Unsteady Aerodynamics," AGARD Conference Proceedings No. 227, Paper No. 23 by U. B. Metha and No. 24 by J. C. Wu, S. Sampath and N. L. Sankar.

4. Sugavanam, A. and Wu, J. C., "Numerical Study of Separated Turbulent Flow over Airfoils," AIAA Paper 80-1441.

5. "An Integral Representation Approach for Time-Dependent Viscous Flows," by Y. Rizk, Ph.D. Thesis, Georgia Institute of Technology, 1980.

6. Sankar, N. L. and Wu, J. C., "Viscous Flow Around Oscillating Airfoil - A Numerical Study," AIAA Paper 78-1225.

7. Sankar, N. L. and Tassa, Y., "Reynolds Number and Compressibility Effects on Dynamic Stall of a NACA 0012 Airfoil," AIAA Paper 80-0010.

8. Shamroth, S. J. and Gibeling, H. J., "The Prediction of the Turbulent Flow Field About an Isolated Airfoil," AIAA Paper 79-1543.

9. Wu, J. C. and Thompson, J. F., "Numerical Solutions of Time-Dependent Incompressible Navier-Stokes Equations Using an Integro-Differential Formulation," J. of Computers and Fluids, Vol. 1, No. 2, pp. 197-215, (1973).

10. Wu, J. C., "Numerical Boundary Conditions for Viscous Flow Problems," AIAA Journal, Vol. 14, No. 8, pp. 1042-1049, (1976).

11. ElRefaee, M., Ph.D. Dissertation, School of Aerospace Engineering, Georgia Institute of Technology, to be published in 1981.

12. Sankar, N. L., Private Communication.

13. Wu, J. C., "Integral Representation of Field Variables for the Finite Element Solution of Viscous Flow Problems," Proceedings of the 1974 Conference on Finite Element Methods in Engineering, pp. 827-840, Clarendon Press, 1974.

14. Roach, P., Computational Fluid Dynamics, Hermosa Publishers, page 73, 1976.

15. Grove, A. S., Shair, F. H., Peterson, E. E. and Acrivos, A., "An Experimental Investigation of the Steady Separated Flow Past a Circular Cylinder,", J. Fluid Mech., Vol. 19, pp. 60-80, 1964.

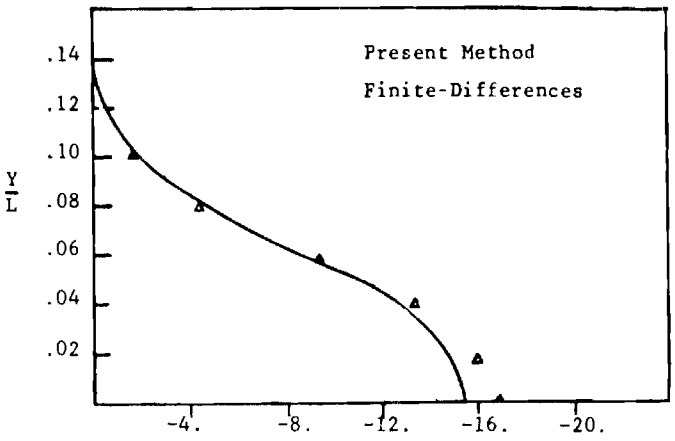

Fig. 1 Vorticity at midplate

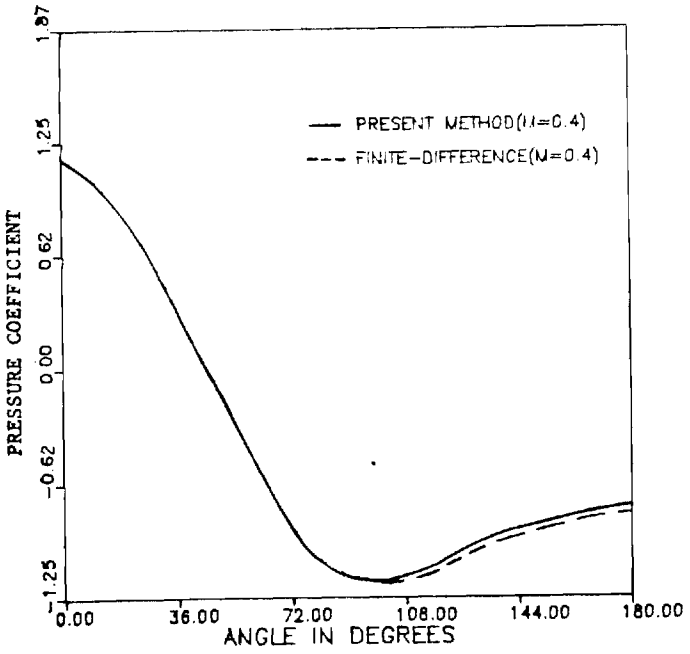

Fig. 2 Pressure distribution on circular cylinder

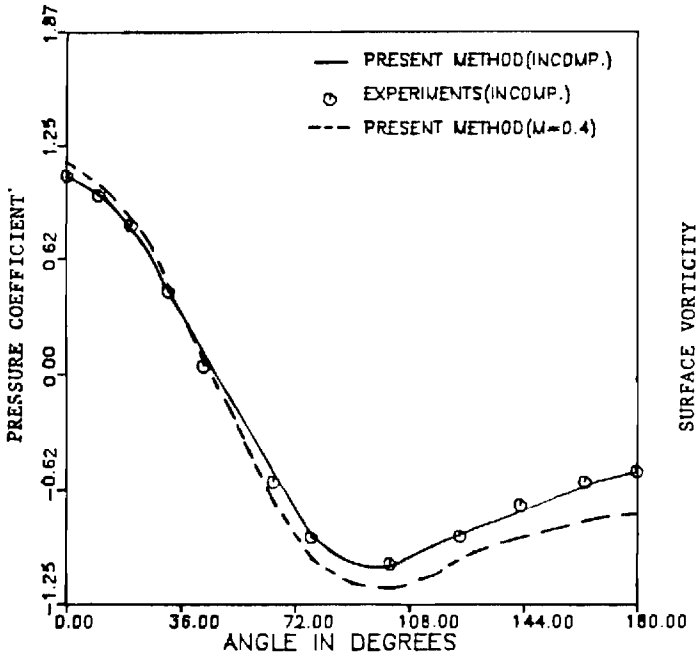

Fig. 3 Pressure distribution on circular cylinder

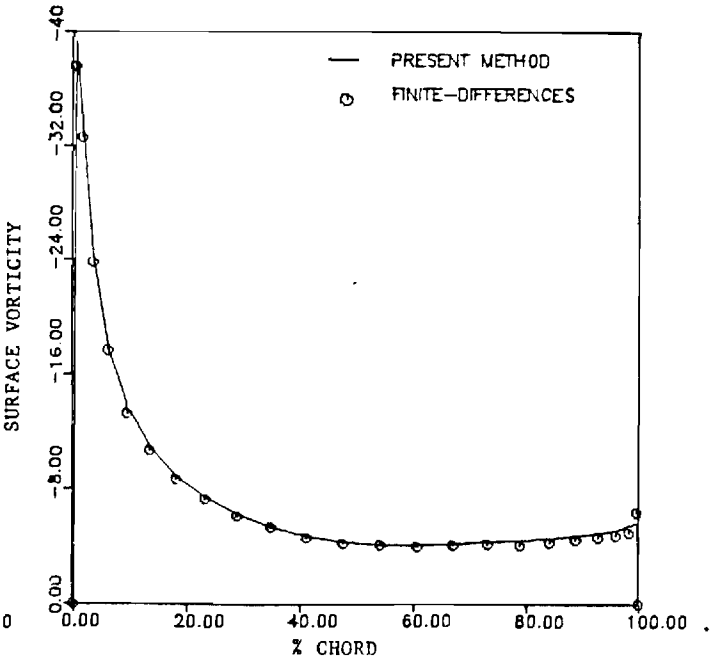

Fig. 5 Surface vorticity distribution

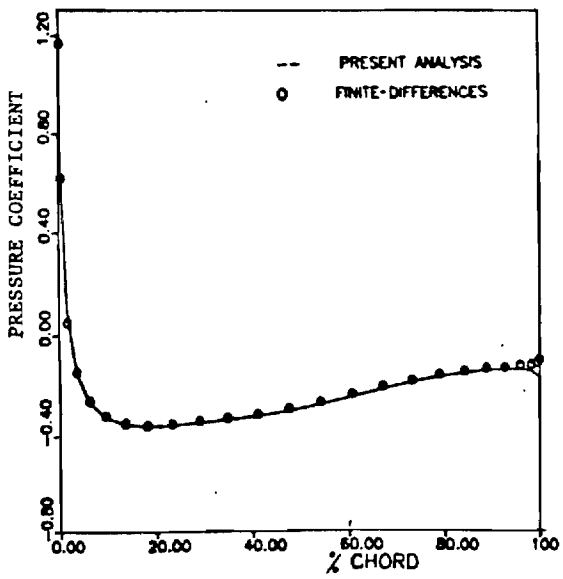

Fig. 4 Surface pressure distribution

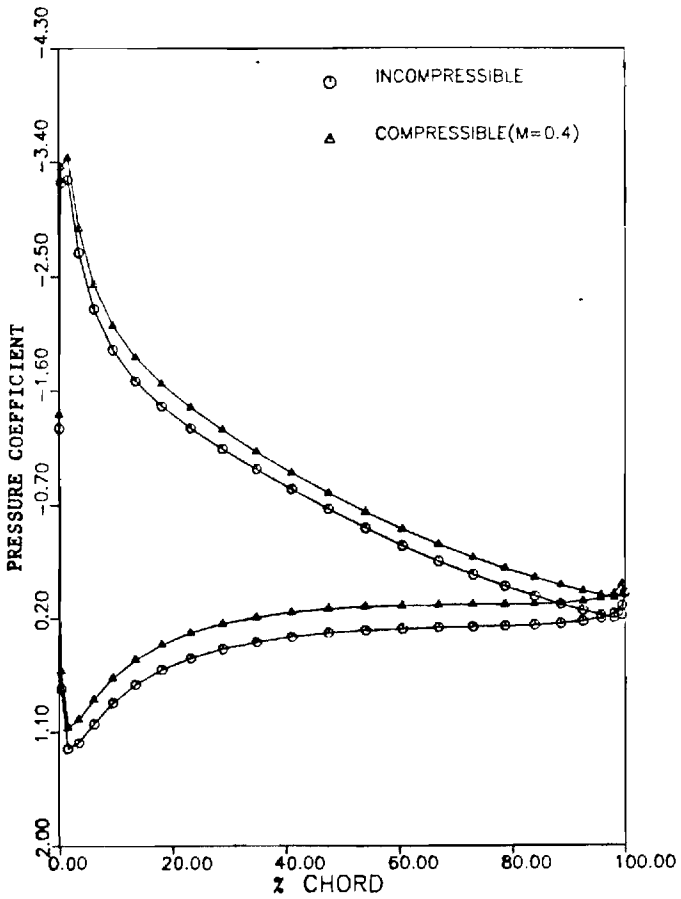

Fig. 6 Surface pressure distribution for T = 0.941

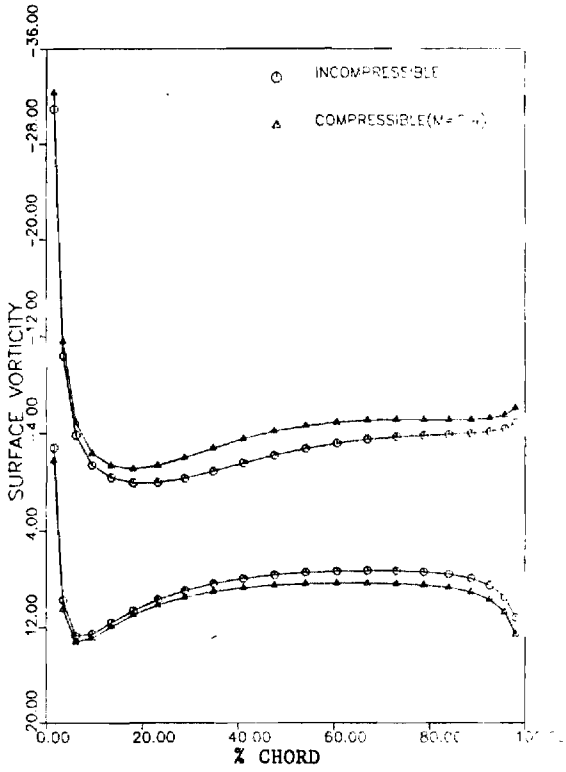

Fig. 7 Surface vorticity distributions for T = 0.941

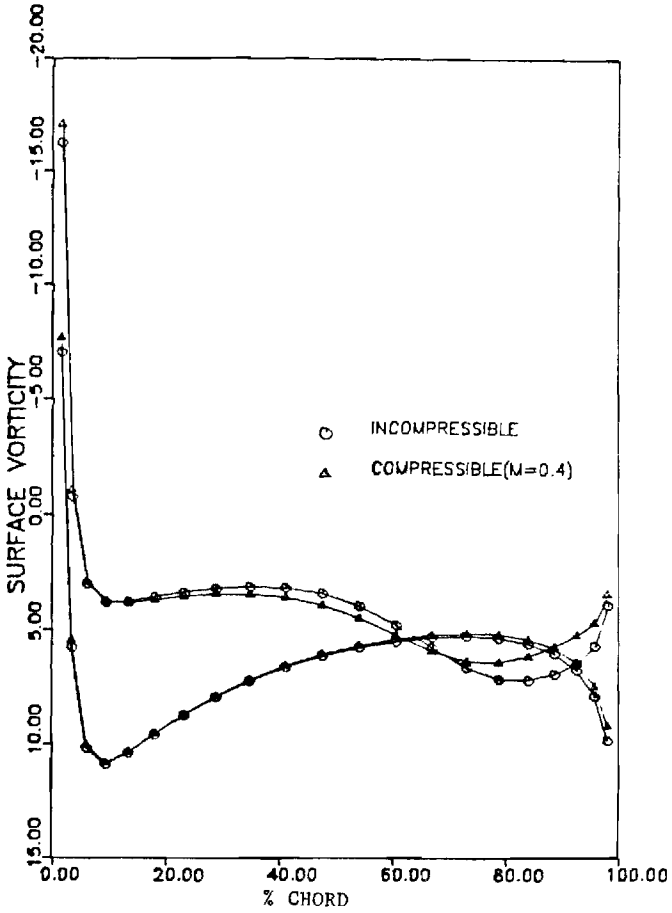

Fig. 9 Surface vorticity distributions for T = 2.557

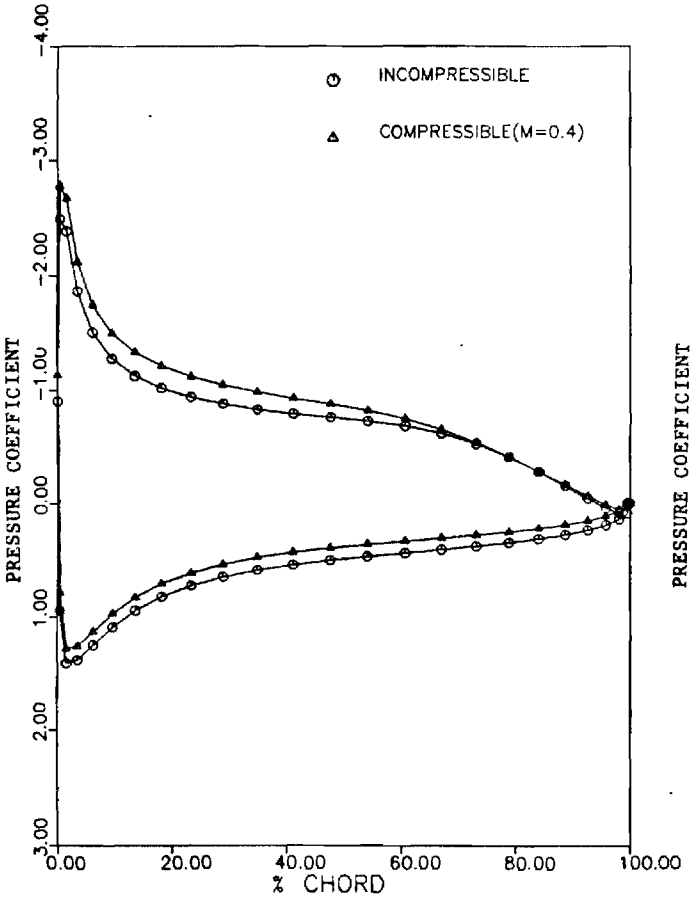

Fig. 8 Surface pressure distribution for T = 2.557

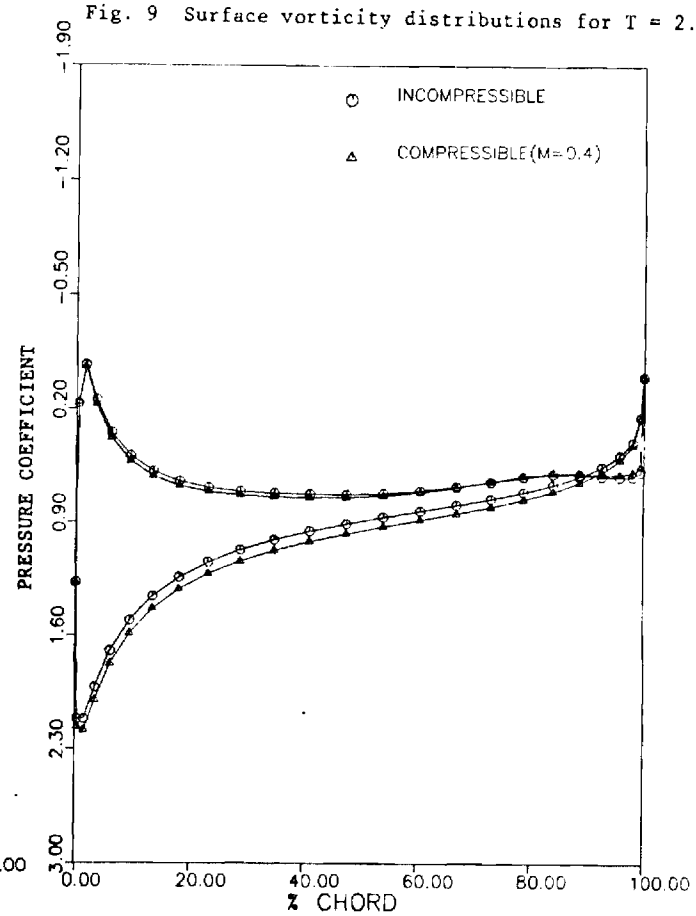

Fig. 10 Surface pressure distributions for T = 5.013

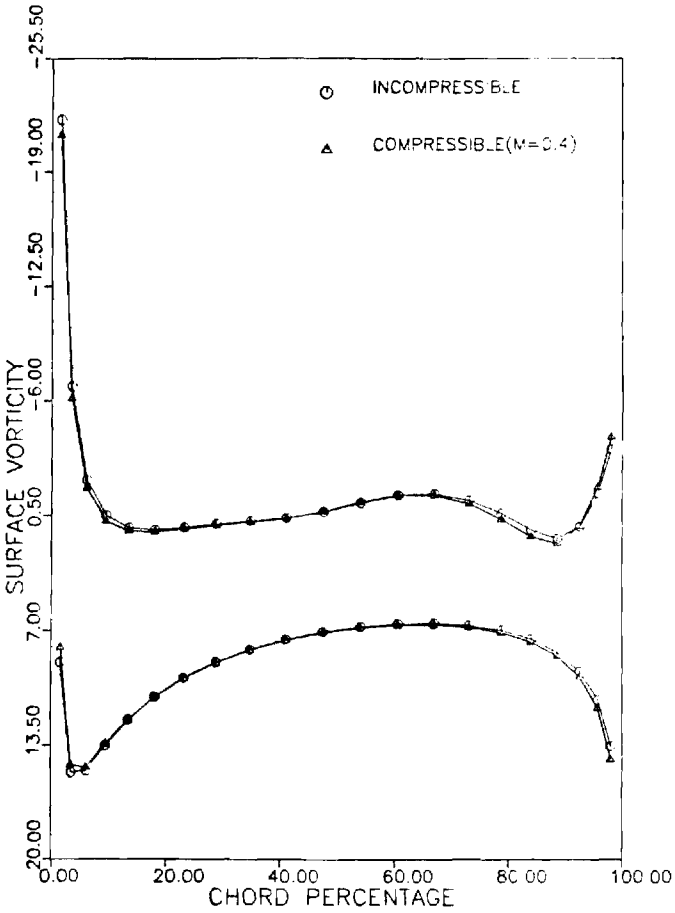

Fig. 11 Surface vorticity distributions for T = 5.013

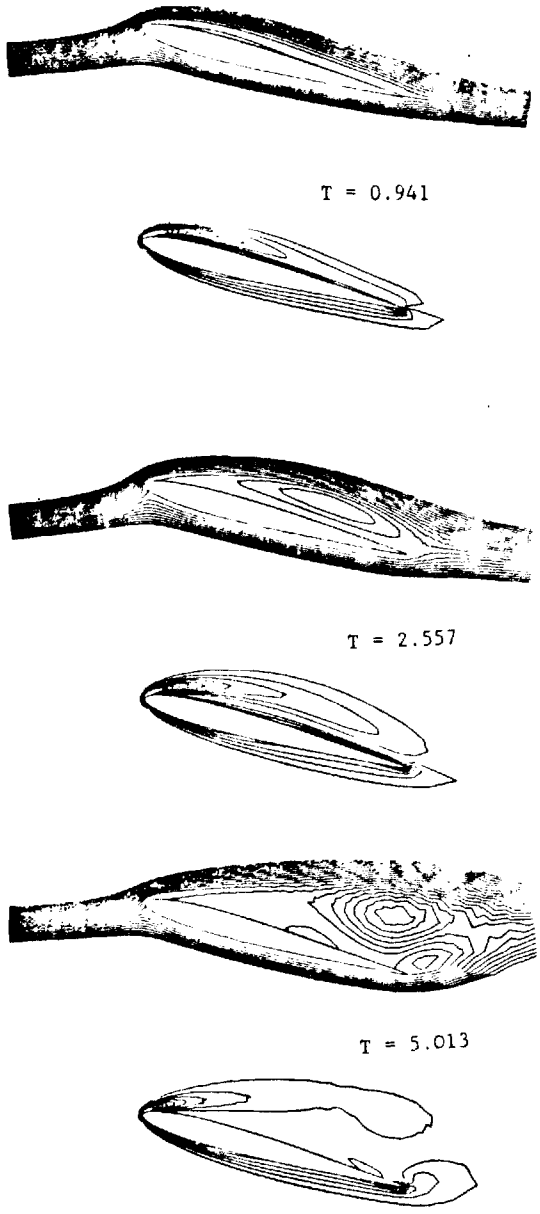

Fig. 12 Streamline-like lines and equal vorticity lines

Appendix

$$\phi = -\omega\beta + \frac{\mu}{\rho^2 R_e}\left(4/3\left|\vec{\nabla}\beta \times \vec{\nabla}\rho\right| - \vec{\nabla}\rho \cdot \vec{\nabla}\omega\right)$$

$$+ \frac{\gamma-1}{\gamma}\vec{\nabla} \ln\rho \times \vec{\nabla}h + \frac{c_1}{R_e} \qquad (A.1)$$

$$c_1 = \frac{1}{\rho}(u_y+v_x)(\mu_{xx}-\mu_{yy}) + \frac{2}{\rho}(v_y-u_x)\mu_{xy} + \mu_x\left\{\frac{2}{\rho}\nabla^2 v\right.$$

$$+ \frac{2}{\rho}u_{xy} - \frac{1}{\rho^2}(\rho_x u_y - v_x\rho_x - 2\rho_y u_x + \frac{2}{3}\rho_y\beta)\Big\} + \mu_y\Big\{-\frac{2}{\rho}$$

$$\nabla^2 u + \frac{2}{\rho}v_{xy} - \frac{1}{\rho^2}(2\rho_x v_y - u_y\rho_y - v_x\rho_y - \frac{2}{3}\beta\rho_x)\Big\} \qquad (A.2)$$

$$\psi = -(u^2{}_x + v^2{}_y + 2u_y v_x) + \frac{\mu}{\rho^2 R_e} - \frac{4}{3}\nabla\rho \cdot \nabla\beta + \left\{\left|\nabla\rho \times \nabla\omega\right|\right\}$$

$$- \frac{\gamma-1}{\gamma}(\nabla^2 h + h\nabla^2 \ln\rho + \nabla h\nabla.\ln\rho) + \frac{c_2}{R_e} \qquad (A.3)$$

$$c_2 = \frac{8}{3\rho}\nabla\beta \cdot \nabla\mu + \frac{2}{3}\left|\nabla\omega \times \nabla\mu\right| - \frac{2}{3\rho}\beta\nabla^2\mu + \frac{2}{\rho}(u_x\mu_{xx}$$

$$+ v_y\mu_{yy}) + (v_x + u_y)\mu_{xy} - \frac{1}{\rho^2}(v_x + \mu_y) + \rho_y\mu_x$$

$$+ \frac{2}{3}\frac{\beta}{\rho^2}\nabla\rho\nabla\mu - \frac{2}{\rho^2}(\rho_x u_x \mu_x + \rho_y v_y \mu_y) \qquad (A.4)$$

$$\Theta = -(\gamma-1)\beta h + \frac{\gamma\mu}{\rho R_e}\left[\frac{\beta^2}{3} + (2u_x - \beta^2) + (2v_x - \omega)^2\right] + \frac{\gamma}{\rho R_e Pr}\vec{\nabla}h.\vec{\nabla}k$$

(A.5)

In the above expression the vector product terms denote the magnitude of the resulting vector.

For low subsonic speeds the variation of viscosity and thermal conductivity have a negligible effect and the "source" terms can be approximated by

$$\phi = -\omega\beta + \frac{\mu}{R_e\rho^2}\left\{4/3(\vec{\nabla}\beta \times \vec{\nabla}\rho).\vec{k} - \nabla\rho \cdot \nabla\omega\right\}$$

$$+ \frac{\gamma-1}{\gamma}(\nabla \ln\rho \times \nabla h).\vec{k} \qquad (A.6)$$

$$\psi = \beta^2 + (\nabla v \times \nabla u).\vec{k} + \frac{\mu}{\rho^2 R_e} + \left\{-4/3\,\vec{\nabla}\rho \cdot \vec{\nabla}\beta + (\vec{\nabla}\rho \times \vec{\nabla}\omega).\vec{k}\right\}$$

$$- (\frac{\gamma-1}{\gamma})(\nabla^2 h + h.\nabla^2 \ln\rho + \nabla h.\nabla\ln\rho) \qquad (A.7)$$

$$\theta = -(\gamma-1)\beta.h + \frac{\mu\gamma}{\rho R_e}\left\{(4/3)\beta^2 + \omega^2 + 4(\nabla v \times \nabla u).\vec{k}\right\} \qquad (A.8)$$

In the above expression, $\vec{k}$ denotes the unit vector normal to the plane of the flow.

Annual Progress Report

for the period September 10, 1979 to September 9, 1980

on NASA-Lewis Research Center

Grant No. NSG 3307

A NEW NUMERICAL APPROACH FOR COMPRESSIBLE VISCOUS FLOWS

by

J. C. Wu, Professor

and

S. G. Lekoudis, Assistant Professor

School of Aerospace Engineering

Georgia Institute of Technology

1. INTRODUCTION

The main objective of the research being conducted under NASA Lewis Research Center grant no. NSG 3307 is the development of a new numerical technique for solving the compressible Navier-Stokes equations. This new technique utilizes an integral representation of the kinematics of the flowfield. In the case of a steady flow, an integral representation of the kinetics of the flowfield can also be utilized.

In the case of an incompressible flow, both the kinetics and the kinematics of the flowfield have been expressed as integral representations (Reference 1 and 2). Compressibility introduces two additional unknowns into the problem. In the present work, the dependent variables selected to represent the new unknowns are the dilitation and the enthalpy. The main advantage of the integral representation is that it permits the computation to be confined to the viscous region of the flow. In the case of an incompressible flow, the viscous region is the region of non-negligible vorticity. In the case of compressible flow, the viscous region is the region of non-negligible vorticity and dilitation.

The progress that has been made towards the attainment of the objectives of this research, both in the analytical formulation and in the numerical procedures, is outlined in the following.

2. PROGRESS IN THE ANALYTICAL FORMULATION

As stated in the introduction, the main objective of this research is the development of a new numerical technique for solving the compressible Navier-Stokes equations. The present research utilizes the experience

gained in solving incompressible Navier-Stokes equations. For incompressible flows, both the kinetics and the kinematics of the flow can be represented in terms of integrals relating the velocity and the vorticity (References 1, 3, 4). If the flow is steady, the integral representation for the kinematics is somewhat simplified (Reference 1).

In the case of steady compressible flow, integral-representation describing both the kinetics and the kinematics of the problem have been derived and were presented in the research proposal (Reference 5) leading to the present project. The development of an integral-differential formulation for the case of unsteady two dimensional compressible viscous flow has been completed and is outlined below.

The vorticity $\vec{\omega}$ and the dilitation β are defined by:

$$\vec{\nabla} \times \vec{v} = \vec{\omega} \tag{1}$$

$$\vec{\nabla} \cdot \vec{v} = \beta \tag{2}$$

where $\vec{v}$ is the velocity vector. Substituting (1) and (2) into the two-dimensional Navier-Stokes equations, one obtains after some lengthy algebra, the following governing equations:

$$\frac{\partial \omega}{\partial t} = - \vec{v} \cdot \nabla\omega + \left(\frac{\mu}{\rho R_e}\right) \nabla^2\omega + \phi \ (\rho, \beta, \omega, h) \tag{3a}$$

$$\frac{\partial \beta}{\partial t} = - \vec{v} \cdot \nabla\beta + \left(\frac{4/3\mu}{\rho R_e}\right) \nabla^2\beta + \psi \ (\rho, \beta, \omega, h) \tag{3b}$$

$$\frac{\partial \ln\rho}{\partial t} = - \vec{v} \cdot \vec{\nabla} \ln\rho - \beta \tag{3c}$$

$$\frac{\partial h}{\partial t} = - \vec{v} \cdot \nabla h + \left(\frac{\gamma k}{\rho R_e P_r}\right) \nabla^2 h + \Theta \ (\rho, \beta, h, \omega) \tag{3d}$$

where ρ is the density and h is the enthalpy of the fluid

$$R_e = \frac{\rho_\infty u_\infty L}{\mu_\infty} \tag{4a}$$

$$P_r = \frac{c_p \mu}{k} \tag{4b}$$

$$\gamma = c_p / c_v \tag{4c}$$

are the usual definition of the Reynolds number, the Prandtl number, the ratio of specific heats, and L, u_∞, ρ_∞ and T_∞ have been used in the nondimensionalization. The terms ϕ, ψ, and Θ, are "source-like" terms, are identically zero in the incompressible case, and are given in the Appendix.

The equations (3) are four equations with six scalar unknowns e, h, β, ω and $\vec{v}$. The needed relation to close the system is obtained from the kinematics of the problem. From (1) and (2) we obtain

$$\vec{v}(\vec{r}_o, t) = - \frac{1}{2\pi} \int_R \frac{\vec{\omega} \times (\vec{r} - \vec{r}_o) + \beta (\vec{r} - \vec{r}_o)}{|\vec{r} - \vec{r}_o|^2} \, dR + \vec{v}_\infty \tag{5}$$

In (5) R is the domain of the flowfield where ω and β are non-negligible.

The analytical formulation for two-dimensional unsteady compressible Navier-Stokes equations in terms of vorticity and dilitation, as described above, has been applied to two test problems and to the flow around an airfoil with and without massive separation.

3. PROGRESS IN THE COMPUTATIONAL ALGORITHMS

3.1 Flow over a flat plate

The compressible flow at a zero angle of attack over a flat plate of length L, at Mach number $M_\infty = 0.5$, Reynolds number of 1,000 and Prandtl number 1, was investigated using the approach discribed in Section 2. The relatively coarse grid had uniform $\Delta x = 0.1L$ and $\Delta y = .04L$. The computational domain was extended 0.5L ahead of the leading edge of the plate, 1.5L behind the trailing edge of the plate and .8L above the plate.

Figures 1 and 2 show the distribution of the streamwise velocity u and the enthalpy h, at midplate, after steady state convergence was obtained, at a nondimensional time level $t = \frac{L}{u_\infty} = 2$. The numerical calculations predict an overshoot at the u profile when compared with the boundary layer theory. This overshoot is due to the boundary-layer displacement effect and is expected. Figure 3 shows the vorticity distribution at midplate from the present method, from boundary layer theory, and from a finite-difference solution of the Navier-Stokes equations. Considering that the Navier-Stokes calculations were done with different grids, the results are in reasonable agreement.

3.2 Flow around a circular cylinder

The second test problem solved using the present method is the flow over a circular cylinder, at $R_e = 40$, $M_\infty = 0.4$ and $P_r = 1$. The computational field is subdivided into three-regions bounded by concentric circles with their center at the center of the cylinder, and with radii 1.35R, 3.525R and 18.916R, where R is the cylinder radius. Inside the first circle the integral representation for the kinematics was used. In the other two regions, a Poisson type differential equation for the

kinematics was solved. However the velocity at the boundaries of the regions was obtained from the integral representation for the kinematics. This segmentation technique was found to accelerate the convergence rates and also reduce the required CPU time.

In the polar grid used, the spacing in the Θ direction was $\pi/20$, and the spacing in the radial direction was exponential with

$$r_j = 1 + \exp\left((j-1)\ \Delta z\right) \quad \text{and } \Delta z = .06$$

The computations were stopped at a time level $t = 15.1 = R/U_\infty$ when a steady state solution has been achieved. The time step was varied gradually from .05 to .15. Small time steps were used at the beginning of the calculation (impulsive start) because the flowfield was varying rapidly.

Figure 4 shows the pressure distribution at the cylinder surface computed from the present method and a finite-difference technique. Considering the difference in grids used, the results are in reasonable agreement. Figure 5 shows again the surface pressure distribution obtained from the present method in the incompressible limit, together with experimental data and from applying the Karman-Tsien (K.T.) rule to the incompressible results. It is recognized that the K.T. rule applies strictly to slender bodies. It seems to underestimate the compressibility effects on the pressure distribution.

Figures 6 and 7 are computer generated plots of the streamlines and equal vorticity lines for the flow around the cylinder, for both the incompressible and the compressible flow case.

In summary, the integral-differential method has been found capable of accurately predicting the compressible flowfield around the circular cylinder with massive separation.

3.3 Flow around a 9% Joukowski airfoil

The method is being applied to the case of a compressible subsonic flow around an airfoil. A conformal transformation is used to map the exterior of the airfoil onto the exterior of a unit circle. The computation is then performed in the circle-plane.

Figures 8 and 9 show the streamlines and the surface pressure distribution for the flow around a 9% thick Joukowski airfoil at zero angle of attack for R_e = 1,000. From figure 9 it can be seen that results from the present method are in good agreement with results from conventional finite-difference techniques.

The method was next applied to the case of the same airfoil at 15^o angle of attack. The flow is generated from an impulsive start at T = 0. In order to check the program, incompressible calculations were done by "switching off" the terms due to compressibility in the program. Figures 10, 12, 14 and 16 show streamline and equal vorticity countours generated from the program, with compressibility neglected, for different nondimensional time levels. Figures 11, 13, 15 and 17 show the corresponding surface vorticity distributions. All the incompressible results are in good qualitative agreement with previous incompressible calculations (Reference 7).

Figures 18 and 19 show streamlines, equal vorticity countours and surface vorticity distributions for a compressible flow around the same airfoil with a freestream Mach number of 0.4.

4. WORK IN PROGRESS

The steady state compressible flow solution of the Navier-Stokes equations has been programmed using integral representations for both the kinematics and the kinetics of the flowfield. The program is at the debugging stage. The method uses triangular elements for the flow in a channel.

Also work continues on the compressible airfoil program to obtain more results, to speed up the program, and to compare results with conventional finite-difference techniques.

PUBLICATIONS

The following documents, have been prepared under support by NASA-Lewis Research Center.

1. J. C. Wu, "Accomodation of Diverse Length-Scales in General Viscous Flows," an invited paper presented in June, 1980, at the Second International Symposium on Innovative Numerical Analysis in Applied Engineering Science and published in the Symposium Proceeding by the University of Virginia Press, June, 1980.
2. Y. M. Rizk, "A Integral-Representation Approach for Time-Dependent Viscous Flows," a Ph.D. Thesis, Georgia Institute of Technology, March 1980.
3. M. M. ElRefaee, "A Numerical Study of Laminar Unsteady Compressible Flow over Airfoils," a Ph.D. thesis proposal, Georgia Institute of Technology, February 1980.

4. J. C. Wu, M. ElRefaee and S. G. Lekoudis, "Solutions of the Unsteady Two-Dimensional Compressible Navier-Stokes Equations using the Integral Representation Method," AIAA Paper 80-0046. To be presented at the 19th Aerospace Sciences Meeting in St. Louis, January 1981.

REFERENCES

1. J. C. Wu, and M. Wahbah, "Numerical Solution of Viscous Flow Equations Using Integral Representations," Proceedings of the Fifth International Conference on Numerical Methods in Fluid Dynamics, Lecture Series in Physics, Springer-Verlag, Vol. 59, pp. 448-453, 1976.

2. M. M. Wahbah, "Computation of Internal Flows with Arbitrary Boundaries Using the Integral Representation Method," Georgia Institute of Technology Report, March, 1978.

3. J. C. Wu, and Y. M. Rizk, "Integral-Representation Approach for Time-Dependent Viscous Flows," Proceedings of the Sixth International Conference on Numerical Methods in Fluid Dynamics, Lecture Notes in Physics, Springer-Verlag, Vol. 90, 1978, pp. 558-564.

4. Y. M. Rizk, "A Integral-Representation Approach for Time-Dependent Viscous Flows," a Ph.D. Thesis, Georgia Institute of Technology, March 1980.

5. J. C. Wu, "A New Numerical Approach for Compressible Viscous Flows," A Research Proposal submitted to NASA-Lewis Research center, Georgia Institute of Technology, April 1979.

6. M. M. ElRefaee, "A Numerical Study of Laminar Unsteady Compressible Flow over Airfoils," a Ph.D. thesis proposal, Georgia Institute of Technology, February 1980.

7. Metha, U. B. and Lavan, J., "Starting Vortex, Separation Bubbles and Stall - A Numerical Study of Laminar Unsteady Flow Around an Airfoil," J. Fluid Mech., Vol. 67, pp. 227-256, 1975.

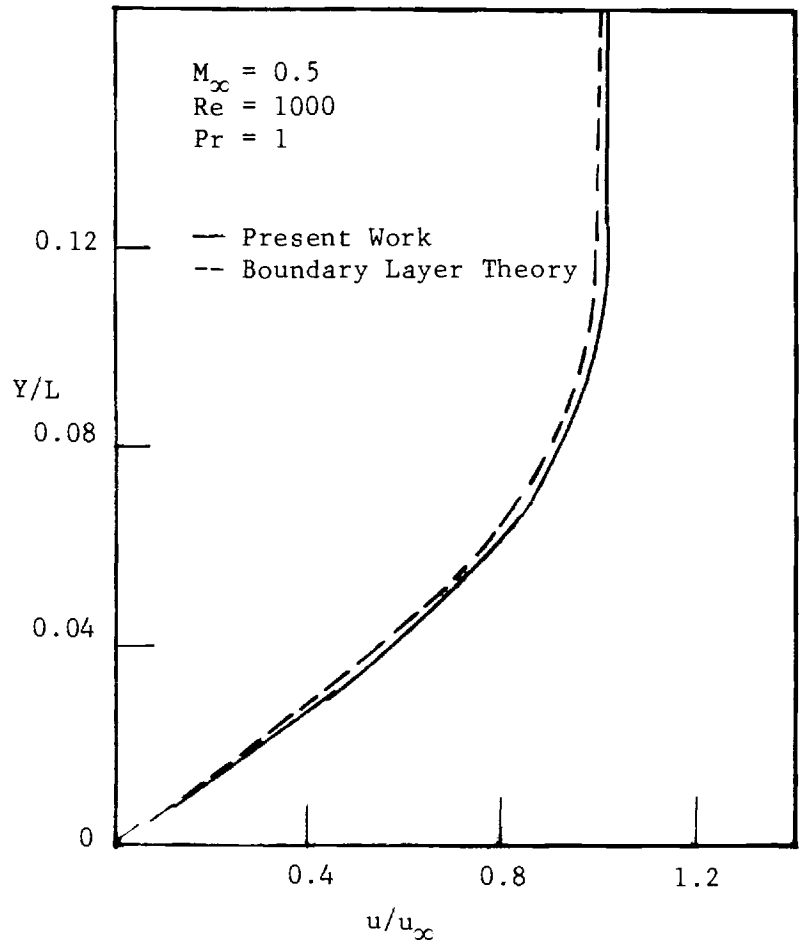

Figure 1. Flat Plate Problem Mid-Plate Velocity Profile

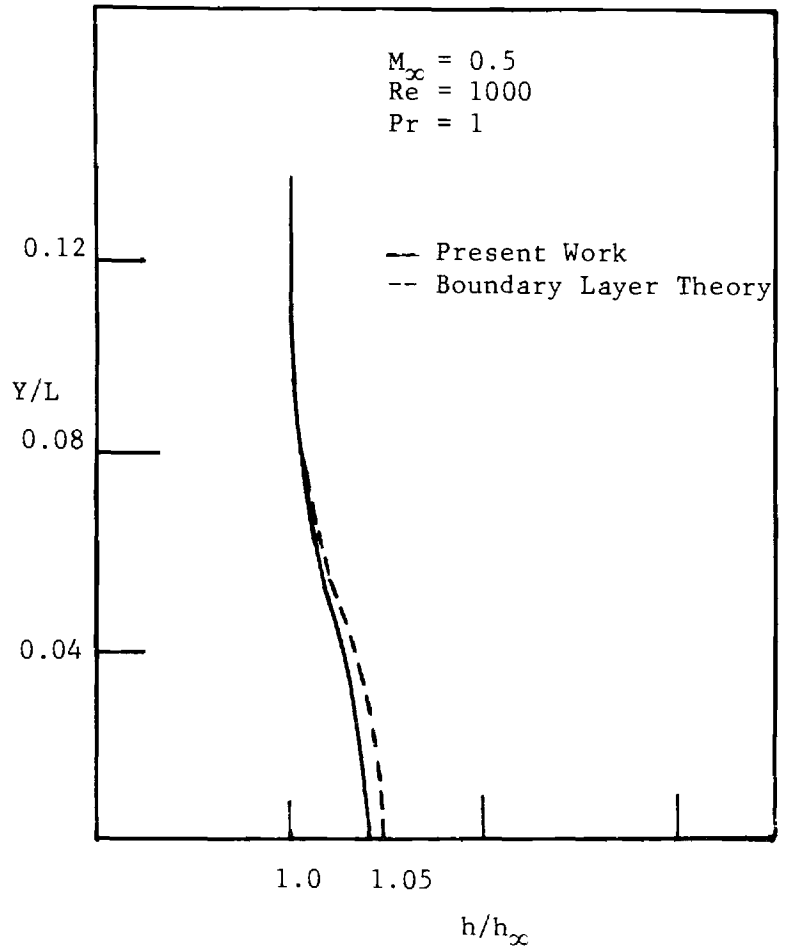

Figure 2. Flat Plate Problem Mid-Plate Enthalpy Profile

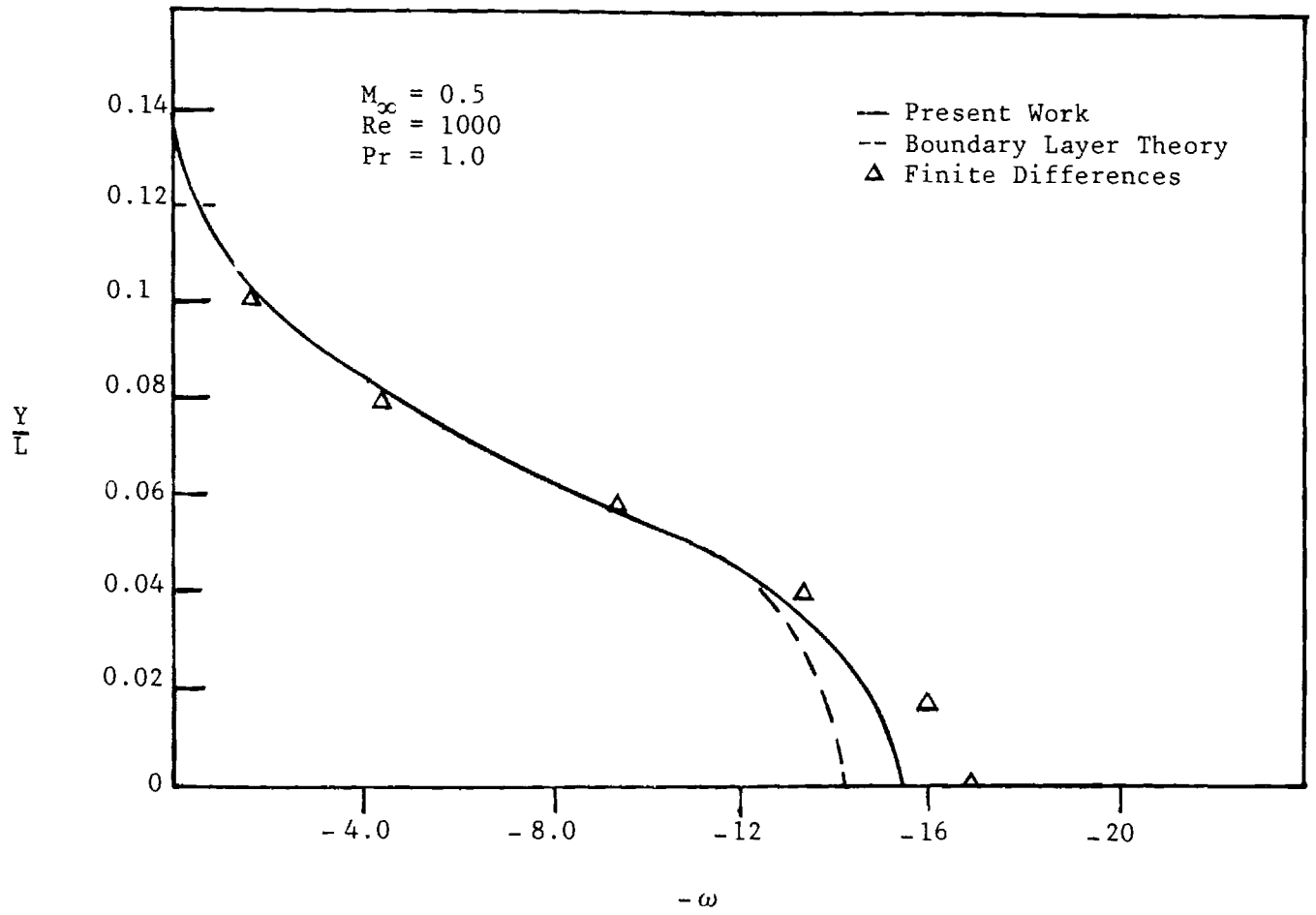

Figure 3. Vorticity Profile at Mid Plate

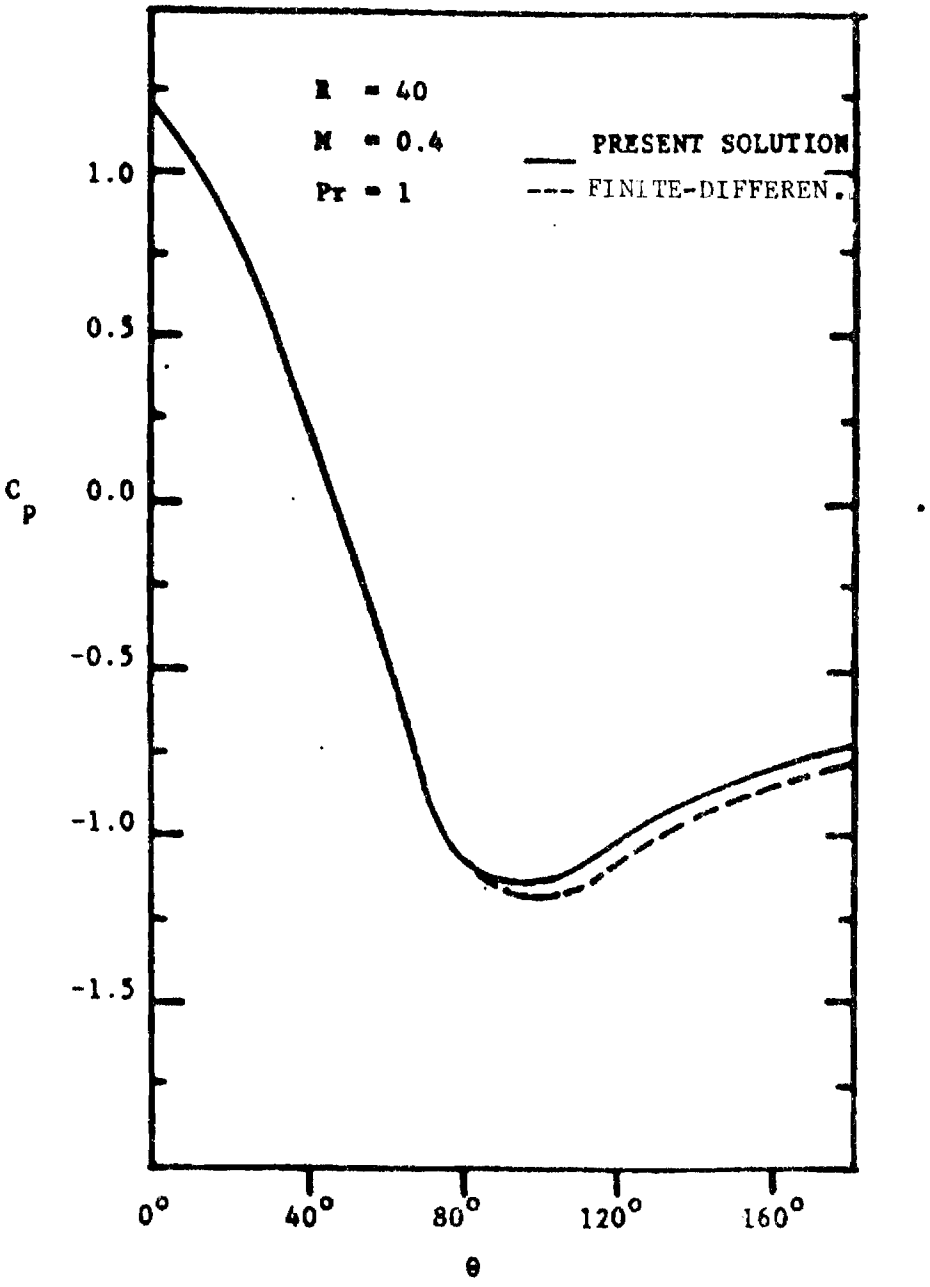

Figure 4. Surface Pressure Distribution on Circular Cylinder

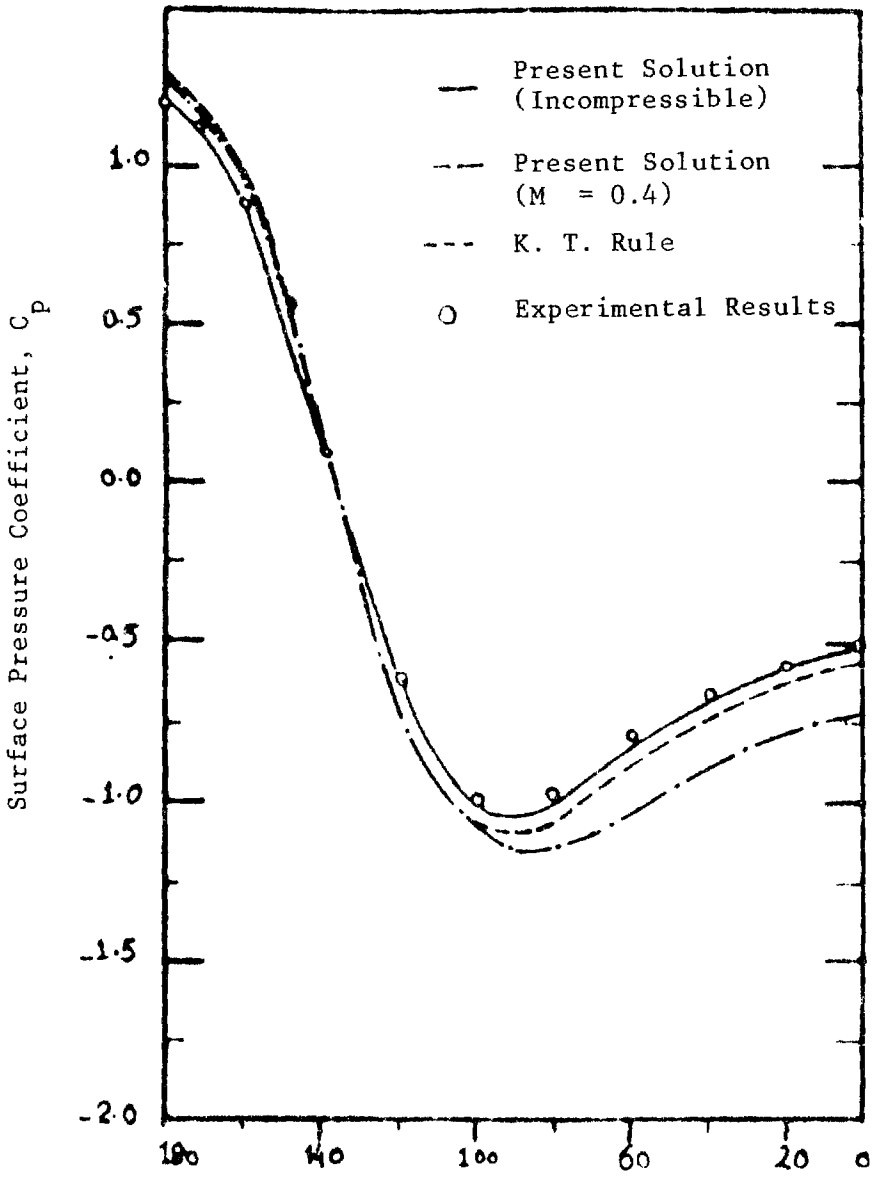

Figure 5. Circular Cylinder Surface Pressure Distribution at Later Time Levels

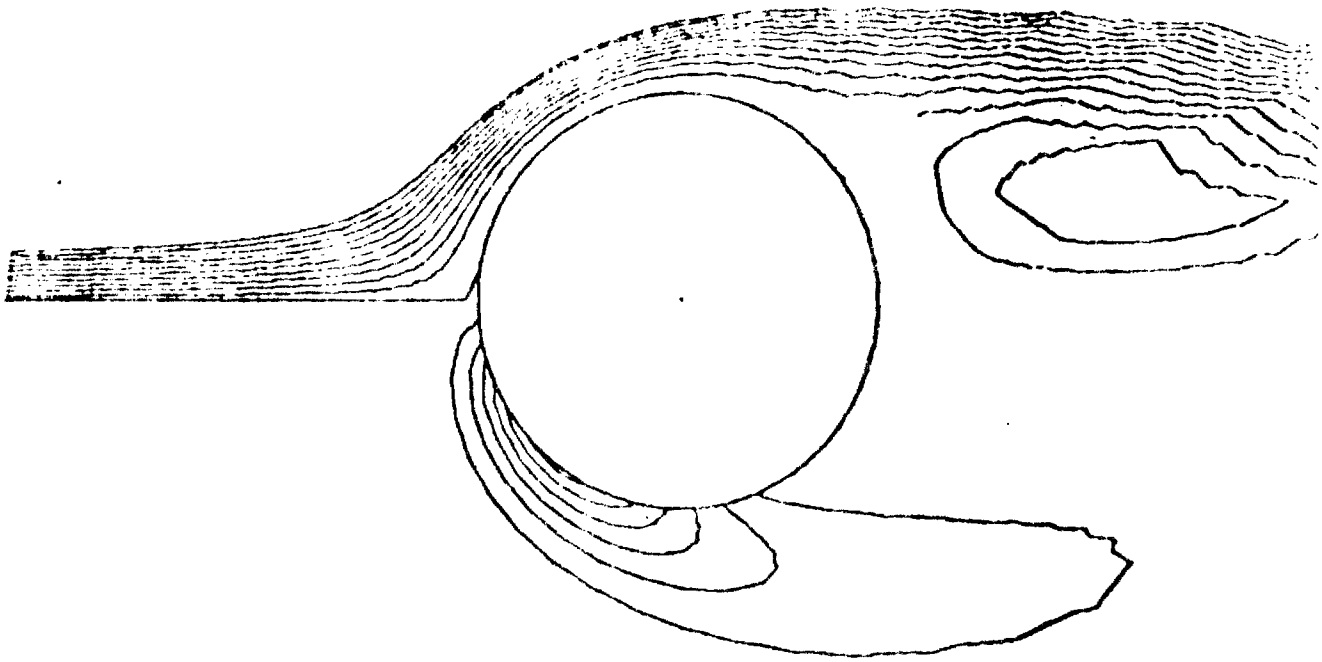

Figure 6. Streamlines and Constant Vorticity Contours for Viscous Incompressible Flow Past a Circular Cylinder (Re = 40)

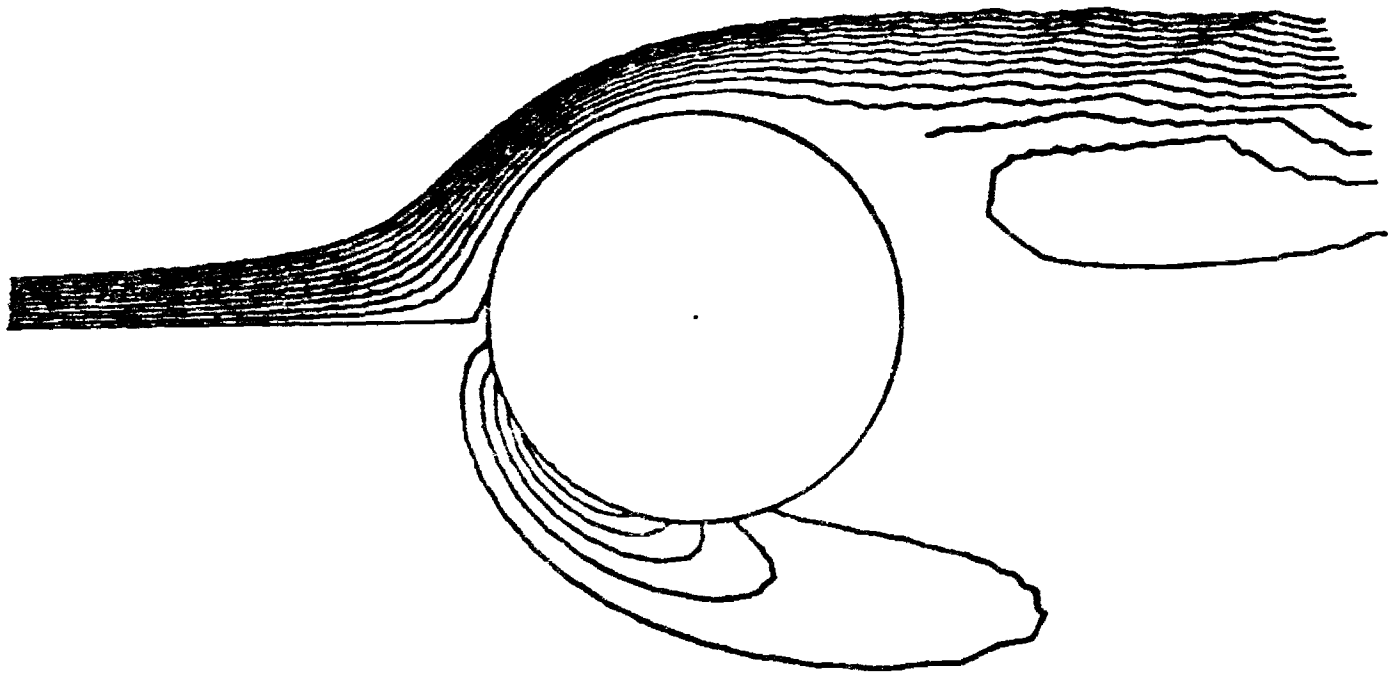

Figure 7. Streamlines and Equal Vorticity Contours from Compressible Flow Around a Circular Cylinder (R = 40, M = 0.4, Pr = 1)

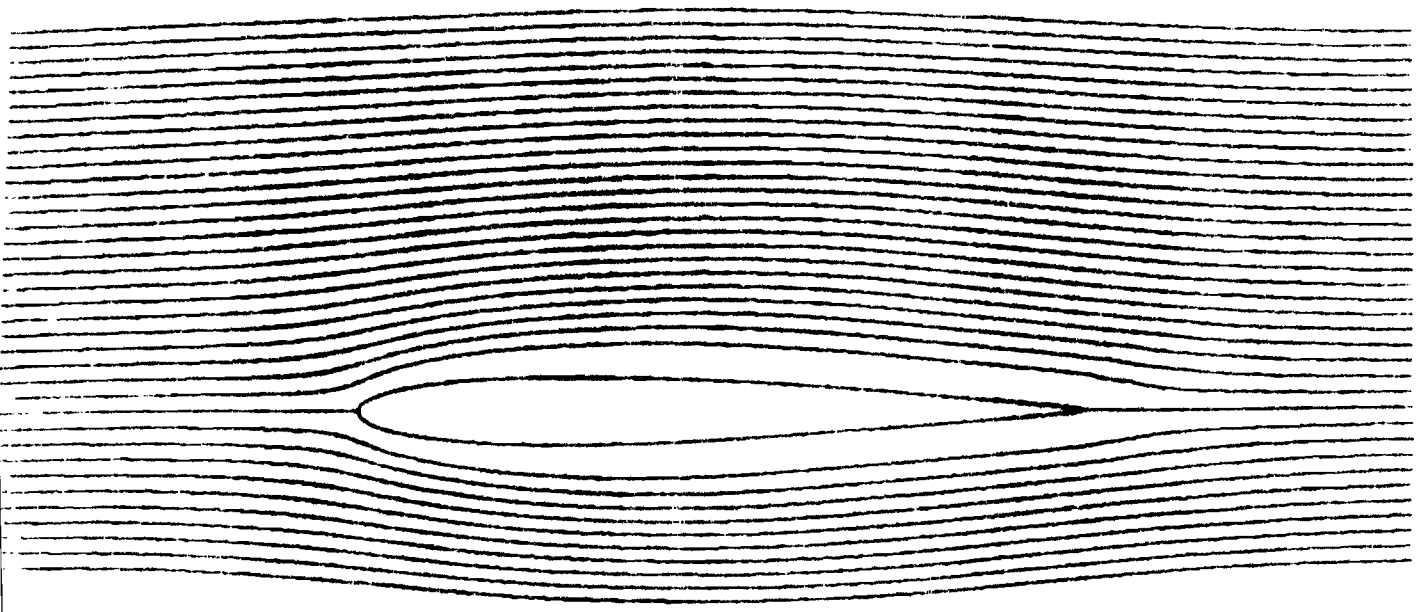

Figure 8. Streamlines around a 9% Joukowski airfoil for R_c = 1,000, M_∞ = 0.4, α = 0°.

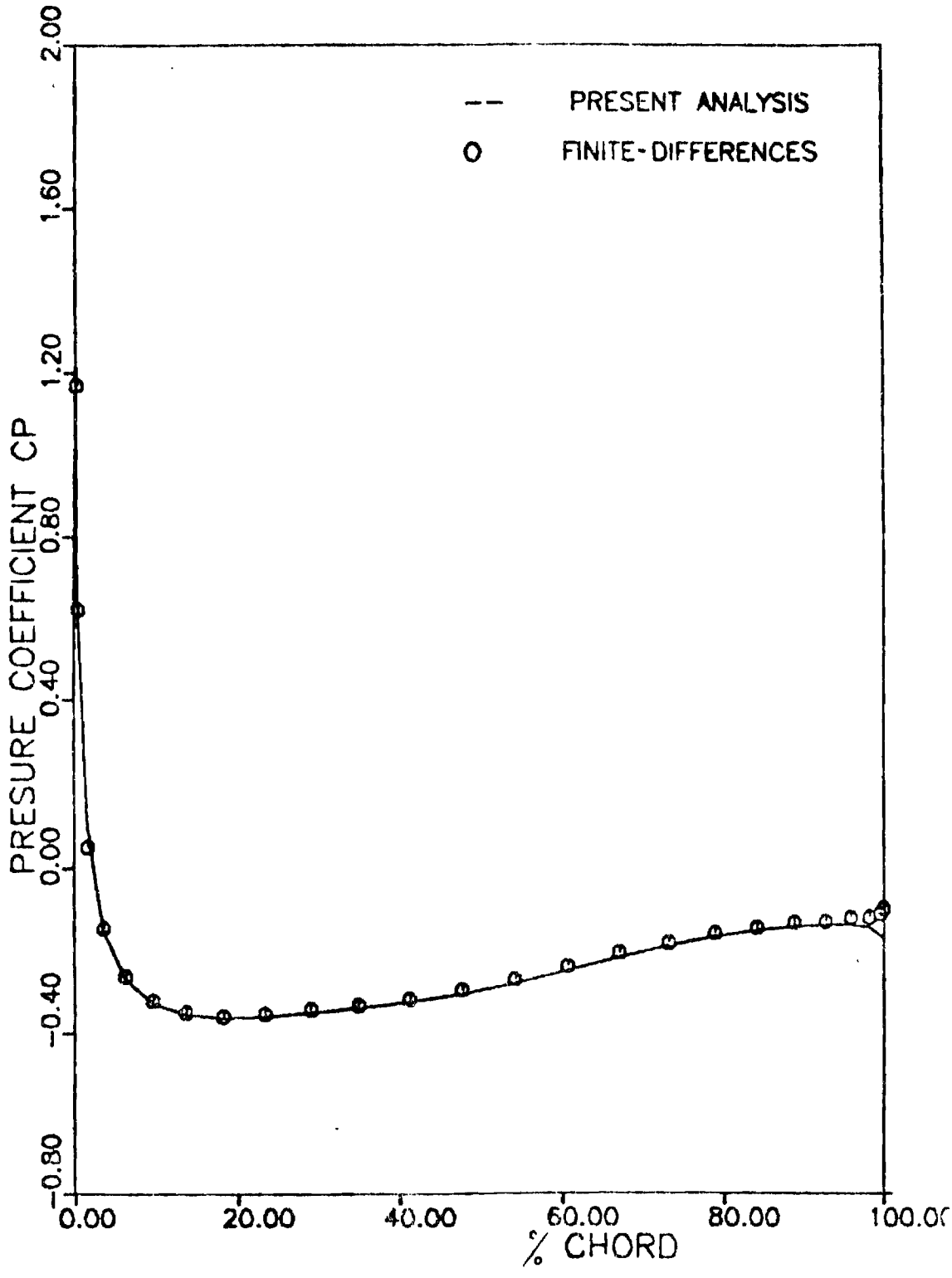

Figure 9. Pressure distribution on a 9% Joukowski airfoil for R_c = 1,000, M_∞ = 0.4, α = 0°.

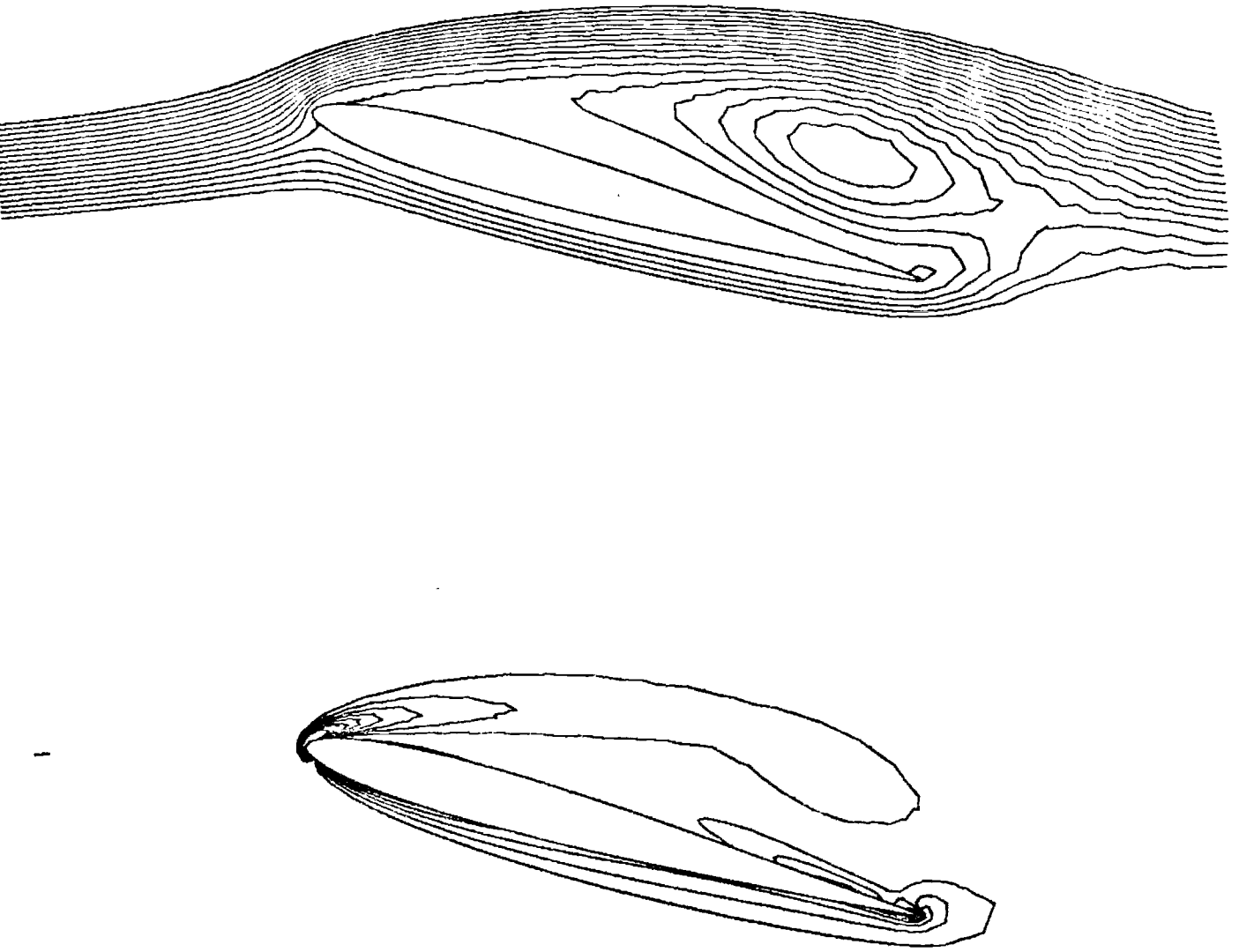

Figure 10. Streamlines and Equal Vorticity Contours Around a 9% Joukowski Airfoil. Incompressible Theory, $\alpha = 15^{\circ}$, R = 1,000, T = 14.05.

Figure 11. Surface Vorticity Distribution on a 9% Joukowski Airfoil. Incompressible Theory, $\alpha = 15^{o}$, R = 1,000, T = 14.05.

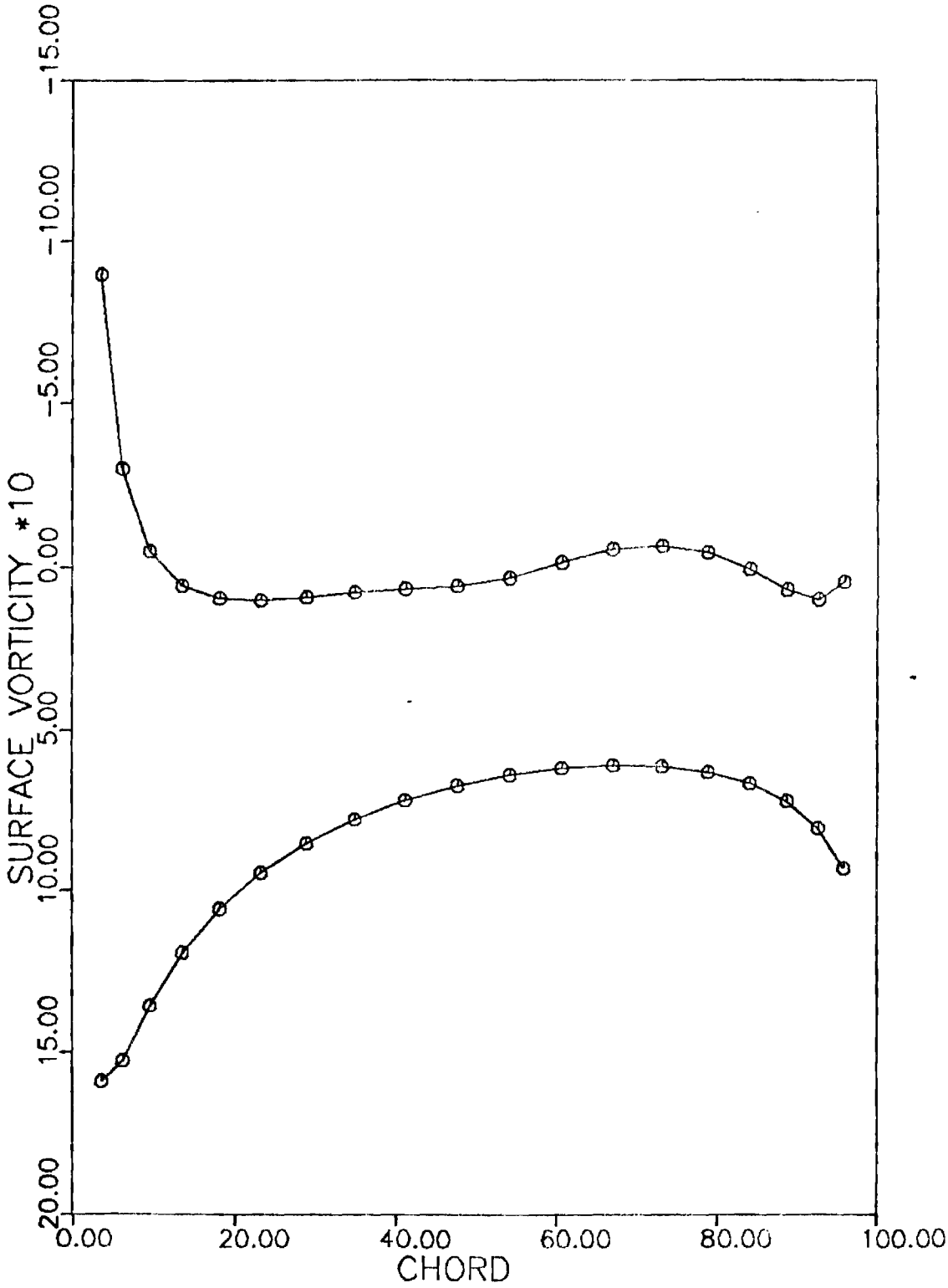

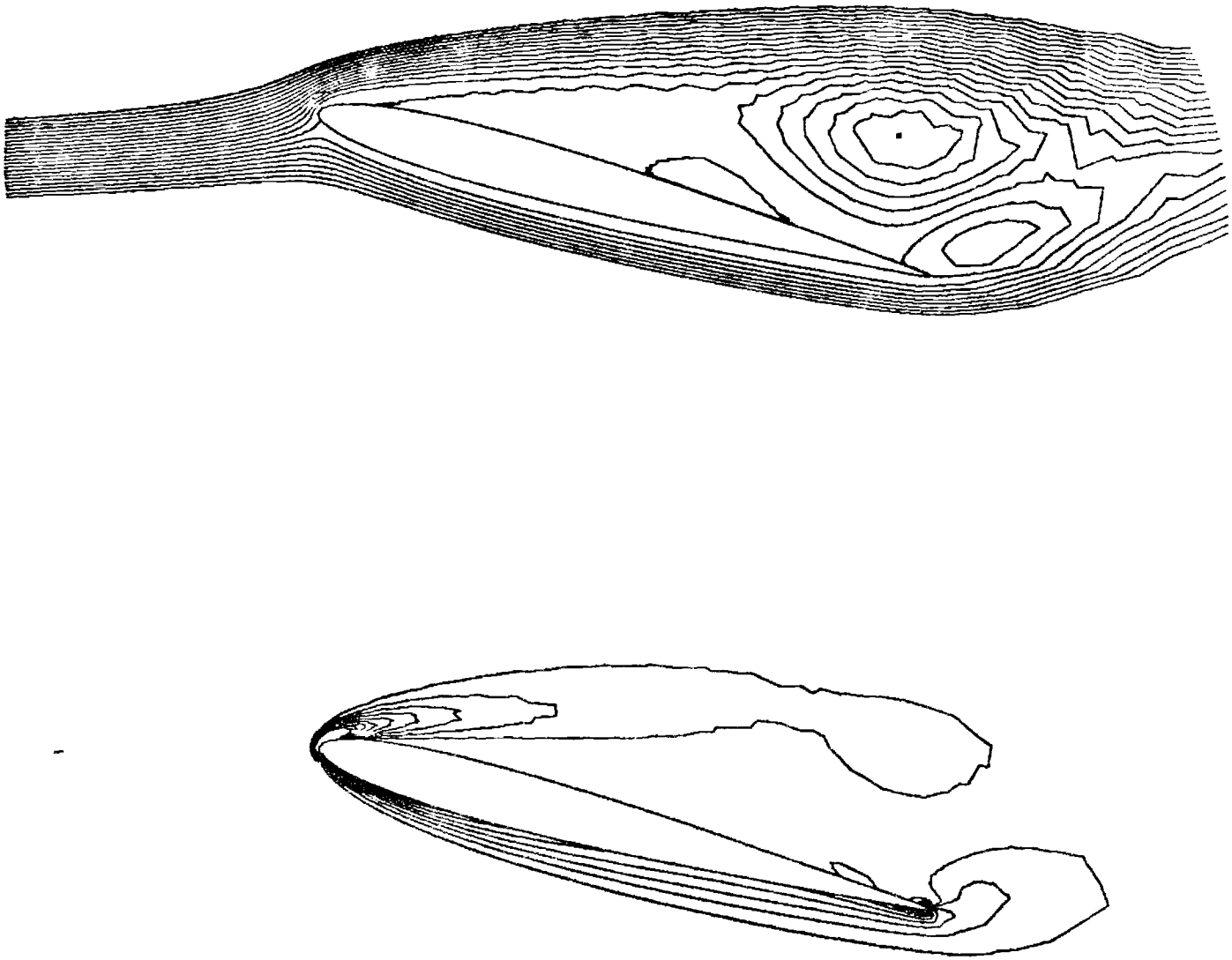

Figure 12. Streamlines and Equal Vorticity Contours Around a 9% Joukowski Airfoil.

Incompressible theory, $\alpha = 15^{o}$, R = 1,000, T = 18.6.

Figure 13. Surface Vorticity Distribution on a 9% Joukowski Airfoil. Incompressible Theory, $\alpha = 15^{o}$, R = 1,000, T = 18.6.

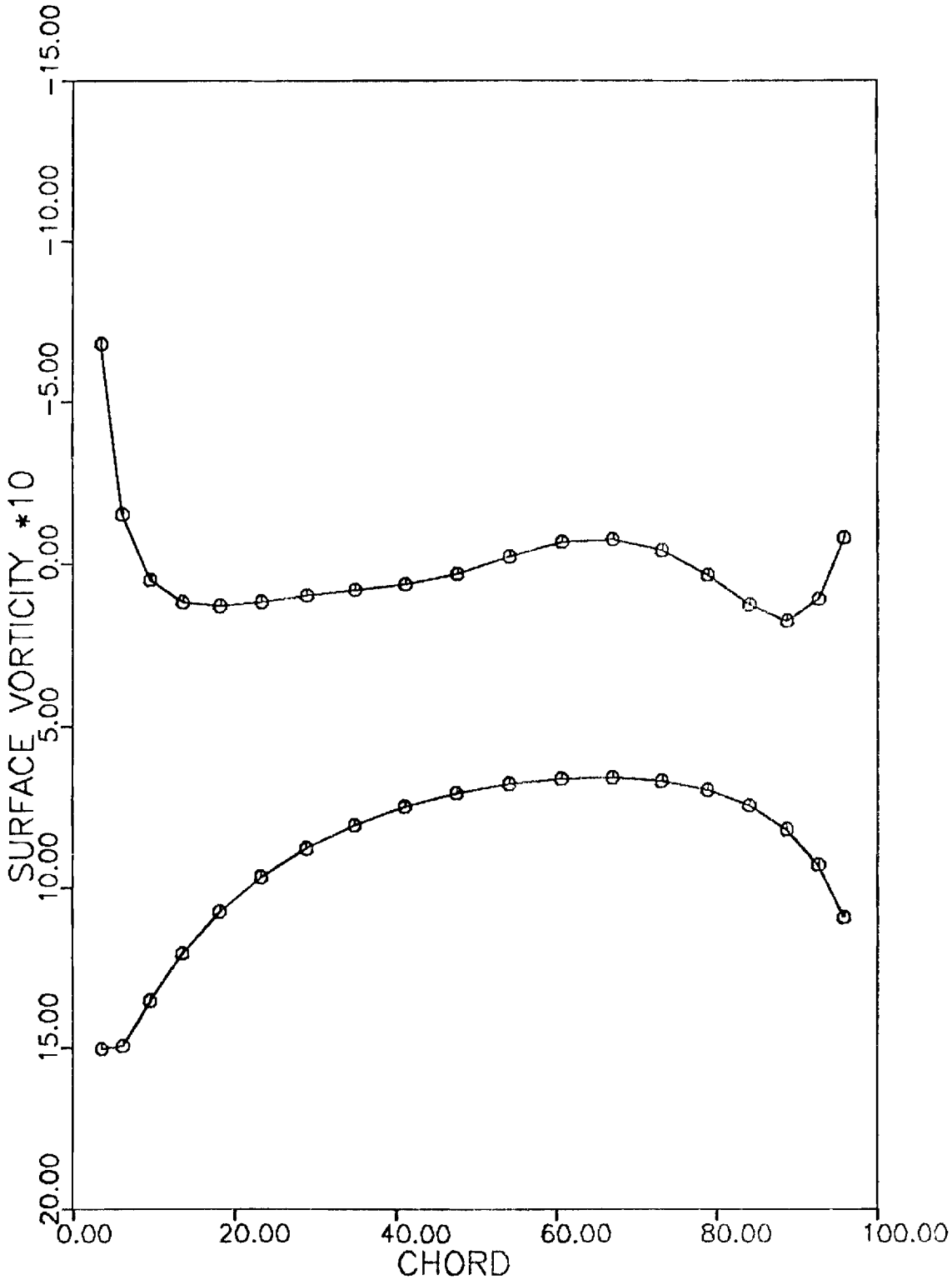

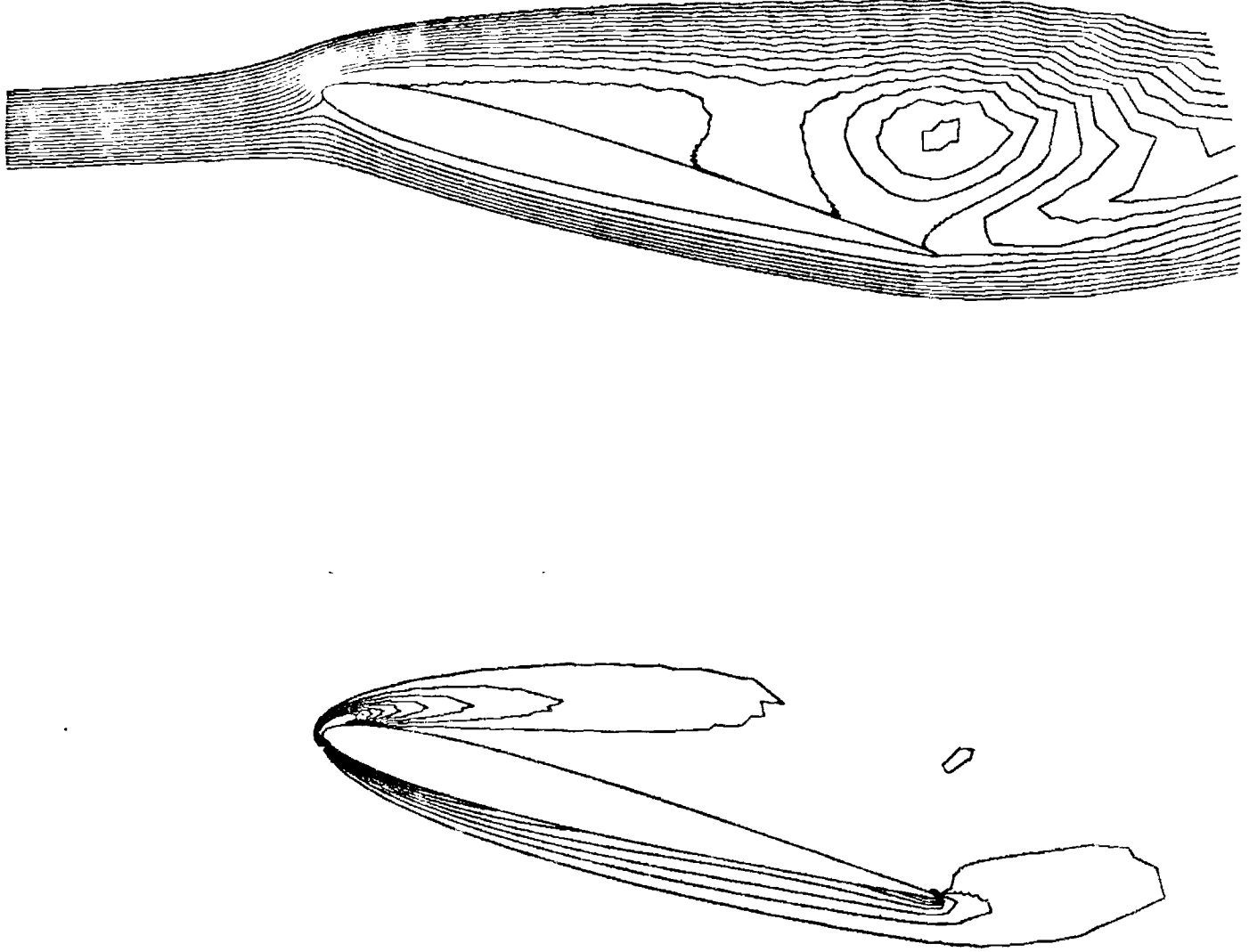

Figure 14. Streamlines and Equal Vorticity Contours Around a 9% Joukowski Airfoil. Incompressible Theory, $\alpha = 15^{o}$, R = 1,000, T = 21.37.

Figure 15. Surface Vorticity Distribution on a 9% Joukowski Airfoil. Incompressible Theory, $\alpha = 15^{o}$, R = 1,000, T = 21.73.

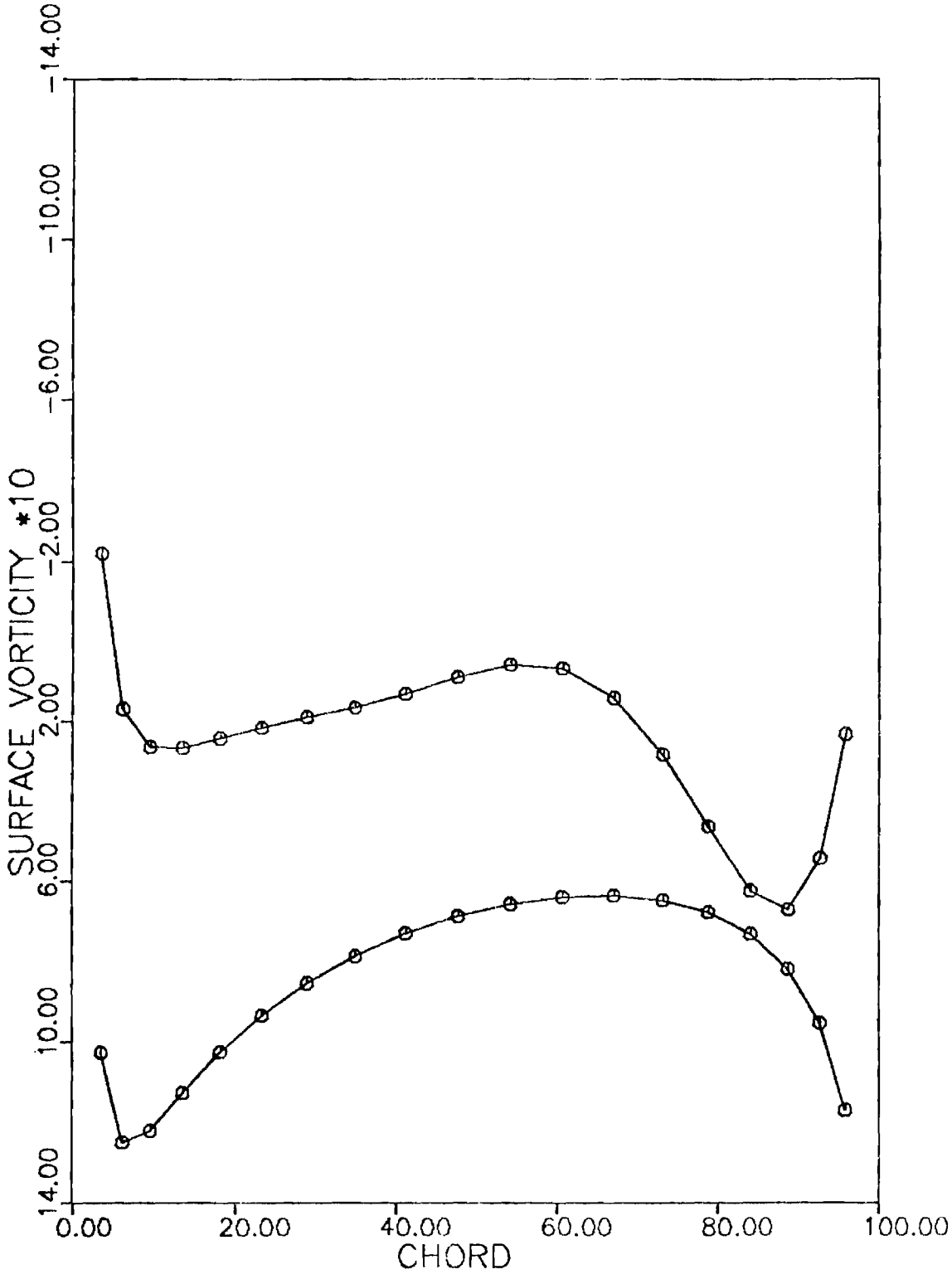

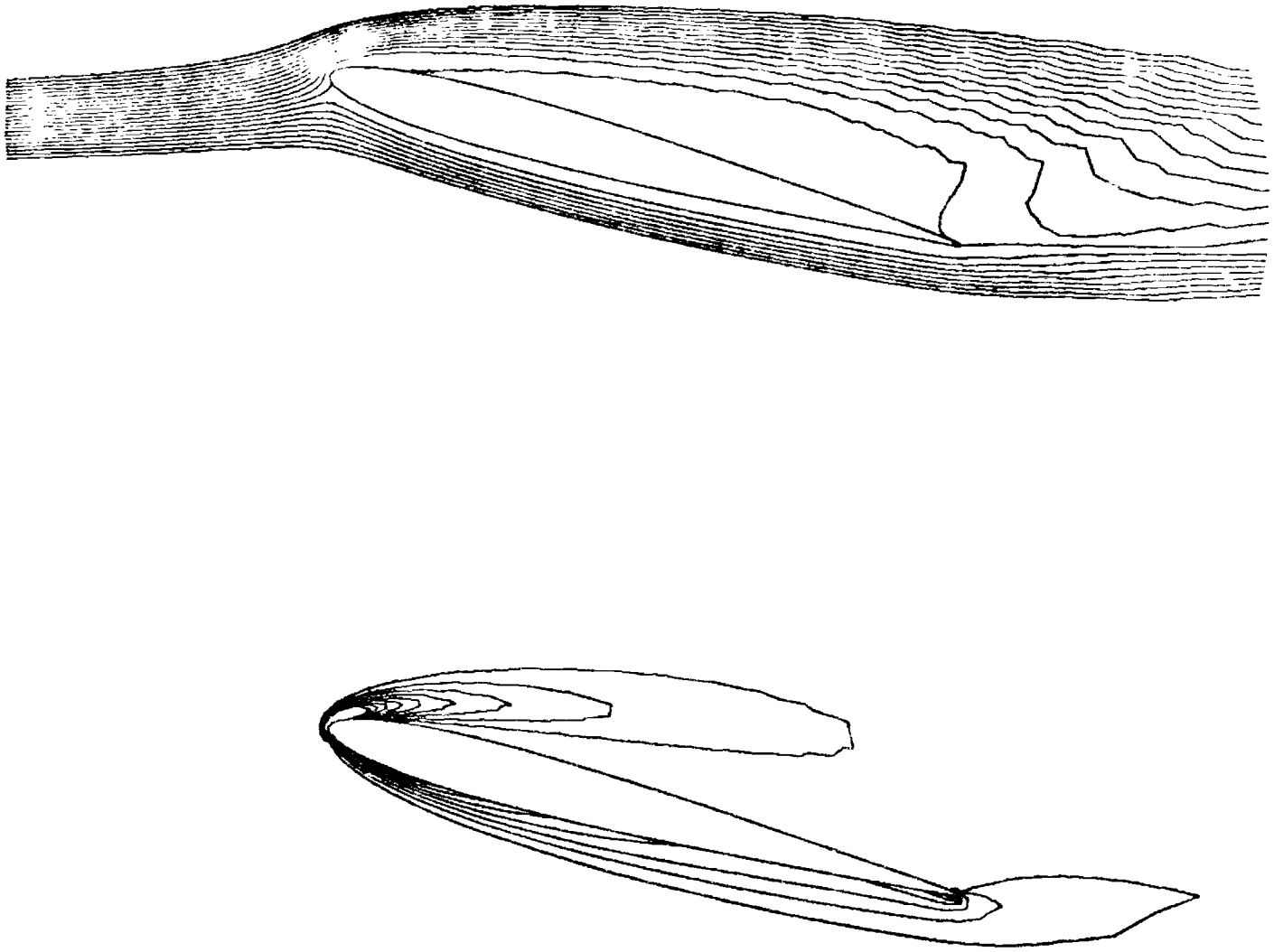

Figure 16. Streamlines and Equal Vorticity Contours Around a 9% Joukowski Airfoil. Incompressible Theory, $\alpha = 15^{o}$, R = 1,000, T = 27.3.

Figure 17. Surface Vorticity Distribution on a 9% Joukowski Airfoil. Incompressible Theory, $\alpha = 15^{o}$, R = 1,000, T = 27.3.

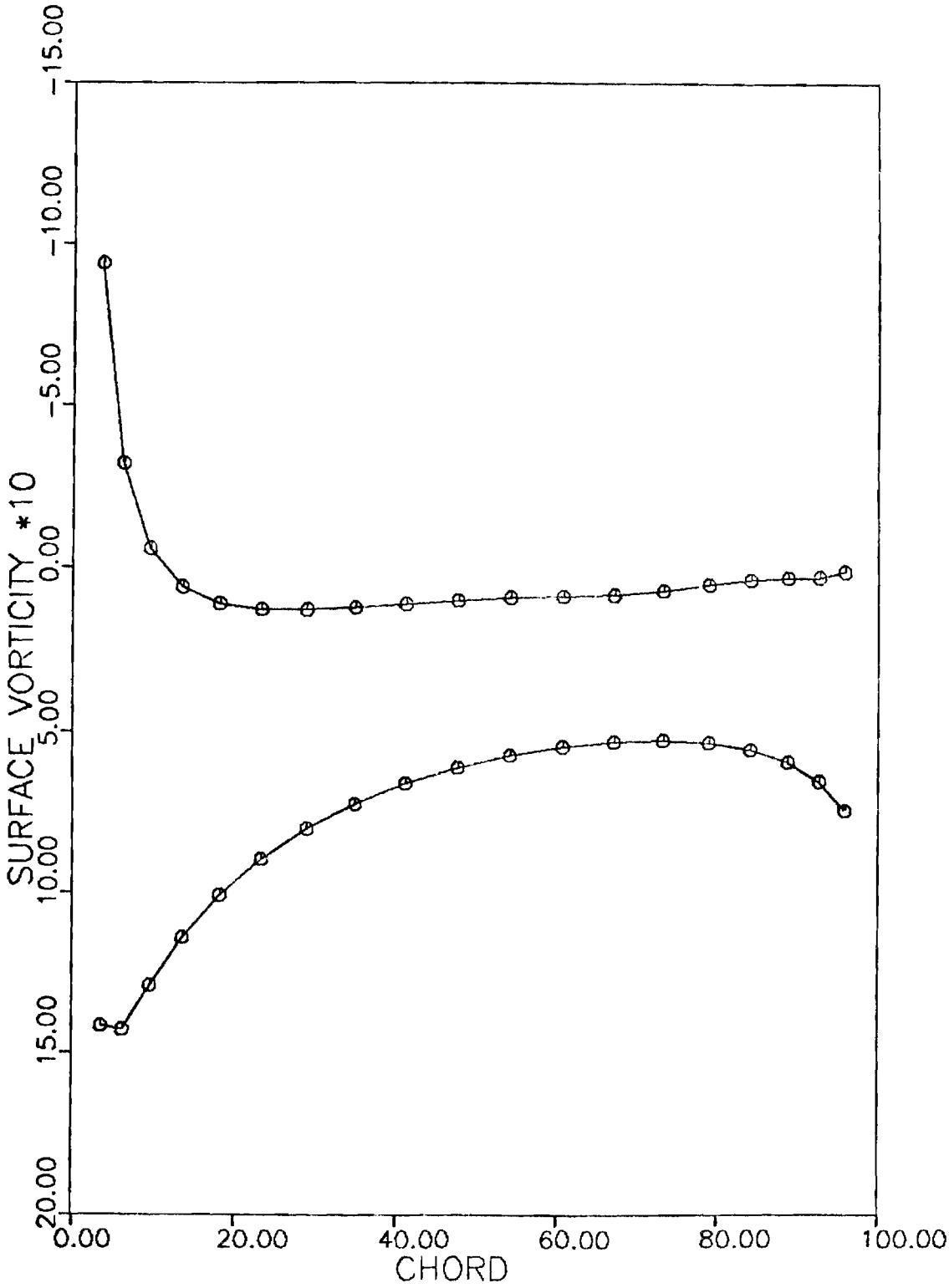

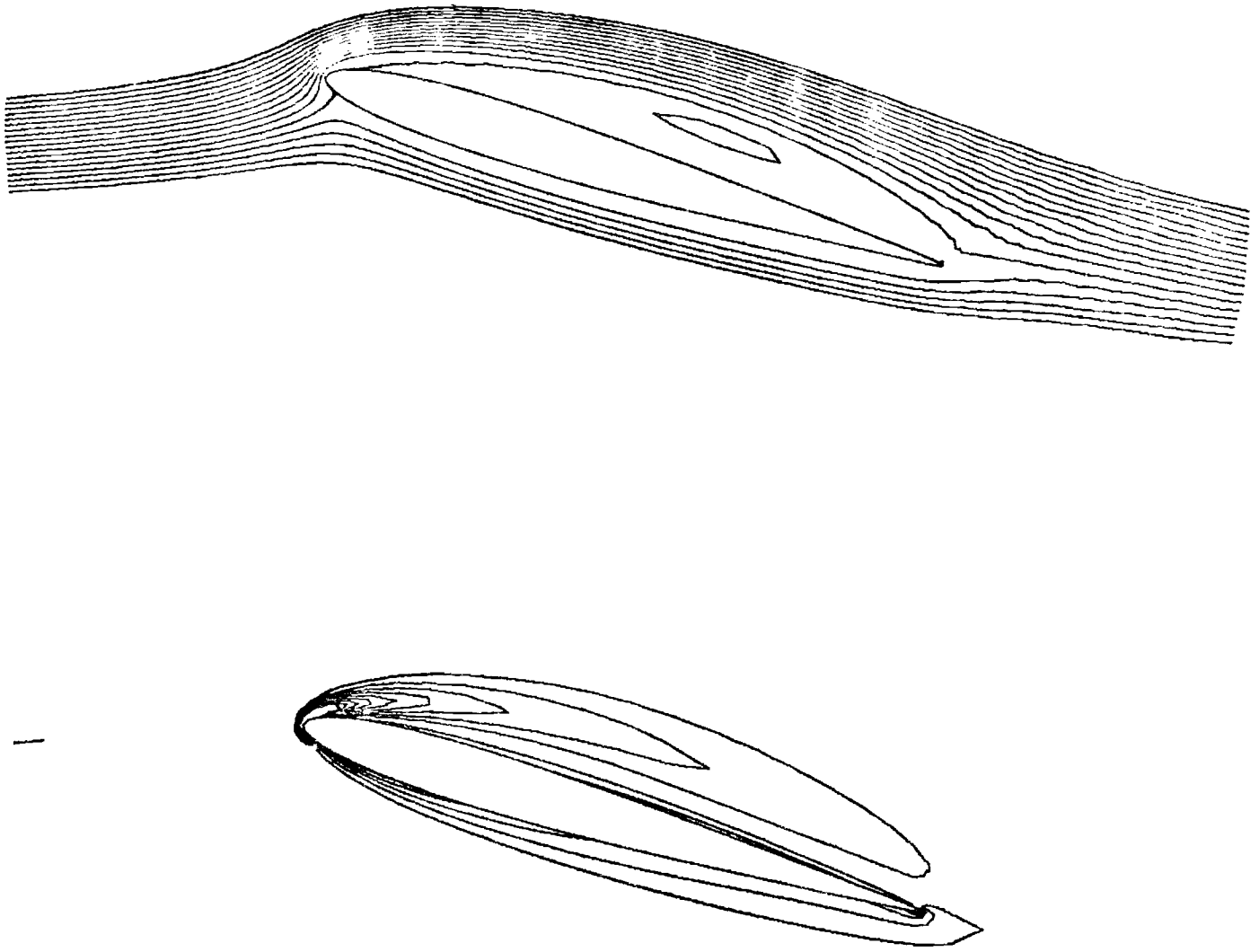

Figure 18. Streamlines and Equal Vorticity Contours Around a 9% Joukowski Airfoil.

Compressible theory, $M_\infty = 0.4$, $\alpha = 15^\circ$, R = 1,000, T = 7.2.

Figure 19. Surface Vorticity Distribution on a 9% Joukowski Airfoil. Compressible theory, $M_\infty = 0.4$, $\alpha = 15^o$, R = 1,000, T = 7.2.

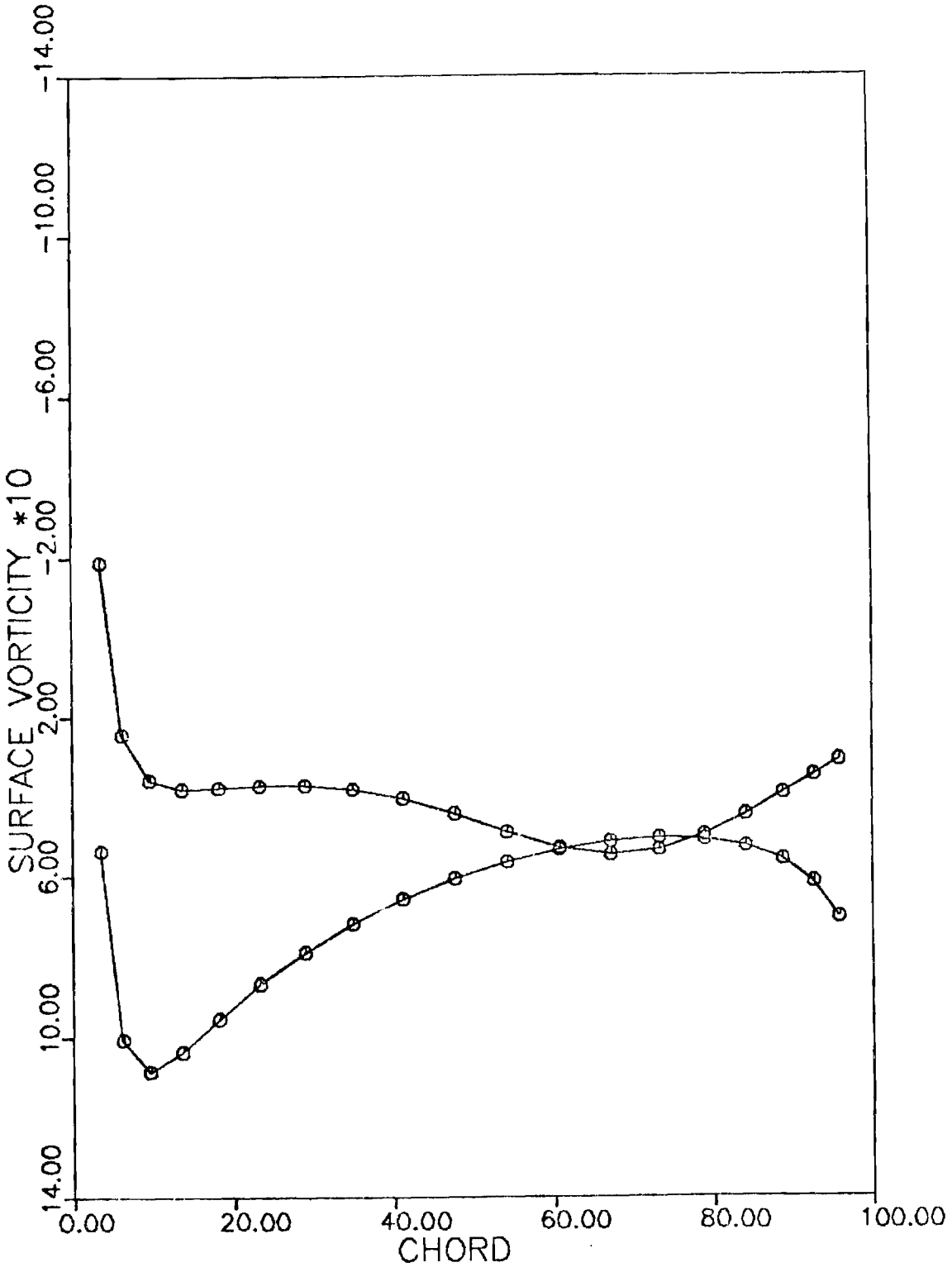

APPENDIX

Definitions of Source-Like Terms

$$\phi = -\omega\beta + \frac{\mu}{\rho^2 R_e}\left(4/3\left|\vec{\nabla}\beta \times \vec{\nabla}\rho\right| - \vec{\nabla}\rho \cdot \vec{\nabla}\omega\right)$$

$$+ \frac{\gamma-1}{\gamma}\vec{\nabla} \ln\rho \times \vec{\nabla}h + \frac{c_1}{R_e} \tag{A.1}$$

$$c_1 = \frac{1}{\rho}(u_y + v_x)(\mu_{xx} - \mu_{yy}) + \frac{2}{\rho}(v_y - u_x)\mu_{xy} + \mu_x\left\{\frac{2}{\rho}\nabla^2 v\right.$$

$$+ \frac{2}{\rho} u_{xy} - \frac{1}{\rho^2}(\rho_x u_y - v_x \rho_x - 2\rho_y u_x + \frac{2}{3}\rho_y \beta)\Big\} + \mu_y \left\{-\frac{2}{\rho}\right.$$

$$\left.\nabla^2 u + \frac{2}{\rho} v_{xy} - \frac{1}{\rho^2}(2\rho_x v_y - u_y\rho_y - v_x\rho_y - \frac{2}{3}\beta\rho_x)\right\} \tag{A.2}$$

$$\psi = -(u^2_x + v^2_y + 2u_y v_x) + \frac{\mu}{\rho^2 R_e}\left\{-\frac{4}{3}\nabla\rho \cdot \nabla\beta + \left|\nabla_\rho \times \nabla\omega\right|\right\}$$

$$- \frac{\gamma-1}{\gamma}(\nabla^2 h + h\,\nabla^2 \ln\rho + \nabla h \nabla \cdot \ln\rho) + \frac{c_2}{R_e} \tag{A.3}$$

$$c_2 = \frac{8}{3\rho}\nabla\beta \cdot \nabla\mu + \frac{2}{3}\left|\nabla\omega \times \nabla\mu\right| - \frac{2}{3\rho}\beta\nabla^2\mu + \frac{2}{\rho}(u_x \mu_{xx}$$

$$+ v_y\mu_{yy}) + (v_x + u_y)\mu_{xy} - \frac{1}{\rho^2}(v_x + \mu_y) + \rho_y\mu_x$$

$$+ \frac{2}{3}\frac{\beta}{\rho^2}\nabla\rho\nabla\mu - \frac{2}{\rho^2}(\rho_x u_x \mu_x + \rho_y v_y \mu_y) \tag{A.4}$$

$$\Theta = -(\gamma - 1)\beta h + \frac{\gamma\mu}{\rho R_e}\left[\frac{\beta^2}{3} + (2u_x - \beta^2) + (2v_x - \omega)^2\right] + \frac{\gamma}{\rho R_e P_r}\vec{\nabla} h \cdot \vec{\nabla} k \tag{A.5}$$

In the above expression the vector product terms denote the magnitude of the resulting vector.

Final Report

on NASA-Lewis Research Center
Grant No. NSG 3307

A NEW NUMERICAL APPROACH FOR COMPRESSIBLE VISCOUS FLOWS

by

J.C. Wu, Professor and
S.G. Lekoudis, Assistant Professor

School of Aerospace Engineering
Georgia Institute of Technology

TABLE OF CONTENTS

1. INTRODUCTION

The objective of the Grant NSG 3307, from the NASA Lewis Research Center to the School of Aerospace Engineering at Georgia Tech, was to develop a new numerical approach for computing unsteady compressible viscous flows. This approach offers the capability of confining the region of computation to the viscous region of the flow. The viscous region is defined as the region where the vorticity is nonnegligible and the difference in dilatation between the potential flow and the real flow around the same geometry is also nonnegligible. The method was developed and tested. Also, an application of the procedure to the solution of the steady Navier-Stokes equations for incompressible internal flows is presented.

2. MATHEMATICAL FORMULATION

In this chapter the mathematical relationships that govern the time history of compressible viscous flow around an arbitrary body are presented. The kinematic and kinetic boundary conditions are stated and a method for estimating the surface vorticity is described. In order to improve readability, the derivations of some of the equations used in this chapter are omitted in the main text and given in the appendices.

Governing Equations

In the absence of body forces, the Navier-Stokes equations for a compressible fluid with density ρ, viscosity ν, thermal conductivity k and ratio of specific heat coefficients γ, may be written in an inertial coordinate system as follows

$$\rho \frac{\partial \vec{V}}{\partial t} + \rho(\vec{V}.\vec{\nabla})\vec{V} = -\vec{\nabla}p + \vec{\nabla}.\vec{\tau} \qquad (2.1)$$

The equation of continuity is given by

$$\frac{\partial \rho}{\partial t} + \vec{\nabla}.(\rho\vec{V}) = 0 \qquad (2.2)$$

The energy equation and the equation of state are given by

$$\rho \frac{\partial h}{\partial t} - \frac{\partial p}{\partial t} + \rho \vec{V}.(\vec{\nabla}h) - \vec{V}.\vec{\nabla}p = -\vec{\nabla}.q + \vec{\nabla}\vec{V}:\vec{\tau} \qquad (2.3)$$

$$p = \rho RT = (\frac{\gamma-1}{\gamma})\rho h \qquad (2.4)$$

Here $\vec{\nabla}\vec{V}:\vec{\tau}$ represents the dissipation function given in cartesian coordinates by

$$\vec{\nabla}\vec{V}:\vec{\tau} = \tau_{ij} \frac{\partial u_j}{\partial x_i}$$

where τ_{ij} is the shear stress tensor and can be expressed as follows;

$$\tau_{ij} = 2\mu e_{ij} + \delta_{ij} \lambda(\vec{\nabla}.\vec{V})$$

Here e_{ij} is the rate of strain tensor and λ is the second coefficient of viscosity.

Kinematics Expressed in Integral Representation

The vorticity $\vec{\omega}$ and the dilatation β are related to the velocity field $\vec{V}$ by:

$$\vec{\nabla} \times \vec{V} = \vec{\omega} \qquad (2.5)$$

$$\vec{\nabla} . \vec{V} = \beta \qquad (2.6)$$

The kinematics of the problem, governed by equations (2.5) and (2.6) are elliptic in nature, requiring the specification of Neumen, Dirichlet or

mixed type of boundary conditions for velocity. These conditions are required both at infinity, known as the farstream condition, and on the solid surface. In the present study, Dirichlet type boundary conditions are prescribed on the boundaries.

The velocity boundary conditions are

$$\vec{V} = \vec{V}_b \qquad \text{on } b \tag{2.7}$$

and R is the fluid domain bounded by the boundary b. For external flow problems, the boundary b consists of the farstream boundary c and the body surface s. On s, the no-slip condition is used, while $\vec{V} = \vec{V}_\infty$ is prescribed on c.

Since the kinematic relationsnips are linear in $\vec{V}$, the velocity vector $\vec{V}$ can be decomposed into a solenoidal part $\vec{V}_1$ and an irrotational part $\vec{V}_2$ with homogeneous boundary condition for the latter. Thus

$$\vec{V} = \vec{V}_1 + \vec{V}_2 \tag{2.8}$$

with

$$\vec{\nabla} \cdot \vec{V}_1 = 0 \tag{2.9a}$$

$$\vec{\nabla} \times \vec{V}_1 = \vec{\omega} \tag{2.9b}$$

having boundary conditions

$$\vec{V}_{1s} = 0 \tag{2.10a}$$

$$\vec{V}_{1c} = \vec{V}_\infty \tag{2.10b}$$

and, for $\vec{V}_2$,

$$\vec{\nabla} \cdot \vec{V}_2 = \theta \tag{2.11a}$$

$$\vec{\nabla} \times \vec{V}_2 = 0 \tag{2.11b}$$

with boundary conditions

$$\vec{V}_{2s} = 0 \tag{2.12a}$$

$$\vec{V}_{2c} = 0 \tag{2.12b}$$

Wu (1) has shown that it is possible to recast the kinematic aspect of the problem into an integral representation for the velocity $\vec{V}$ in terms of the vorticity $\vec{\omega}$ and the dilatation β. For two dimensional flows this means

$$\vec{V}(\vec{r}_o, t) = -\frac{1}{2\pi}\int_R \frac{\vec{\omega}\times(\vec{r}-\vec{r}_o) + \beta(\vec{r}-\vec{r}_o)}{|\vec{r}-\vec{r}_o|^2}\, dR + \vec{V}_\infty \tag{2.13}$$

In (2.13) R is the region where the vorticity and dilatation are non-negligible. At high and moderate Reynolds number the dilatation is significant at distances from the body where the vorticity is already negligible. Hence the approach does not seem as advantageous as in the incompressible case. However, by using the potential flow solution around the same body, it will be shown in the next section that the domain of the computations can be reduced to include only the region where the vorticity and the difference in dilatation between the viscous flow and potential

flow are both non-negligible.

Use of the Potential Flow Solution to Reduce the Domain of Computations

Equation (2.13) can be written in the following form

$$\vec{V}(\vec{r}_o,t) = -\frac{1}{2\pi}\int_{R1}\frac{\vec{\omega}\times(\vec{r}-\vec{r}_o)+\vec{B}(\vec{r}-\vec{r}_o)}{|\vec{r}-\vec{r}_o|^2}\,dR$$

$$-\frac{1}{2}\int_{R2}\frac{3(\vec{r}-\vec{r}_o)}{|\vec{r}-\vec{r}_o|^2}+\vec{V}_\infty \qquad (2.14)$$

where R1 is the region of the flow where vorticity is non-negligible and R2 is the rest of the domain, extending to infinity for external flow problems. This expression can be written for the potential flow around the same body as follows:

$$\vec{V}_p(\vec{r}_o) = -\frac{1}{2\pi}\int_{R1}\frac{\beta_p(\vec{r}-\vec{r}_o)dR}{|\vec{r}-\vec{r}_o|^2}-\frac{1}{2\pi}\int_{R2}\frac{\beta_p(\vec{r}-\vec{r}_o)dR}{|\vec{r}-\vec{r}_o|^2}$$

$$-\frac{1}{2\pi}\int_{s}\frac{\gamma_p\times(\vec{r}-\vec{r}_o)dS}{|\vec{r}-\vec{r}_o|^2}+\vec{V}_\infty \qquad (2.15)$$

where the subscript p indicates potential flow and γ_p is the vortex sheet strength on the surface, s, of the body due to the potential flow. Because equation (2.15) is a limiting case of the general viscous compressible flow relation (2.14), it gives the potential velocity everywhere except at the surface where the equation is identically zero.

If region R1 extends far enough from the body, the combination of (2.14) and (2.15) gives

$$\vec{V}(\vec{r}_o,t) = -\frac{1}{2\pi}\int_{R1}\frac{\vec{\omega}x(\vec{r}-\vec{r}_o)+(\beta-\beta_p)(\vec{r}-\vec{r}_o)}{|\vec{r}-\vec{r}_o|^2}\,dR$$

$$-\frac{1}{2\pi}\int_{s}\frac{\gamma_p x(\vec{r}-\vec{r}_o)ds}{|\vec{r}-\vec{r}_o|^2}+\vec{V}_p \qquad (2.16)$$

The relation (2.16) implies the following. First, $(\beta-\beta_p)$ in region R2 is small enough so that its effect on the velocity in region R1 is negligible (a detailed discussion of this aspect is given in Reference 11). Second, one needs to solve only in region R1, which is a smaller region than the region where β is significant.

The kinematic boundary condition for the external flow problem requires that the velocity has to reach the freestream velocity at an infinite distance away from the solid surfaces. This requirement is referred to in this work as the farfield boundary conditions. This requirement is satisfied by equation (2.16). However, if a finite-difference method is used without any coordinate transformation, this boundary condition is difficult to satisfy since the computational domain to be included becomes very large.

Kinetics - The Vorticity, Dilatation, Density, and Energy Transport Equations

By taking the curl of equation (2.1) and using equation (2.4) one obtains

$$\frac{\partial \vec{\omega}}{\partial t} = \vec{\nabla} \times \vec{V} \times \vec{\omega} + \left(\frac{\gamma-1}{\gamma}\right) \vec{\nabla} \ln\rho \times \vec{\nabla} h + \vec{\nabla} \times \left(\frac{1}{\rho} \vec{\nabla} \cdot \vec{\tau}\right) \tag{2.17}$$

Similarly, taking the divergence of equation (2.1) and using equation (2.4) results in

$$\frac{\partial \beta}{\partial t} = -\vec{\nabla} \cdot \left[(\vec{V} \cdot \vec{\nabla})\vec{V}\right] - \left(\frac{\gamma-1}{\gamma}\right)\nabla^2 h - \left(\frac{\gamma-1}{\gamma}\right) h \nabla^2 \ln\rho - \left(\frac{\gamma-1}{\gamma}\right) \vec{\nabla} h \cdot \vec{\nabla} \ln\rho$$

$$+ \vec{\nabla} \cdot \left(\frac{1}{\rho} \vec{\nabla} \cdot \vec{\tau}\right) \tag{2.18}$$

Specializing the equations for two-dimensional case, rearranging the terms in equations (2.17) and (2.18), and collecting the coefficients of β and ω, equations (2.17) and (2.18) become

$$\frac{\partial \omega}{\partial t} = -\vec{\nabla} \cdot (\vec{V}\omega) + \left(\frac{\mu}{Re \cdot \rho}\right)\nabla^2 \omega + \Phi(\rho, \beta, \omega, h) \tag{2.19}$$

$$\frac{\partial \beta}{\partial t} = -\vec{\nabla} \cdot (\vec{V}\beta) + \left(\frac{4\mu}{3 \cdot Re \cdot \rho}\right)\nabla^2 \beta + X(\rho, \beta, \omega, h) \tag{2.20}$$

The full details of the derivation of the above equations are given in appendix B.

The density and energy equations can be also written in terms of the derived variables ω and β as follows

$$\frac{\partial \ln\rho}{\partial t} = -\vec{\nabla} \cdot (\vec{V} \ln\rho) - \Gamma \tag{2.21}$$

$$\frac{\partial h}{\partial t} = -\vec{\nabla} \cdot (\vec{V} h) + \left(\frac{\gamma k}{Re \cdot Pr \cdot \rho}\right)\nabla^2 h + \Theta(\rho, \beta, \omega, h) \tag{2.22}$$

where ω denotes the magnitude of the vorticity vector. The terms Φ, χ, Γ and Θ look like source terms and are given in appendix B.

The governing equations (2.19) to (2.22) have been non-dimensionalized by normalizing the variables with respect to the following reference quantities: distance, L; velocity, V_∞; density, ρ_∞; enthalpy, V_∞^2; and time, L/V_∞, where L is the characteristic length of the body. This type of normalization leads to the following non-dimensional parameters: Mach number, M_∞; Reynolds number, Re; and Prandtl number, Pr.

Formulation for the Study of an Impulsively Started Airfoil

In this section, the mathematical formulation discussed above is specialized and applied to the study of compressible laminar flow past an impulsively started airfoil. The airfoil geometry and the grid system are generated through a conformal transformation which transforms the airfoil into a unit circle. The airfoil chosen for the numerical study is a modified 9% Joukowski airfoil.

By using the transformation relations given in appendix , the governing equations (2.19-2.22) are written in the transformed plane and in a conservation form as shown below.

The vorticity transport equation is

$$\frac{\partial \omega}{\partial t} = \frac{1}{H^2}\left(-\vec{\nabla}\cdot(\vec{V}\omega)\right) + \frac{1}{H^2}\left(\frac{\mu}{\rho Re}\right)\nabla^2\omega + \frac{1}{H^2}\Phi \qquad (2.23)$$

where H is the scale factor.

The dilatation transport equation is

$$\frac{\partial \beta}{\partial t} = \frac{1}{H^2}\left(-\vec{\nabla}.(\vec{V}\beta)\right) + \frac{1}{H^2}\left(\frac{4.\mu}{3.Re.\rho}\right)\nabla^2\beta + \frac{1}{H^2}\chi \qquad (2.24)$$

The density transport equation is

$$\frac{\partial \ln\rho}{\partial t} = \frac{1}{H^2}\left(-\vec{\nabla}.(\vec{V}\ln\rho)\right) - \Gamma \qquad (2.25)$$

The energy transport equation is

$$\frac{\partial h}{\partial t} = \frac{1}{H^2}\left(-\vec{\nabla}.(\vec{V}h)\right) + \frac{1}{H^2}\left(\frac{\gamma k}{Re.Pr.\rho}\right)\nabla^2 h + \Theta \qquad (2.26)$$

where $\vec{V}$ is the apparent velocity in the transformed plane and the divergence and Laplacian operators are applied in the transformed plane. The source terms ϕ, χ, Γ and Θ are given in appendix A.

The radial and tangential components of the velocity in the transformed plane are

$$\vec{V}_\theta(\vec{r}_o,t) = \frac{1}{2\pi}\int_s \frac{\gamma_p.H(r\cos(\theta-\theta_o)-r_o)ds}{|\vec{r}-\vec{r}_o|^2} + V_{\theta_p}$$

$$- \frac{1}{2\pi}\int_{R1} \frac{\omega H^2(r\cos(\theta-\theta_o)-r_o)dR}{|\vec{r}-\vec{r}_o|^2} - \frac{1}{2\pi}\int_{R1} \frac{H^2(\beta-\beta_p)r^2\sin(\theta-\theta_o)dR}{|\vec{r}-\vec{r}_o|^2} \qquad (2.27)$$

$$V_r(\vec{r}_o,t) = -\frac{1}{2\pi}\int_s \frac{\gamma_p H.r\sin(\theta-\theta_o)ds}{|\vec{r}_s-\vec{r}_o|^2} + \frac{1}{2\pi}\int_{R1} \frac{\omega H^2 r\sin(\theta-\theta_p)dR}{|\vec{r}-\vec{r}_o|^2}$$

$$- \frac{1}{2\pi} \int_{R1} \frac{(\beta-\beta_p)(r\cos(\theta-\theta_o)-r_o)dR}{|\vec{r}-\vec{r}_o|^2} + V_{r_p} \qquad (2.28)$$

Equations (2.27) and (2.28) are essentially the same as the two components of equation (2.16) in cylinderical coordinates, except for the scale factor H.

Surface Vorticity Determination

The vorticity values away from the surface are determined using the vorticity transport equation (2.23). In order to solve this equation, it is necessary to prescribe the vorticity values on the solid surface at all time levels. To do that, the viscous region is conveniently divided into a vortex sheet of strength γ located on the surface, and an outer vorticity field where the vorticity ω and the dilatation β are assumed to be known. Applying equation (2.27) on the surface of the body yields

$$V_\theta(r_s,t) = 0 = - \frac{1}{2\pi} \int_s \frac{H(\gamma-\gamma_p)(r_s\cos(\theta-\theta_o)-r_s)d\theta}{r_s^2+r_s^2-2r_s^2\cos(\theta-\theta_o)} + V_t \qquad (2.29)$$

Here γ represents the integrated value of ωdn on the first cell adjacent to the surface and r_s is the position vector for the points on the surface where the tangential component is calculated. V_t is the tangential velocity at the body surface due to both the outer vorticity field and the whole dilatation field in R1, and is given by

$$V_t = -\frac{1}{2\pi}\int_{R1}\frac{\omega H^2(r\cos(\theta-\theta_o)-r_o)rdrd\theta}{r^2+r_o^2-2rr_o\cos(\theta-\theta_o)} - \frac{1}{2\pi}\int_{R1}\frac{(\beta-\beta_p)H^2 r\sin(\theta-\theta_o)rdrd\theta}{r^2+r_o^2-2rr_o\cos(\theta-\theta_o)} \tag{2.30}$$

It must be noted that the region R1 in the first integral does not include points on the solid surface.

If r approach r_s, the first integral on the right-hand side of equation (2.29) becomes [20].

$$-\frac{1}{2\pi}\int_s\frac{(\gamma-\gamma_p)H\,(r_s\cos(\theta-\theta_o)-r_s)rd\theta}{r_s^2+r_s^2-2r_s^2\cos(\theta-\theta_o)} = \frac{1}{4\pi}\int_o^{2\pi}(\gamma-\gamma_p)Hds - \frac{1}{2}(\gamma-\gamma_p)H \tag{2.31}$$

The principle of conservation of total vorticity gives

$$\frac{1}{4\pi}\int_o^{2\pi}\gamma H\, r_s\, d\theta = -\frac{1}{4\pi}\int_{(R1-s)} H^2\omega\, dR \tag{2.32}$$

and, since the solution is started by a non-circulatory potential flow, it follows that

$$\frac{1}{4\pi}\int_o^{2\pi}\gamma_p.H\, r_s\, d\theta = 0 \tag{2.33}$$

Substituting equations (2.30-2.33) into equation (2.29) yields

$$\gamma H=\frac{1}{2\pi r_s}\int_{(R1-s)}\frac{(r_s^2-r^2)\omega H^2\, rdrd\theta}{r_s^2+r^2-2rr_s\cos(\theta-\theta_o)} - \frac{1}{\pi}\int_{R1}\frac{H^2(\beta-\beta_p)r\sin(\theta-\theta_o)rdrd\theta}{r_s^2+r^2-2rr_s\cos(\theta-\theta_o)} + \gamma_p H \tag{2.34}$$

In equation (2.34) the region (R1-s) is the computation region R1 excluding the surface s. Since the radius of the circle in the transformed plane is taken to be unity, equation (2.34) is rewritten as

$$\gamma = \frac{1}{2\pi H}\int_{(R1-s)} \frac{\omega H^2(1-r^2)rdrd\theta}{1+r^2-2r\cos(\theta-\theta_o)} - \frac{1}{\pi H}\int_{R1} \frac{H^2(\beta-\beta_p)r\sin(\theta-\theta_o)rdrd\theta}{1+r^2-2r\cos(\theta-\theta_o)} + \gamma_p \qquad (2.35)$$

Segmentation of the Velocity Field

The advantage of using equation (2.27) to calculate exterior flow problems stems from its explicit nature. Thus, the integral formulation permits the determination of the velocity on the boundaries of rectangular regions without regard to the interior nodes. In several cases, since rapid finite-difference computational schemes are available for solving the Poisson's equation in regions with rectangular boundaries, a combination of equation (2.27) and such schemes can provide a faster way to compute velocities in exterior flow problems. For this reason, the computational domain is divided into compartments in which the kinematic computations are performed independently of each other. The choice of the scheme, to be applied in each compartment, depends upon the shape of the body surface and on the relative distance between the body surface and the compartment. For example, as will be shown later in the static stall case, the integral relation (2.27) is used in the whole wake and in inner regions adjacent to the airfoil surface in order to compute the velocities. The

Poisson's equation is used in the rest of the computational domain and the velocity on the boundaries is calculated using the integral relation (2.27).

The Poisson's equation for the tangential velocity in the transformed plane is derived as follows:

The vorticity and dilatation can be written as

$$\vec{\nabla} \times \vec{V} = \vec{\omega} H^2 = \vec{\omega}_o \tag{2.36}$$

$$\vec{\nabla} \cdot \vec{V} = \beta H^2 = \beta_o \tag{2.37}$$

Upon taking the curl of the terms in equation (2.36), the equation becomes

$$\vec{\nabla} \times \vec{\omega}_o = \vec{\nabla} \times \vec{\nabla} \times \vec{V} = \vec{\nabla}(\vec{\nabla} \cdot \vec{V}) - \nabla^2 \vec{V} \tag{2.38}$$

Substituting equation (2.37) in equation (2.38) one obtains:

$$\nabla^2 \vec{V} = \vec{\nabla} \beta_o - \vec{V} \times \vec{\omega}_o \tag{2.39}$$

Writing equation (2.39) in polar coordinates

$$\left(\frac{1}{r} \frac{\partial \omega_o}{\partial \theta} - \frac{\partial \beta_o}{\partial r} \right) \vec{e}_r - \left(\frac{\partial \omega_o}{\partial r} + \frac{1}{r} \frac{\partial \beta_o}{\partial \theta} \right) \vec{e}_\theta + \nabla^2 V_\theta \vec{e}_\theta + \nabla^2 V_r \vec{e}_r = 0 \tag{2.40}$$

By singling out the tangential component terms in equation (2.40) one gets

$$\nabla^2 V_\theta = \frac{1}{r} \frac{\partial \beta_o}{\partial \theta} + \frac{\partial \omega_o}{\partial r} \tag{2.41}$$

Equation (2.41) is the Poisson's equation for the tangential velocity written in the transformed plane.

Once the tangential component of the velocity, V_θ, is determined the radial component of the velocity is calculated explicitly by using the definition of the dilatation in the transformed plane, namely

$$\vec{\nabla} \cdot \vec{V} = \beta H^2 = \beta_o$$

$$\frac{\partial V_r}{\partial r} + \frac{V_r}{r} + \frac{1}{r} \frac{\partial V_\theta}{\partial \theta} = \beta_o \tag{2.42}$$

Pressure and Shear Calculations

Since the surface pressure details are needed for any load estimation on the body surface, the equation of state (2.4) is used to determine the pressure on the surface as follows:

$$p = \left(\frac{\gamma-1}{\gamma}\right)\rho h \tag{2.43}$$

A pressure coefficient can be written as

$$C_p = \frac{p-p_o}{\left(\frac{1}{2}\rho V_\infty^2\right)} \tag{2.44}$$

where p_o is a reference pressure.

As will be shown later, the gradients of the flow variables on the upper surface of a stalled airfoil are very sensitive to small disturbances created either by using different approximations to the governing equations or by adopting different boundary conditions. Compressibility effects are expected to be small for $M_\infty = 0.4$, and in order

to capture these small effects, it was decided to compare the present compressible results with incompressible results obtained by using exactly the same mathematical and numerical procedures. For this reason, a different (from that employed in the test cases) scheme for computing the surface pressure, similar to the scheme used in the incompressible case [7], is developed and presented below.

In the body-fitted coordinate system, the vector momentum equation is

$$\rho \frac{\partial \vec{V}}{\partial t} + \rho(\vec{V}.\vec{\nabla})\vec{V} = -\vec{\nabla}p + \vec{\nabla}.\ \vec{\vec{\tau}} \tag{2.45}$$

At the surface, the momentum equation is reduced to the following simple form because of the no-slip condition.

$$\vec{\nabla}p = \vec{\nabla}.\ \vec{\vec{\tau}} \tag{2.46}$$

Taking the dot product of the above equation with the tangential unit vector $\vec{t}$ at the surface, defined positive in the counterclockwise sense one gets

$$\frac{\partial p}{\partial s} = (\vec{\nabla}.\vec{\vec{\tau}}).\vec{t} \tag{2.47}$$

where s is the coordinate direction tangential to the surface, and is measured positive in the counterclockwise sense.

The surface vector $\vec{t}$ is defined by

$$\vec{t} = \frac{dx}{ds}\vec{i} + \frac{dy}{ds}\vec{j} \tag{2.48}$$

For simplicity, it is assumed that the fluid is a perfect gas with constant molecular viscosity, thermal conductivity and specific heat. These assumptions are reasonable for low subsonic flows. By using these assumptions the right-hand side of equation (2.47) can be written as follows:

$$\vec{\nabla} \cdot \vec{\vec{\tau}} = \mu\nabla^2\vec{V} + 1/3\mu\vec{\nabla}\beta \tag{2.49}$$

Inserting equation (2.49) into equation (2.47) one gets

$$\frac{\partial p}{\partial s} = \mu\nabla^2 V_t + \left(\frac{1}{3}\right)\mu\frac{\partial \beta}{\partial s} \tag{2.50}$$

Also,

$$\nabla^2 V_t = \frac{\partial^2 V_t}{\partial s^2} + \frac{\partial^2 V_t}{\partial n^2} \tag{2.51}$$

where $\vec{n}$ is the unit normal vector on the body surface, measured positive in the direction away from the solid surface. Because of the no-slip condition, V_t and $\frac{\partial^2 V_t}{\partial s^2}$ are zero everywhere on the surface. Thus,

$$\nabla^2 V_t = \frac{\partial^2 V_t}{\partial n^2} = \frac{\partial \omega}{\partial n} \tag{2.52}$$

Combining the terms, equation (2.47) reduces to

$$\frac{\partial p}{\partial s} = \mu \frac{\partial \omega}{\partial n} + (1/3)\mu \frac{\partial \beta}{\partial s} \tag{2.53}$$

If the pressure is non-dimensionalized with respect to the dynamic pressure at infinity, and all quantities are non-dimensionalized with respect to the reference quantities mentioned earlier, equation (2.53) becomes

$$\frac{\partial C_p}{\partial s} = \frac{2C}{Re} \left(\frac{\partial \omega}{\partial n} + 1/3 \frac{\partial \beta}{\partial s}\right) \tag{2.54}$$

where, $C_p = \dfrac{p-p_o}{(\frac{1}{2}\rho V_\infty^2)}$ and C is the chord length.

The dimensionless shear stress at the surface is given by;

$$C_f = -\frac{2C}{Re}\omega \tag{2.55}$$

knowing the surface pressure and the surface shear stress distributions, other quantities of interest such as lift, drag and moment can be easily obtained.

Calculation of Loads

Once the surface pressure and shear stress distributions are known, the loads are obtained from the following expressions.

$$C_N = C_{N_p} + C_{N_F} \tag{2.56}$$

$$C_T = C_{T_p} + C_{T_F} \tag{2.57}$$

$$C_M = C_{M_p} + C_{M_F} \tag{2.58}$$

where

$$C_{N_p} = \frac{1}{C} \int_0^{2\pi} C_p(\theta) \frac{dx}{d\theta} \, d\theta \tag{2.59}$$

$$C_{N_F} = \frac{2}{Re} \int_0^{2\pi} \omega(\theta) \frac{dy}{d\theta} \, d\theta \tag{2.60}$$

$$C_{T_p} = -\frac{1}{C} \int_0^{2\pi} C_p(\theta) \frac{dy}{d\theta} \, d\theta \tag{2.61}$$

$$C_{T_F} = \frac{2}{Re} \int_0^{2\pi} \omega(\theta) \frac{dx}{d\theta} \, d\theta \tag{2.62}$$

$$C_{M_p} = \frac{1}{C^2} \int_0^{2\pi} C_p(\theta) \left\{ x \frac{dx}{d\theta} + y \frac{dy}{d\theta} \right\} d\theta \tag{2.63}$$

$$C_{M_F} = \frac{2}{Re \cdot C} \int_0^{2\pi} \omega(\theta) \left\{ x \frac{dy}{d\theta} - y \frac{dx}{d\theta} \right\} d\theta \tag{2.64}$$

The C_N and C_T are force coefficients directed normal and tangential to the airfoil chord, and C_M is the moment coefficient. The subscripts p and F denote the pressure and the skin friction contribution respectively. The moment is taken about the origin of the coordinate system and is positive in the counterclockwise direction.

The lift and drag coefficients referred to the wind axes are obtained from:

$$C_L = C_N \cos\alpha - C_T \sin\alpha \tag{2.65}$$

$$C_D = C_N \sin\alpha + C_T \cos\alpha \tag{2.66}$$

where α is the angle of attack.

Initial and Boundary Conditions

The non-circulatory potential flow solution is used as an initial condition in the present work. Along the body surface, the vanishing normal derivatives of enthalpy h and density ρ were used as boundary conditions for h and ρ. These conditions are convenient for an adiabatic wall. The surface values of the dilatation δ were obtained using a three-point extrapolation formula during each iteration of the dilatation transport equation. The boundary values of δ were relaxed and set to be zero whenever the solution approached steady state. The integral expression (2.35) was used to compute the surface vorticity at each iteration while iterating the vorticity transport equation.

The potential flow values were used as in flow boundary conditions, while the vanishing second derivatives for β, h, ρ and zero vorticity were used as downstream boundary conditions. The wake never approached the downstream boundary during the calculations. The aforementioned boundary conditions preserve the elliptic nature of the problem.

3. RESULTS AND DISCUSSION

The procedure developed was tested on two problems in order to demonstrate the ability of the approach to compute attached and separated flows. The test problems considered are: (i) laminar compressible flow around a circular cylinder, (ii) laminar compressible flow over an airfoil at zero angle of attack. Finally, the method was applied to the static stall problem.

In the results discussed below, the non-dimensionalization is done with respect to the free stream velocity and the characteristic length of the body in the transformed plane. In the airfoil case and other test cases, the solid body was set into motion impulsively. Since the time rate of change of all flow variables is very high after the impulsive start, very small values of the time step, Δt, are used to obtain proper timewise resolution at the initial time levels. As the gradients with respect to time decrease, large values of Δt are used. The under-relaxation parameter, which sometimes controls the acceleration of the convergence of the iterations, is varied depending upon the type of problem considered.

Laminar Compressible Flow Past a Circular Cylinder

The present scheme also has been applied to the study of laminar compressible flow past a circular cylinder at a Reynolds number of 40, Mach number of 0.4 and Prandtl number of 1. The Reynolds number is based on the cylinder diameter and the free stream velocity. This classical test case is chosen to demonstrate the ability of the approach to handle flows with massive separation.

The grid system consists of lines of constant radii and lines of constant angle θ. The lines of constant θ are equally spaced with $\pi/20$ intervals. In the radial direction, a stretching relation is assumed as follows:

$$r = e^{s}, \qquad s = (j-1)\Delta s, \quad j = 1, Jmax$$

By varying s uniformly, with $\Delta s = 0.06$, an exponential variation is obtained. The total number of grid points used is 2000 points. It should be noted that with the present formulation not all of these grid points are involved in the computations at all time levels. At the earlier time levels, the computational region contained about 40% of the total number of grid points. As the solution progressed in time, the number of points in the computational domain increased. When the computations were terminated at a time level of 15.1, the computational region contained all the 2000 points.

In order to compute the kinematic part of the problem the segmentation technique, explained in chapter II was used. The computational domain is divided into three annular regions R', R'' and R'''. The inner region, R', consists of 240 nodes. The intermediate region, R'', consists of 600 nodes, while the outer region, R''', contains 1160 nodal points. Regions R', R'' are matched at a distance of .35 radii away from the surface; likewise the regions R'' and R''' are matched at a distance of 2.525 radii away from the surface. The far-field boundary is located 17.916 radii away from the surface. The integral formula is used to compute the tangential velocity in region R' and on all of the boundaries. Then, the Poisson's equation is iterated to get the velocities in R'' and R'''.

The kinetic equations (2.19), (2.20), (2.21) and (2.22) are approximated by an implicit finite-difference scheme in the polar coordinates and are solved by using the 'point successive under-relaxation' technique. Central differences are used to approximate the convection terms. It should be noted that no symmetry was assumed regarding this present case.

The solid body was set into motion impulsively. At this impulsive start, the flow was prescribed by the potentialflow solution about a circular cylinder immersed in a uniform stream. The time step varied gradually from 0.05 to 0.15. The solution was terminated at t = 15.1. At this time level the drag coefficient had converged to three digits. In the present case, the time is non-dimensionalized relative to the cylinder radius and the free stream velocity.

In Figure 1 the surface pressure distribution at steady state is compared with the numerical solution obtained by Sankar and Tassa [2]. The agreement is quite good.

In Table 1, the present compressible and incompressible results are compared with the compressible results of Reference 2. In this Table, the separation angle $\theta_{sep.}$ is measured from the rear axis, and obtained as the point on the surface where the vorticity changes sign. The length of the standing vortex (L/R) represents the distance between the center of the cylinder and the point on the centerline where the velocity changes sign. These comparisons indicate that the present solution and the finite-difference method give results that are in satisfactory agreement.

TABLE 1

Comparison Between the Present Method and Reference 2

	Presents Results		Reference 2
	Incompressible (M=0)	Compressible (M=0.4)	Compressible (M=0.4)
θ_{sep}	53.5	53.7	52.5
Length of Standing Vortex (L/R)	5.80	5.85	5.08
Pressure Drag Coefficient C_{D_P}	1.025	1.230	1.32
Friction Drag Coefficient C_{D_F}	0.555	.520	.561
Total Drag Coefficient C_{D_T}	1.580	1.750	1.881
Minimum Surface Vorticity $\omega_{min.}$	-6.60	-6.12	-5.82

Compressible Laminar Flow Past an Airfoil at Zero Angle of Attack

The computational procedure developed here is next applied to the case of compressible laminar flow past a symmetric 9% thick Joukowski airfoil at a zero angle of attack. The airfoil is obtained by means of a conformal transformation of a unit circle. The chord Reynolds number

considered in this case is 1000. The Mach number is 0.4 and the Prandtl number is unity. The normalizing reference time is obtained by dividing the transformed circular cylinder radius by the free steam velocity. All of the quantities are non-dimensionalized with respect to the free stream velocity and cylinder radius.

The tangential velocity, V_θ , in the transformed plane, is calculated using the integral relation for the set of nodes on the first coordinate line next to the surface and at the outer boundaries. The Poisson's equation is then solved by using a 'successive point over-relaxation' technique in the rest of the domain. The difference kinetic equations, written in the transformed plane, are solved using a 'point under-relaxation' iterative technique. The circular domain is discretized with 60 equally spaced points in the direction and 40 points in the radial direction. The time step is gradually varied from 0.0025 to 0.1 during the course of the computations. The computations are initiated with an impulsive start. The initial surface vortex sheet strength is computed from the potential flow velocity values. The kinematic computations are done with the finite Fourier series method. At a time level of 6.5, a steady state is determined to have been reached based upon the agreement (within 1%) of the computed surface vorticity values with those of the previous time level.

In Figures 2, 3 the present surface pressure and surface vorticity values are compared with the corresponding values obtained in Reference 2 . Both solutions are in very close agreement. The reference pressure

used in these figures is the free stream pressure.

Laminar Compressible Flow Past an Airfoil at an Angle of Attack

The airfoil used in the present study is the 9% thick symmetrical Joukowski airfoil described in appendix E. The chord Reynolds number considered is 1000. The Mach number is 0.4, the Prandtl number is 1.0 and the angle of attack is 15^{o}.

A number of publications (1, 2, 3, 5, 6, 7) have treated this problem before by incompressible flow. It can be seen from these results that the solutions are not quantitatively comparable. However, there is a qualitative similarity between the results. In the static stall case, the results depend on a number of factors such as grid resolution, specification of the far-field boundary conditions and the numerical scheme. Therefore, in order to capture the small compressibility effects expected here, the compressible results have been compared with incompressible results obtained using the same computer program after 'switching off' the compressibility effects.

Consequently, before solving the compressible static stall problem, it was appropriate to conduct first a series of incompressible numerical experiments to : (i) test the code, (ii) inspect the sensitivity of this solution with the change of mesh size in the θ direction, (iii) examine the role of the time increment on the accuracy of the solution, (iv) examine the cyclic behavior of the solution, and (v) obtain incompressible data to be compared later with the compressible data. The difference between the two solutions represents the effect of compressibility.

Incompressible Solution

The incompressible solution for the static stall case was obtained by following the same procedure used later for the compressible case. In order to demonstrate the accuracy of the scheme, the incompressible solution has been compared with the numerical results of Mehta [7]. As shown in Figure 4, the present results agree very well with Mehta's results at the early time levels. As expected, the two solutions differ quantitatively at the later time levels. However, the qualitative behavior is similar at these later time levels.

To illustrate the effect of the grid resolution on the solution, two sequences of solution were obtained for $\Delta\theta = \pi/24$ and $\Delta\theta = \pi/30$. Figure 5 shows the history of a load comparison between the two solutions. It is seen from this figure that the two solutions are comparable. Although there is no drastic difference between the two solutions, there still exists enough of a difference that there could be a misinterpretation of the results obtained for two different mesh size solutions, one compressible and the other incompressible. This experiment demonstrates the importance of using the same grid size whenever small compressibility effects are examined.

The continuation of the cyclic behavior of the solution for more than one cycle and the validity of the present method for a number of cycles of vortex shedding was demonstrated. The solution was advanced in time up to a dimensionless time level of 62 (the reference time being the transformed circle radius divided by the free-stream velocity). Figure 5 shows the time history of loads which illustrate the cyclic behavior of the

solution with time. Note that there are two cycles observed in the prescribed time range. This exercise provides considerable confidence in the formulation of the problem and in the computer program.

Finally, in order to study the effect of the time step on the solution, three numerical experiments, with three different time increments, were performed. Table 2 shows the comparisons among these three solutions. Each solution has been started at time level of 20.175, and then advanced in time up to a time level of 21.615 and 24.735. The good agreement among the solutions is apparent in Table 2. It could be concluded that, within the prescribed time range, the size of the time step plays a minor role in the accuracy of the solution.

Table 2

Comparison Among Three Different Time Increments Solutions

Time Level	Δt	C_L	C_D	$-C_M$	$\omega_{s,min}$
	0.06	0.2582	0.1641	0.1160	-89.26
t = 21.615	0.12	0.2574	0.1654	0.1150	-89.41
	0.24	0.2623	0.1683	0.1127	-89.58
	0.06	0.3475	0.1722	0.1225	-93.971
t = 24.735	0.12	0.3516	0.1718	0.1235	-94.28
	0.24	0.3527	0.1686	0.1257	-94.46

Compressible Solution

In the Figures that follow, the chordwise distance denoted "chord percentage" is measured from the leading edge of the airfoil. The force coefficients are normalized with respect to the free-stream velocity and the radius of the unit circle. The normalized reference time is obtained by dividing the radius of the unit circle by the free-stream velocity.

The grid system contains 48 equally spaced points in the θ-direction and 40 points in the radial direction. The exponential relation given in appendix E is applied for placing the points in the r direction. The time increment used in this numerical study is progressively increased from Δt = 0.0005 to Δt = 0.24. A total of 255 time steps were used to march the solution to a time level of 31.275, when the computations were terminated.

Using the flowfield segmentation technique described earlier in chapter II, the velocity is obtained everywhere in the computational

domain. Figure 6 shows the segmented compartments and the kinematic relation used in each of them.

The iterative procedure used in solving the kinetic equations were varied to study their effects on the solution. Switching the iteration direction in the tangential coordinates was used to accelerate the convergence. The convergence criteria used in solving the vorticity transport equation was based on the maximum vortex strength variations between two consecutive iterations, where the vortex sheet strength is defined by $\gamma = \omega H^2 dr$. Invariably, the maximum variation between two consecutive iterations occured near the trailing edge, which can be explained by examining equation (2.35). It is seen that the scale factor H appears in the denominator. Because the scale factor is very small near the trailing edge, it amplifies any error in the calculated value of the surface vortex sheet strength. The above criteria for convergence allows more tolerance for the vortex sheet strength near the trailing edge than anywhere else. The tolerance level specified for the vortex sheet strength was 0.002 at the earlier time levels and is subsequently reduced to 0.0005 at later time levels. Continuation of the iteration beyond the above tolerance limit was not found effective in reducing the residue. The residue instead oscillated around a minimum value without showing any tendency to reach zero.

The maximum tolerance criterion used in iterating the enthalpy and density transport equations are 0.1% and .5% of the previous iteration, respectively. In iterating for the dilatation transport equation, a stringent tolerance limit in the vicinity of the airfoil was assumed in order to ensure proper convergence. In the outer regions and near the trailing edge, this limit is relaxed to accelerate the convergence. At

associated with the formation of both the secondary and the trailing edge bubbles, and (iv) reattachment of the primary bubble. The initial attached bubble which expands with time is referred as the 'primary bubble'.

The convention used is that the upper surface vorticity is negative for attached flows while positive vorticity indicates flow reversal. The opposite is true for the lower surface.

The first stage of the flow field development reflects the effects of the impulsive start. Immediately after the impulsive start, the vorticity is only non-zero at the surface, while potential flow exists in the rest of the fluid. The rear stagnation point is located on the upper surface of the airfoil. Within a short time, the rear stagnation point moves close to the trailing edge. This movement is associated with the formation of a "starting vortex". At subsequent time levels the boundary layer starts growing on the upper and lower surfaces of the airfoil. The thickness of the boundary layer on both the upper and lower surfaces increases with time, as is observed from the displacement of the 'streamline-like' lines near the surface. For convenience, the 'streamline like' lines will be called 'streamlines'. The thickness of the boundary layer on the lower surface is smaller than the thickness of the boundary layer on the upper surface due to the existence of a favorable pressure gradient on most of the lower surface. The extent of the region of adverse pressure gradient on the upper surface is shown in the pressure distribution plot. It is also observed, at this stage, that the magnitude of the surface vorticity near the leading edge on the upper surface continues to decrease with time, forecasting the onset of separation in that neighborhood when the surface vorticity changes sign. However, the separation does not actually occur until a time level of 1.88. During this

first stage, and after the decay of the influence of the impulsive start, the value of C_L starts increasing due to the growth of circulation after first reaching a minimum value at T = 1.0 as shown in Figure 7. The value of C_D continually decreases because the decrease in the friction force on the lower surface as the positive vorticity decreases with time.

The second stage of flow development describes the occurrence of separation, together with the formation and growth of the primary bubble. The separation first takes place at 20% chord at T = 1.88. The size of the separation bubble increases with time until it covers most of the upper surface. This is expected, since the separation point moves forward towards the leading edge and the reattachment point moves rearward towards the trailing edge. At time level 7.214, the separation and the reattachment points are about 95% chord length apart. The increases in the size of the separation bubble increases the effective thickness of the airfoil, and the increase of the intensity of the reversed flow inside the bubble causes additional suction pressure on the upper surface. The above two factors result in an increase in the value of C_L with time. During the duration of the primary bubble, the drag coefficient remains approximately constant.

In the third stage of flow development, the primary bubble is ruptured and an open bubble is formed, indicating the cyclic start of vortex shedding. The reattachment point of the primary bubble lifts off at a time level of 7.214 causing separated flow over almost the entire upper surface. The increase in the number of streamline loops inside the separated bubble, indicates an intensification of the reversed flow inside the bubble. The flow rotation inside the bubble is clockwise, with the fluid next to the surface moving upstream. The pressure plots at T = 9.494, Figure 37, show a small region near the trailing edge where

later time levels, the maximum allowable tolerance in the inner regions, is taken to be 0.8%. This represents the maximum percentage variation between two consecutive iterations.

As described earlier, the total number of nodes are 1980. However not all of these nodes were involved in the computations at all time levels. At early time levels, the vortical region is confined to only about 25% of the maximum computational region. The computational time per time step depends on the extent of the computational boundary and varies from as little as 70 CPU seconds at the early time levels to 154 CPU seconds at later time levels on the CYBER-70 computer with a CDC 6400 CPU.

The average computational time required in the present study to advance the solution for one dimensionless time is 16 CPU minutes. Sankar and Tassa [2] used an ADI scheme to solve the primitive variable system of finite-difference equations, and took 11.5 CPU minutes to advance the solution for one dimensionless time on the same computer. It should be emphasized here that, in the present study, at later time levels the memory requirements are larger than those required in Reference [2]. However, due to computer memory restrictions, the present computer program could not utilize the maximum capacity of the CYBER-70 computer. Therefore, unnecessary computations have been carried out for a number of time steps. Alternatively, if more computer core is used, along with using more sophisticated numerical procedures, it is believed that the computational time required to advance the solution for one dimensionless time can be reduced below 11.5 CPU minutes.

Table 3 gives the details of the time steps versus the computer time for the present computations.

Table 3

Sequence of Changing the Time Increment and Summary of Computer Time

No. of Time Steps	Δt	Time Level T	Average CPU Time in Sec.*
10	0.0005	0.005	70
10	0.001	0.015	80
10	0.0015	0.03	85
10	0.0045	0.075	92
10	0.008	0.155	94
10	0.016	0.315	98
10	0.032	0.635	100
10	0.064	1.275	105
20	0.09	3.075	108
20	0.12	5.475	119
30	0.12	9.075	128
25	0.12	12.075	130
80	0.24	31.275	154

* CYBER-70/Model 74-6400 CPU.

Flow Development

The development of the flow field may be viewed as occuring in four stages. These are: (i) impulsive start, (ii) formation and growth of the primary bubble, (iii) the bursting of the primary bubble which is

there is a decrease in the pressure in the direction of the main flow outside the bubble. This is equivalent to an adverse pressure gradient for the flow near the surface. A small counterclockwise separation bubble appears near the trailing edge at T = 11.775 as a result of the above mentioned pressure gradient. The size of this bubble increases slowly with time until it can be clearly seen at T = 14.05%. At this time level, a similar adverse pressure gradient develops at about 58% chordwise distance from the trailing edge. This results in the appearance of a secondary counterclockwise bubble at T = 16.71. The direction of the flow inside this bubble is counterclockwise, with the fluid near the surface moving downstream toward the trailing edge. The intensity of the flow rotation in the trailing edge bubble is larger than it is inside the secondary bubble, as indicated by the number of streamline loops inside that bubble. The size of the two bubbles increases with time. As time progresses, the primary bubble starts to shrink while the other two small bubbles enlarge. The secondary bubble expands locally in the normal direction, whereas the trailing edge bubble gets enlongated in the downstream direction. At this stage of flow development, the lift coefficient keeps on increasing, due to the extent of the primary bubble beyond the trailing edge, until it reaches a maximum at T = 10.75. Meanwhile, the drag coefficient starts increasing very slowly after the time level 4.8. This slow increase in the drag is due to the increase in the effective thickness of the airfoil as judged by the shape of the zero streamline. This causes an increase in the pressure drag. The value of C_D continuously increases until it reaches a maximum at T = 12. The downstream motion of the center of the ruptured clockwise bubble, which is accompanied by the appearance of the two small counter-

clockwise bubbles, causes a general drop in the value of C_L after T = 10.75. The reason for this drop is that the negative pressure sustained by the primary bubble is partly removed by the formation of the two counterclockwise bubbles. This also results in a decrease in the pressure drag, which explains the drop of C_D after reaching a maximum at T = 12.

The fourth stage of flow development involve the opening up of the secondary bubble, the lifting off of the trailing edge bubble, and the reattachment of the upstream part of the primary bubble. The streamlines and equi-vorticity lines show the following flow development during this stage: (1) the secondary bubble splits the primary bubble and opens up to the outside flow at a time level of 20.51; (2) the trailing edge bubble moves downstream until it lifts off the airfoil by T = 21.95; (3) the downstream part of the primary bubble starts to disengage from the surface at a time level of 25.455; and (4) as time progresses, the upstream part of the primary bubble spreads in the downstream direction until the reattachment point reaches the trailing edge at a time level of 31.275, indicating the completion of the first cycle of vortex shedding. The streamline pattern at T = 31.275 looks similar to the pattern at the start of the cycle (T = 7.214), which indicates that the second cycle of oscillatory behavior is going to start at T = 31.275. As the secondary bubble opens up to the main stream, the reattachment point of the upstream part of the primary bubble starts to move downstream, increasing the region of the clockwise reversed flow. This reversed flow is able to sustain more suction pressure which results in an increase in the value of C_L. The lift-off of the trailing edge bubble and the shedding of the downstream part of the primary bubble into the downstream flow enables the upstream

part of the primary bubble to cover most of the airfoil. This will lead to a continuous increase in C_L and C_D, as indicated in Figures 8 and 9.

Judging either from the contour plots of the streamlines or from the time histories of the loads plots, it is estimated that one cycle of vortex shedding occurs during the time period from T = 7.214 to T = 31.275. With the airfoil chord as the characteristic length, the Strouhal number, defined by C/(TV), where T is the period of the cycle, is then found to be 0.155.

Comparison Between the Compressible and Incompressible Solutions

In order to predict the compressibility effect for the present static stall case at a Mach number of 0.4, the compressible and the incompressible solutions obtained using the same grid are quantitatively compared in Table 4. The importance of using the same grid size in both solutions was demonstrated earlier in this chapter.

Based on the comparison shown in Table 4, the observations made may be summarized as follows:

(i) At the earlier time levels, the compressibility seems to decrease the rate of thickening of the boundary layer.

(ii) The onset of the separation of the primary bubble begins to appear at a later time level in the compressible case.

(iii) Compressibility seems to play a minor role in the growth of the primary bubble.

(iv) The compressibility delays the appearance of both the secondary and the trailing edge bubbles. These two bubbles grow at a faster rate in the compressible case than they grow in the incompressible case as shown in Figures (8-10).

(v) When the first cycle of vortex shedding starts, the difference in the force coefficients between the compressible and the incompressible solutions is small. As time advances, the difference between the two solutions gradually increases, indicating the increased influence of the compressibility. At a time level of approximately 21 the compressibility effect becomes very small. At this time level, the time rate of change of flow variables decreases to a minimum. At later time levels, T = 23 - 31.275, the compressibility effect appears to increase again but at a slower rate.

(vi) The effect of compressibility on the force coefficients is shown in Figures (8-10). This effect is comparable to the one computed in Reference 2, as shown in Figures 11 and 12.

Table 4

Quantitative Comparison Between the Present Incompressible and Compressible Solutions

Flow Events	Compressible Data	Incompressible Data
Onset of separation of the primary bubble	T = 1.88	T = 1.76
Separation location from leading edge	20%	23%
Cycle begins at T =	7.214	6.821
Cycle ends at T =	31.275	29.815
First appearance of trailing edge bubble	T = 11.775	T = 11.24
First appearance of secondary bubble	T = 16.70	T = 15.374
Opening up of the secondary bubble	T = 20.51	T = 19.81
Strouhal number $C/(TV_\infty)$	0.15478	0.16146
$C_{L_{max.}}$	1.32	1.29
$C_{L_{min.}}$	0.254	0.262

* The force coefficients are given after the recovery from the impulsive start.

Comparison With Other Numerical Solutions

The flow around a 9% symmetric Joukowski airfoil at an angle of attack of 15°, chord Reynolds number of 1000, Mach number of 0.4 and Prandtl number of one, has been solved numerically by Sankar and Tassa [2].

The computational procedures of Reference 2 are significantly different from those used in the present study, and it is very important to bear this in mind when comparing the results of the two studies. The procedures of Reference 2 are as follows: (1) the primative variables (u,V,ρ,h) are used as the unknown flow variables; (2) the governing equations are discretized using central difference formulas for the spatial derivatives; (3) a second order artificial diffusion is added to the real diffusion term to stabilize the solution; (4) an ADI procedure is used to solve the system of difference equations generated from the governing equations: (5) a fourth order dissipation term is added to the governing equations to eliminate the wiggles arising in the solutions; (6) the outer boundary is located at six chord lengths away from the airfoil (in the present study the outer bounday is located at about 10 chord lengths away from the surface); and (7) a uniform flow is used to start the solution impulsively.

Table 6 show typical comparison between the present results and the results obtained in Reference 15.

The stability requirement for non-linear problems may impose more restrictions on the size of the time step even in the case of implicit schemes [8] However, Desideri et al [9] and Ballhaus et al. [10], in separate studies, have shown that a cyclic variation of the size of the time step between two limits is helpful in obtaining convergence in the (ADI) schemes. In the present solution, no such restriction on the time step was required. It is believed that the use of the under-relaxation technique in solving the difference equations has a stabilizing effect on the solution. The maximum time step used in Reference 2 is 0.064,

whereas, in the present study, the time size was successfully increased up to 0.24. More details about the work can be found in Reference 11.

Table 5

Quantitative Comparison Between the Present Results and Those of Reference 2

Flow Feature	Present Results	Reference 2
Onset of separation of the primary bubble	T = 1.88	T = 2.1719
Separation location from leading edge	20%	24%
Cycle begins at T =	7.214	6.3117
Cycle ends at T =	31.275	27.376
First appearance of the trailing edge bubble	T = 11.775	T = 10.695
First appearance of the secondary bubble	T = 16.70	T = 12.52
Opening up of the secondary bubble	T = 20.51	T = 18.056
Strouhal number $C/(TV_\infty)$	0.15478	0.17626
C_L max.	1.32	1.34
C_L min.	0.254	0.251
C_D max.	0.346	0.364
C_D min.	0.165	0.141

4. THE USE OF THE INTEGRAL REPRESENTATION METHOD WITH SERIES SOLUTIONS FOR SOLVING THE NAVIER-STOKES EQUATIONS

The use of orthogonal functions in solving the Navier-Stokes equations has offered high accuracy for certain problems. The reason is the rapid decrease of the truncation error as the number of these functions used increase in a series representation of the solution (16). In this section of the report, the use of Fourier series with the integral representation method (1) is developed. The procedure is applied to simple test problems.

The Navier-Stokes equations, for steady incompressible flow, in a region R, with boundary B, can be written as follows (1):

$$\vec{v}(\vec{r}) = -\frac{1}{2\pi}\int_R \frac{\vec{\omega}_o \times (\vec{r}_o - \vec{r})}{|\vec{r}_o - \vec{r}|^2}\, dR_o + \frac{1}{2\pi}\int_B \frac{(\vec{v}_o \cdot \vec{n}_o)(\vec{r}_o - \vec{r})}{|\vec{r}_o - \vec{r}|^2}\, dB_o - \frac{1}{2\pi}\int_B \frac{(\vec{v}_o \times \vec{n}_o)\times(\vec{r}_o - \vec{r})}{|\vec{r}_o - \vec{r}|^2}\, dB_o \tag{4.1}$$

$$\vec{\omega} = -\frac{Re}{2\pi}\int_R \frac{(\vec{v}_o \times \vec{\omega}_o)\times(\vec{r}_o - \vec{r})}{|\vec{r}_o - \vec{r}|^2}\, dR_o + \frac{Re}{2\pi}\int_B \frac{h_o\, \vec{n}_o \times (\vec{r}_o - \vec{r})}{|\vec{r}_o - \vec{r}|^2}\, dB_o - \frac{1}{2\pi}\oint_B \frac{(\vec{\omega}_o \times \vec{n}_o)\times(\vec{r}_o - \vec{r})}{|\vec{r}_o - \vec{r}|^2}\, dB_o \tag{4.2}$$

Where $\vec{v}$ and $\vec{\omega}$ are the velocity and the vorticity vector respectively, $\vec{r}$ is the position vector and $\vec{n}$ is the unit vector on B directed outwards. The

subscript o indicates that a variable or an integration is evaluated in the $\vec{r}_o$ space. Notice that (4.2) is nonlinear because it is equivalent to our familiar vorticity transport equation.

In a polar (r, θ) coordinate system, the vector equations (4.1) and (4.2) give the following scalar equations.

$$
\begin{aligned}
v_r = \frac{1}{2\pi} & \int_R \frac{\omega_o r_o \sin(\theta_o - \theta)}{r_o^2 + r^2 - 2r_o r \cos(\theta_o - \theta)} \, dR_o \\
& + \frac{1}{2\pi} \oint_B \frac{v_{r_o}\left[r_o \cos(\theta_o - \theta) - r\right]}{r_o^2 + r^2 - 2r_o r \cos(\theta_o - \theta)} \, dB_o \\
& - \frac{1}{2\pi} \oint_B \frac{v_{\theta_o} r_o \sin(\theta_o - \theta)}{r_o^2 + r^2 - 2r_o r \cos(\theta_o - \theta)} \, dB_o
\end{aligned}
\tag{4.3}
$$

$$
\begin{aligned}
v_\theta = & -\frac{1}{2\pi} \int_R \frac{\omega_o r_o \cos(\theta_o - \theta) - r}{r_o^2 + r^2 - 2r_o r \cos(\theta_o - \theta)} \, dR_o \\
& + \frac{1}{2\pi} \oint_B \frac{v_{r_o} r_o \sin(\theta_o - \theta)}{r_o^2 + r^2 - 2r_o r \cos(\theta_o - \theta)} \, dB_o \\
& + \frac{1}{2\pi} \oint_B \frac{v_{\theta_o}\left[r_o \cos(\theta_o - \theta) - r\right]}{r_o^2 + r^2 - 2r_o r \cos(\theta_o - \theta)} \, dB_o
\end{aligned}
\tag{4.4}
$$

$$
\omega = -\frac{Re}{2\pi} \int_R \frac{v_{r_o} \omega_o \left[r_o - r \cos(\theta_o - \theta)\right] + v_{\theta_o} \omega_o r \sin(\theta - \theta_o)}{r_o^2 + r^2 - 2r_o r \cos(\theta_o - \theta)} \, dR_o
$$

$$+ \frac{Re}{2\pi} \oint_B \frac{h_o r \sin(\theta_o - \theta)}{r_o^2 + r^2 - 2r_o r \cos(\theta_o - \theta)} dB_o$$

$$+ \frac{1}{2\pi} \oint_B \frac{\omega_o \left[r_o - r \cos(\theta_o - \theta) \right]}{r_o^2 + r^2 - 2r_o r \cos(\theta_o - \theta)} dB_o \qquad (4.5)$$

In (4.3) - (4.5) v_r and v_o denote the velocity components in the r and θ direction respectively. Because we are looking at a periodic in the θ-direction flowfield we can assume a solution in the form of finite Fourier series.

$$v_r = s_o + \sum_{n=1}^{N} (s_n \cos n\theta + t_n \sin n\theta) \qquad (4.6)$$

$$v_\theta = p_o + \sum_{n=1}^{N} (p_n \cos n\theta + q_n \sin n\theta) \qquad (4.7)$$

$$\omega = \alpha_o + \sum_{n=1}^{N} (\alpha_n \cos n\theta + \beta_n \sin n\theta) \qquad (4.8)$$

In these equations, the Fourier coefficients α_o, α_n's, β_n's, s_o, s_n's, t_n's, p_o, p_n's, q_n's are dependent on r only.

Using the method of residuals (Appendix C), the integrals in equations (4.3), (4.4) and (4.5) could be evaluated explicitly and only the Fourier coefficients are left to be determined (Appendix C):

$$s_o = 0 \qquad (4.9)$$

$$s_n = \frac{1}{2} \int_o^r \beta_n \left(\frac{r_o}{r}\right)^{n+1} dr_o + \frac{1}{2} \int_r^1 \beta_n \left(\frac{r}{r_o}\right)^{n-1} dr_o$$

$$+ \frac{1}{2} s_n(1)\, r^{n-1} - \frac{1}{2} q_n(1)\, r^{n-1} \qquad (4.10)$$

$$t_n = -\frac{1}{2}\int_o^r \alpha_n\left(\frac{r_o}{r}\right)^{n+1} dr_o - \frac{1}{2}\int_r^1 \alpha_n\left(\frac{r}{r_o}\right)^{n-1} dr_o$$

$$+ \frac{1}{2}\, t_n(1)\, r^{n-1} + \frac{1}{2}\, p_n(1)\, r^{n-1} \qquad (4.11)$$

$$p_o = \int_o^r \alpha_o\left(\frac{r_o}{r}\right) dr_o \qquad (4.12)$$

$$p_n = \frac{1}{2}\int_o^r \alpha_n\left(\frac{r_o}{r}\right)^{n+1} dr_o - \frac{1}{2}\int_r^1 \alpha_n\left(\frac{r}{r_o}\right)^{n-1} dr_o$$

$$+ \frac{1}{2}\, t_n(1)\, r^{n-1} + \frac{1}{2}\, p_n(1)\, r^{n-1} \qquad (4.13)$$

$$q_n = \frac{1}{2}\int_o^r \beta_n\left(\frac{r_o}{r}\right)^{n+1} dr_o - \frac{1}{2}\int_r^1 \beta_n\left(\frac{r}{r_o}\right)^{n-1} dr_o$$

$$- \frac{1}{2}\, s_n(1)\, r^{n-1} + \frac{1}{2}\, q_n(1)\, r^{n-1} \qquad (4.14)$$

$$\alpha_o = \alpha_o(1) - \mathrm{Re}\int_r^1 \xi_o\, dr_o \qquad (4.15)$$

$$\alpha_n = \alpha_n(1)\, r^n - \frac{\mathrm{Re}}{2}\, r^n \int_o^1 (\xi_n - \zeta_n)\, r_o^n\, dr_o$$

$$+ \frac{\mathrm{Re}}{2}\int_o^r (\xi_n - \zeta_n)\left(\frac{r_o}{r}\right)^n dr_o$$

$$- \frac{\mathrm{Re}}{2}\int_r^1 (\xi_n + \zeta_n)\left(\frac{r}{r_o}\right)^n dr_o \qquad (4.16)$$

$$\beta_n = \beta_n(1)\, r^n - \frac{\mathrm{Re}}{2}\, r^n \int_o^1 (\eta_n + \mu_n) r_o^n\, dr_o$$

$$+ \frac{\mathrm{Re}}{2}\int_o^r (\eta_n + \mu_n)\left(\frac{r_o}{r}\right)^n dr_o$$

$$+ \frac{Re}{2} \int_r^1 (\eta_n - \mu_n)\left(\frac{r}{r_o}\right)^n dr_o \qquad (4.17)$$

where $1 \leq n \leq N$, the quantities $s_n(1)$, $t_n(1)$, $p_n(1)$, $q_n(1)$ are the known velocity Fourier coefficients on boundary (or at r=1) and ξ, ζ, η, μ are the coefficients from convective terms:

$$\omega v_r = \xi_o + \sum_{n=1}^{N} (\xi_n \cos n\theta + \eta_n \sin n\theta) \qquad (4.18)$$

$$\omega v = \mu_o + \sum_{n=1}^{N} (\mu_n \cos n\theta + \zeta_n \sin n\theta) \qquad (4.19)$$

Once the Fourier coefficients of the velocities and the vorticity are determined, the velocity field and the vorticity field are easily calculated using equations (4.3) - (4.5).

Equations (4.9)-(4.17) are solved using an iterative procedure for the problem of steady flow inside a circle. The Fourier coefficients of the boundary velocities are assumed to be known.

Starting with known values of the Fourier coefficients of the vorticity , α_o^i, α_n^i's, β_n^i's, the superscript "i" being the iteration counter, the following steps constitute one iteration loop.

(i) Determine the boundary values $\alpha_o^i(1)$, $\alpha_n^i(1)$'s and $\beta_n^i(1)$'s.

The boundary values of the velocities need to be satisfied by equations (4.9)-(4.14) during each iteration. Thus with one set of α_o^i, α_n^i's and β_n^i's in R, the boundary values of $\alpha_o^i(1)$, $\alpha_n^i(1)$'s and $\beta_n^i(1)$'s are determined by

$$\int_o^1 \alpha_o r_o \, dr_o = p_o(1) \qquad (4.20)$$

$$\int_o^1 \alpha_n \, r_o^{n+1} \, dr_o = p_n(1) - t_n(1) \tag{4.21}$$

$$\int_o^1 \beta_n \, r_o^{n+1} \, dr_o = s_n(1) + q_n(1) \tag{4.22}$$

The equations (4.20)-(4.22) are the constrains on the boundary vorticity values derived from equations (4.9)-(4.14) when r=1. The $p_o(1)$, $p_n(1)$'s, $q_n(1)$'s, $s_n(1)$'s, $t_n(1)$'s are the Fourier coefficients of the velocities on the boundary which are assumed to be known. With the proper numerical integration of the integrals in equations (4.20)-(4.22), the values of α_o^i, α_n^i's and β_n^i's at r=1 are easily determined.

(ii) Compute the Fourier coefficients of the velocities in R.

With the proper numerical integration, equations (4.9)-(4.14) give explicit, point by point, calculation of s_n^i's, t_n^i's, p_o^2, p_n^i's, q_n^i's in the flow region R.

(iii) Compute the Fourier coefficients of the convective terms.

Because the Fourier coefficients of the velocities and of the vorticity are known at this stage, the Fourier coefficients ξ_o^i, ξ_n^i's, η_n^i's, μ_n^i's, ζ_n^i's can be determined using equations (4.18) and (4.19). The coefficient μ_o need not to be determined because it will not get into the calculation of the Fourier coefficients of the vorticity. This quantity is associated with the static pressure level and it remains arbitrary when the flow is incompressible.

(iv) Compute the vorticity Fourier coefficients α_o^{i+1}, α_n^{i+1}'s and β_n^{i+1}'s in R.

Equations (4.15)-(4.17) permit explicit evaluation of α_o^{i+1}, α_n^{i+1}'s and β_n^{i+1}'s using quadratures if $\alpha_o^i(1)$, $\alpha_n^i(1)$'s, $\beta_n^i(1)$'s and ξ_o^i, ξ_n^i's, ζ_n^i's, μ_n^i's, η_n^i's are known on the right hand side of these equations.

In the above iteration loop, it was found necessary to employ a point under-relaxation technique to obtain converged solutions. The new values of α_o^{i+1}, α_n^{i+1}'s and β_n^{i+1}'s in R are computed from

$$\alpha_o^{i+1} = \lambda_o \alpha_o^* + (1 - \lambda_o)\alpha_o^i \tag{4.23}$$

$$\alpha_n^{i+1} = \lambda \alpha_n^* + (1 - \lambda)\alpha_n^i \tag{4.24}$$

$$\beta_n^{i+1} = \lambda \beta_n^* + (1 - \lambda)\alpha_n^i \tag{4.25}$$

where $1 \leq n \leq N$, λ_o, λ are the under-relaxation parameter and α_o^*, α_n^*'s and β_n^*'s are the values computed in step (iv).

Converged solution of a particular problem is assumed to exist when the following criterion is satisfied.

$$D_{max} = \max_j \left| \alpha_{oj}^{i+1} - \alpha_{oj}^i, \alpha_{nj}^{i+1} - \alpha_{nj}^1, \beta_{nj}^{i+1} - \beta_{nj}^i \right| \leq \varepsilon; \quad \left| \leq n \leq N \right. \tag{4.26}$$

where subscript "j" denotes the Fourier coefficients at $r=r_j (r_j < 1)$. A good value for ε was found to be 10^{-4}.

The new numerical approach was tested and some of its features are discussed as the Reynolds number increases.

(i) Flow without separation

This is a closed streamline flow problem. The boundary velocities are:

$$v_{r_b} = 0 \tag{4.27}$$

$$v_{\theta_b} = \frac{1}{2} + \frac{1}{2}\cos\theta \qquad (4.28)$$

This example was treated by Burggraf (12). He used the Oseen approximation, which took a rigid-body rotation as the basic flow. The solution of such linearized differential equation is only applicable to the case in which the whole flow field forms a singular circular eddy. The asymptotic vorticity value of the inviscid core at high Re he obtained is too low compared to Batchelor's (13) suggested model, which is proven to be quite adequate by Imai (14) and the present calculations.

Using the present approach, converged solutions are obtained at different Reynolds numbers, from 0 to 1,000. The number of iterations, under-relaxation parameters and stream function values at the origin are presented in Table 6. The grid system is equivalent to 21 x 41 mesh points. The variation of maximum deviation D_{max} (in equation 4.22) versus the iteration number is shown in Figure 13 for Re = 1,000. In this case, the process of escalating the Reynolds number has not been used, i.e., the lower Reynolds number solution is not utilized as the initial solution to start the iteration procedure. This has otherwise been very effective in the calculations.

The computer time for each iteration is about 1 second. Compared with the computer time that Imai had used at different Reynolds numbers (14) this approach showed speedup by a factor 2 to 3.

The streamline patterns at Re = 0, 50, 300 are in Figure 14. The vorticity values at θ = 0 with different Re are presented in Figure 15. As Re increases, the value of vorticity in the inviscid core eventually goes to the value suggested by Batchelor and Wood (13)*. Also in this figure,

* Wood actually calculated this value exactly after using the Von Mises transformation in the closed boundary layer region as $Re \to \infty$. Stated simply, the vorticity value in the inviscid core is determined by the root-mean-square speed of the closed boundary surface.

the boundary layer structure is clearly seen as the Reynolds number increases. Figure 16 shows the migration of the vortex center with increasing Reynolds number. It is clearly seen that the ultimate location of the vortex center for Re $\to\infty$ will be the center of the circle.

(ii) Flow consisting of two unsymmetric recirculating regions

This is also a flow with closed streamlines. The boundary conditions are

$$v_{r_b} = 0 \tag{4.29}$$

$$v_{\theta_b} = \frac{1}{3} + \frac{2}{3}\cos\theta \tag{4.30}$$

The streamlines and vorticity values at different Reynolds numbers are in Figure 17and Figure 18. Notice that the asymptotic flow pattern for high Reynolds numbers cannot be found in a simple way as in the last example, since the form of the separation line is not known in advance.

(iii) Unflow - outflow problem

The flow problem together with the boundary velocities are depicted in Figure 19 In this case, the flow is symmetric about the x-axis, thus the Fourier expression could be simplified to

$$\omega = \sum_{n=1}^{N} \beta_n \sin n\theta \tag{4.31}$$

$$v_r = \sum_{n=1}^{N} s_n \cos n\theta \tag{4.32}$$

$$v_o = \sum_{n=1}^{N} q_n \sin n\theta \tag{4.33}$$

and

$$\omega v_r = \sum_{n=1}^{N} n \sin n\theta \tag{4.34}$$

$$\omega v_\theta = \mu + \sum_{n=1}^{N} \mu_n \cos n\theta \tag{4.35}$$

Due to the velocity discontinuity at the boundary, a larger number of grid points is used in the agrimuthal direction. The grid system used in this case is equivalent to 21 x 81 mesh points in the whole plane. The 81 points along the circumferential direction were proven adequate. The use of 121 points in that direction generated differences of the streamfunction values less than 1 percent compared with the results that used 81 points. The effect of the grid size in radial direction has also been tested, as shown in Table 7. The computer time for each iteration, on the 21 x 81 grid system, is about 1.3 seconds, a CDC 6600.

The streamline patterns with different Reynolds numbers are depicted in Figure 20. The occurrence and growth of the separation bubble are clearly seen in this figure, as the Reynolds number increases.

Table 6

Re	λ_o	λ	ITER	ψ_o
0	.1	.1	3	.250
16	.1	.1	56	.256
32	.1	.1	51	.268
50	.1	.1	40	.279
75	.1	.1	62	.289
100	.1	.1	66	.293
128	.1	.1	128	.295
200	.01	.05	430	.296
300	.001	.01	475	.297
1000	.001	.001	4114	.289

Table 7

Re	Δr	λ, λ_o	ITER	ψ_{MAX}
100	.1	.2	47	.111
	.05	.1	80	.123
200	.1	.06	130	.116
	.05	.05	211	.132
300	.1	.03	230	.115
	.05	.002	440	.131

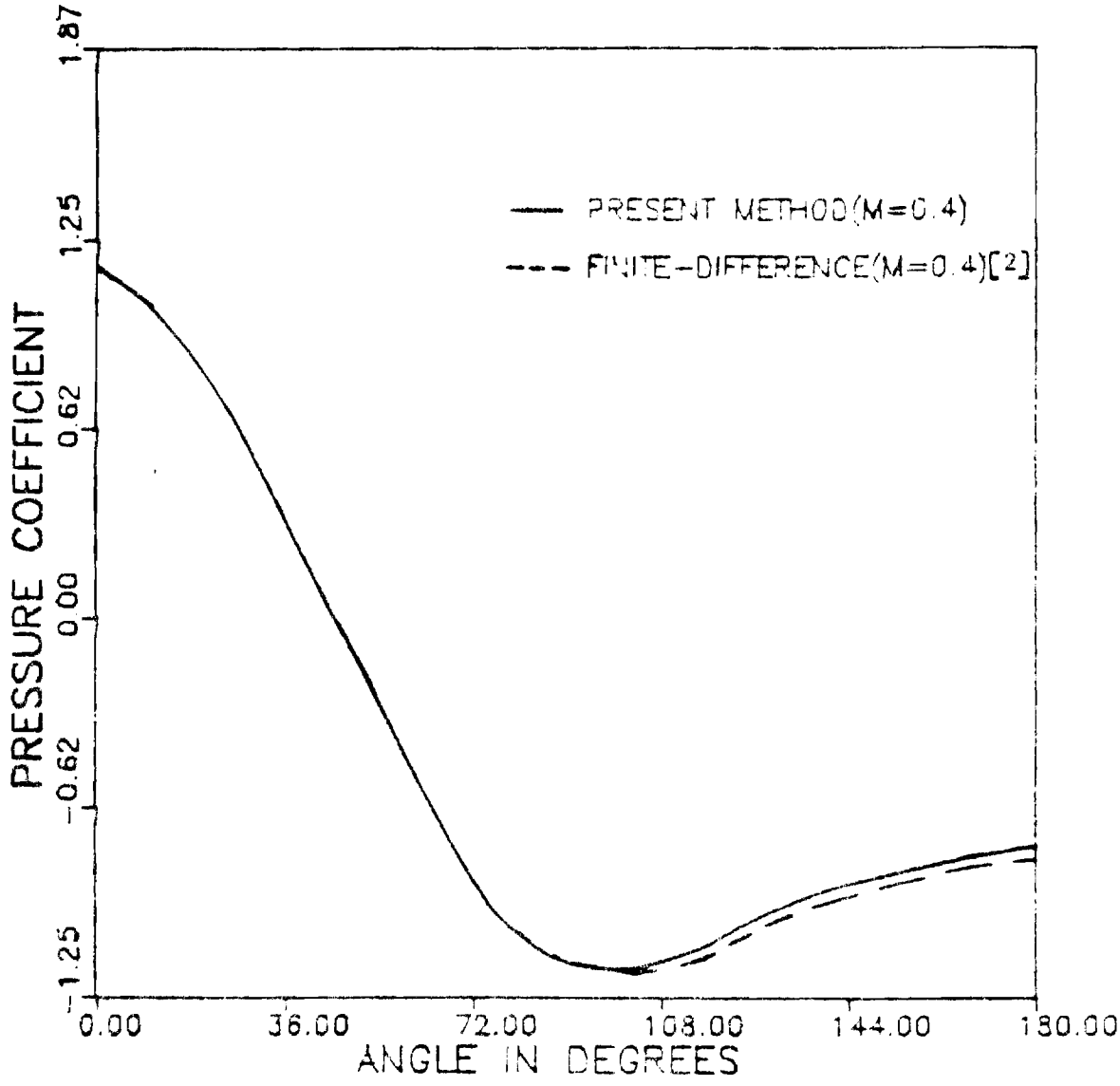

FIGURE (1) PRESSURE DISTRIBUTIONS ON CIRCULAR CYLINDER

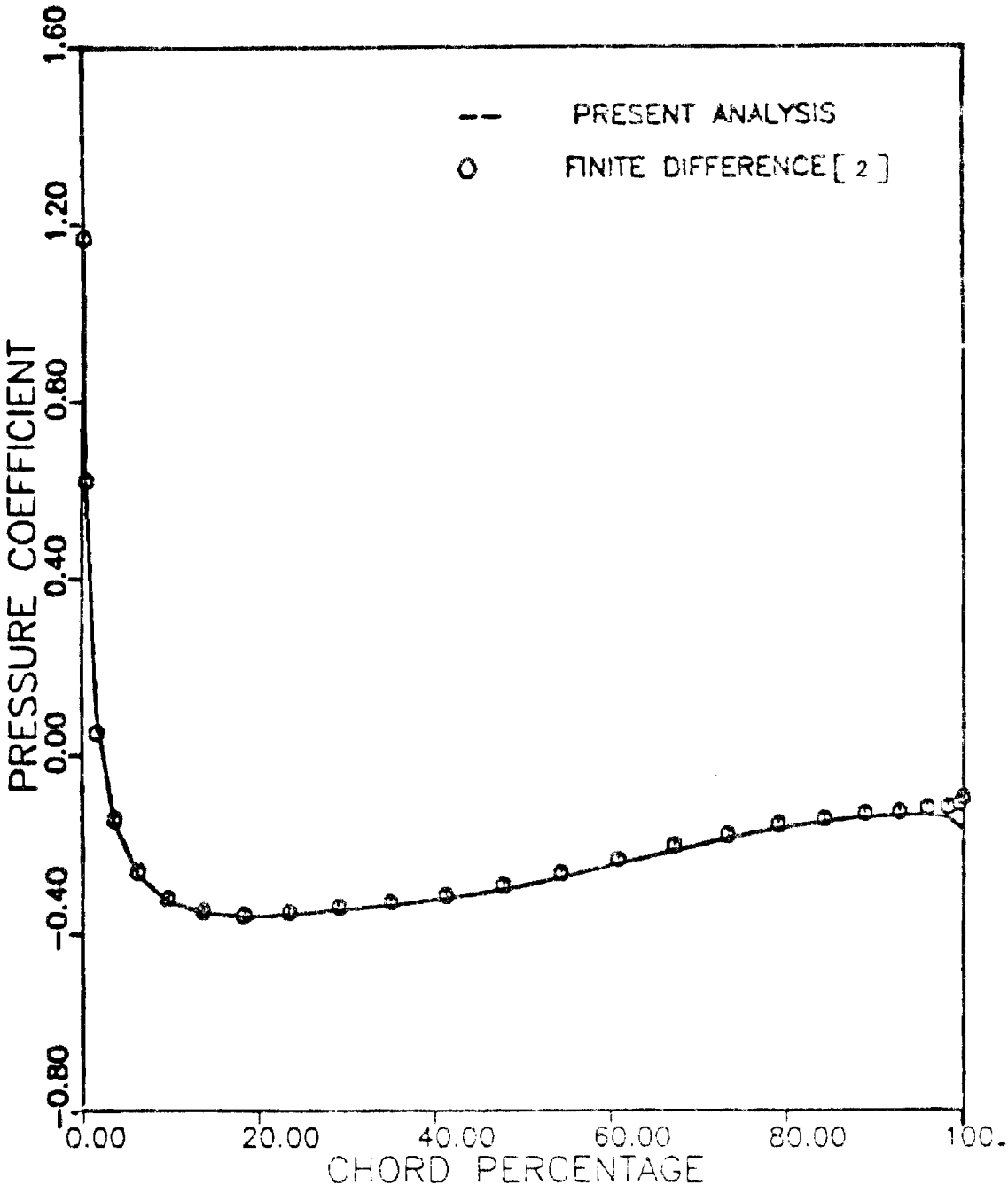

FIGURE(2) JOUKOWSKI 9%AIRFOIL AT ZERO ANGLE OF ATTACK

SURFACE PRESSURE DISTRIBUTION AT STEADY STATE

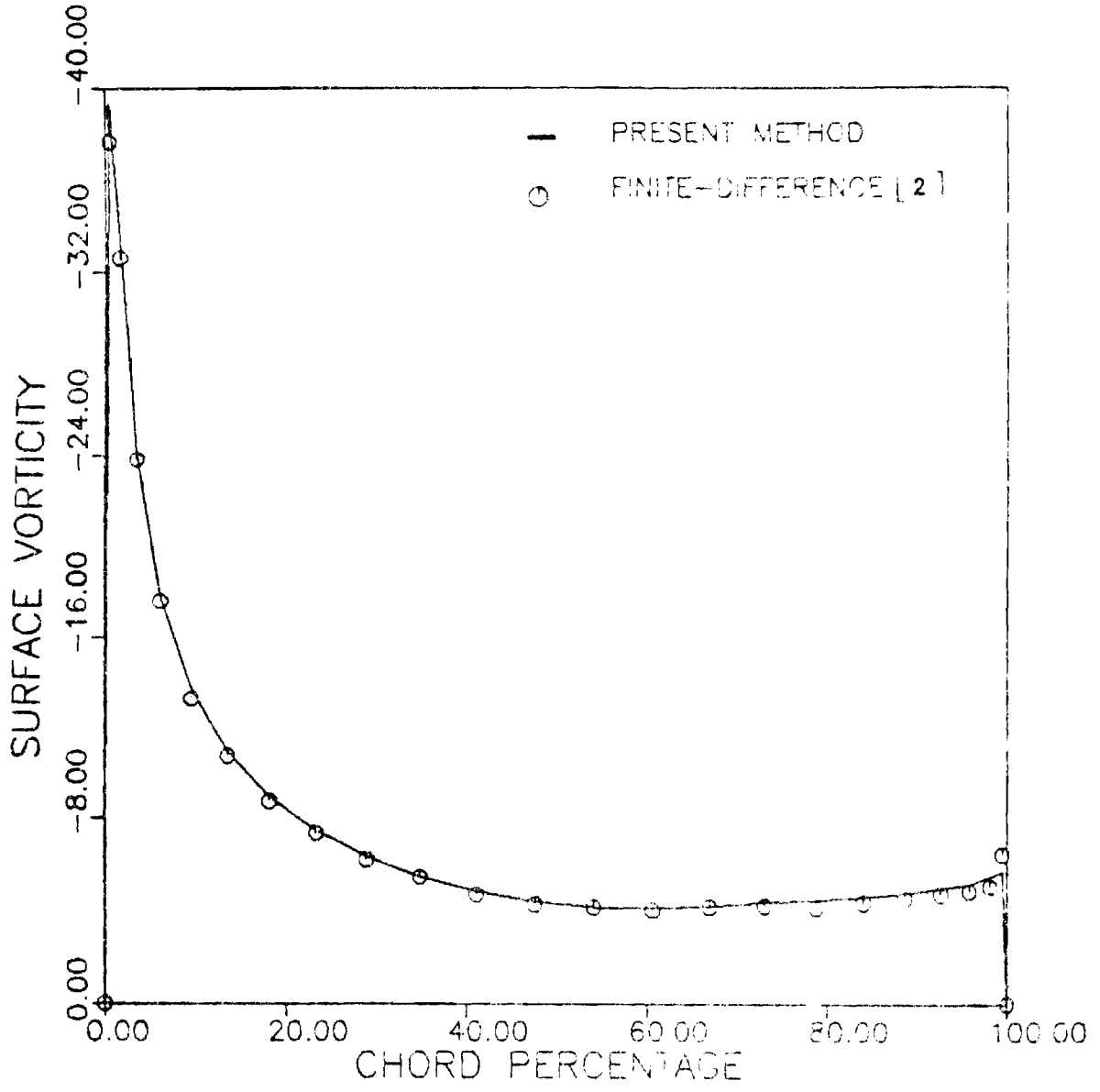

FIGURE(3) JOUKOWSKI 9% AIRFOIL AT ZERO ANGLE OF ATTACK--
SURFACE VORTICITY DISTRIBUTION AT STEADY STATE

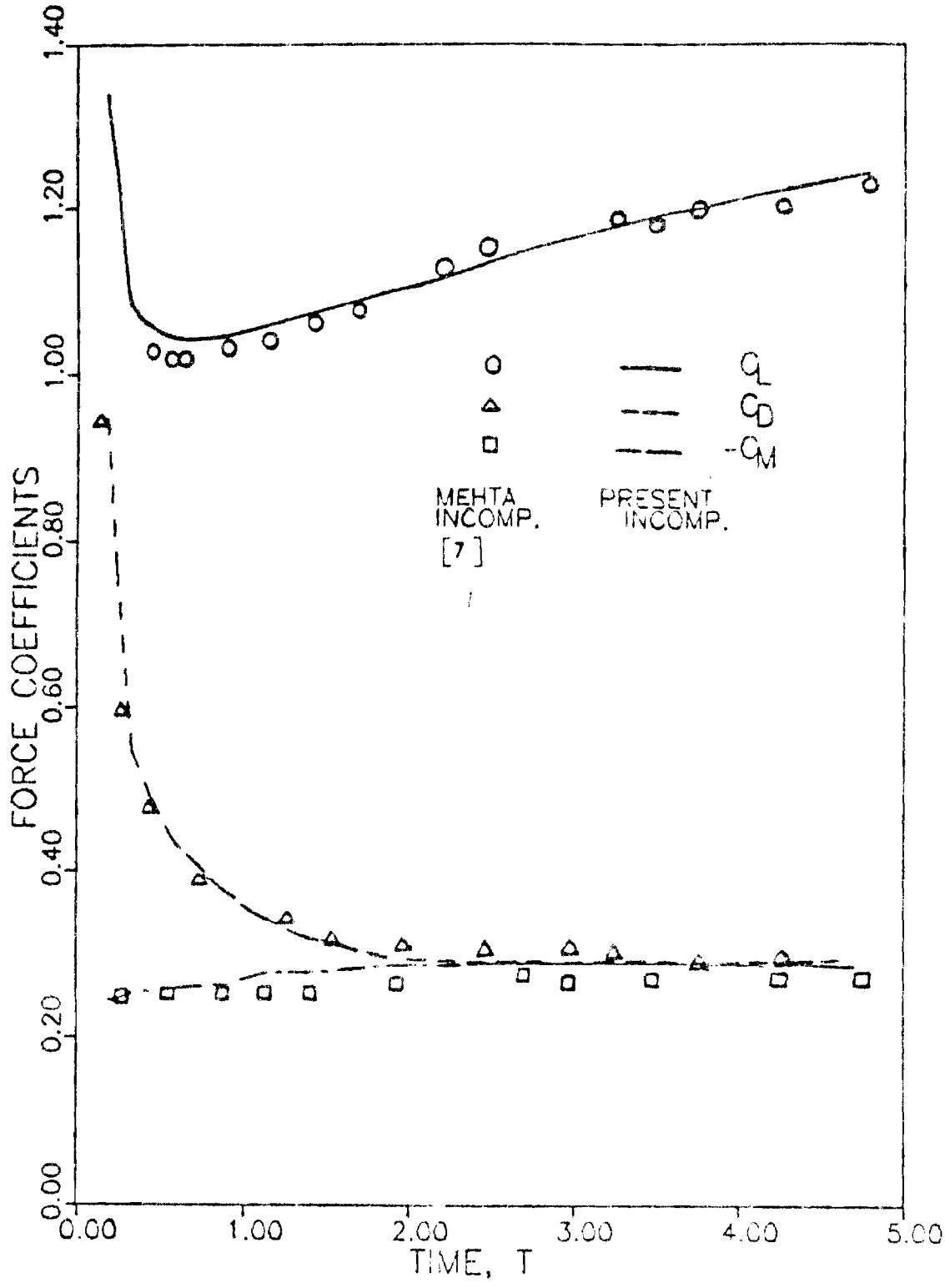

FIGURE (4) COMPARISON OF FORCE COEFFICIENTS BETWEEN THE PRESENT INCOMPRESSIBLE RESULTS AND THOSE OF REFERENCE

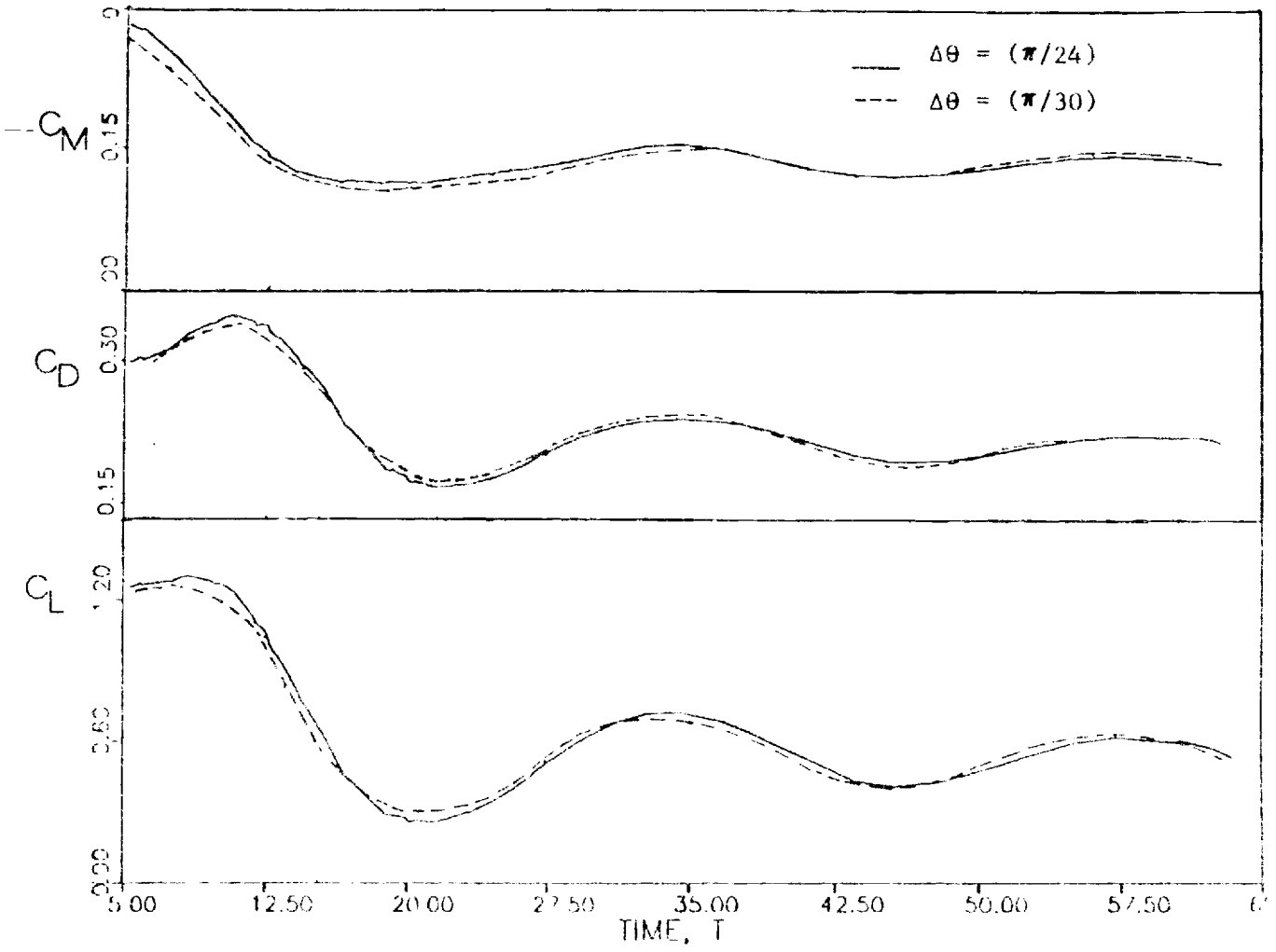

FIGURE(5). TIME HISTORIES OF LOADS

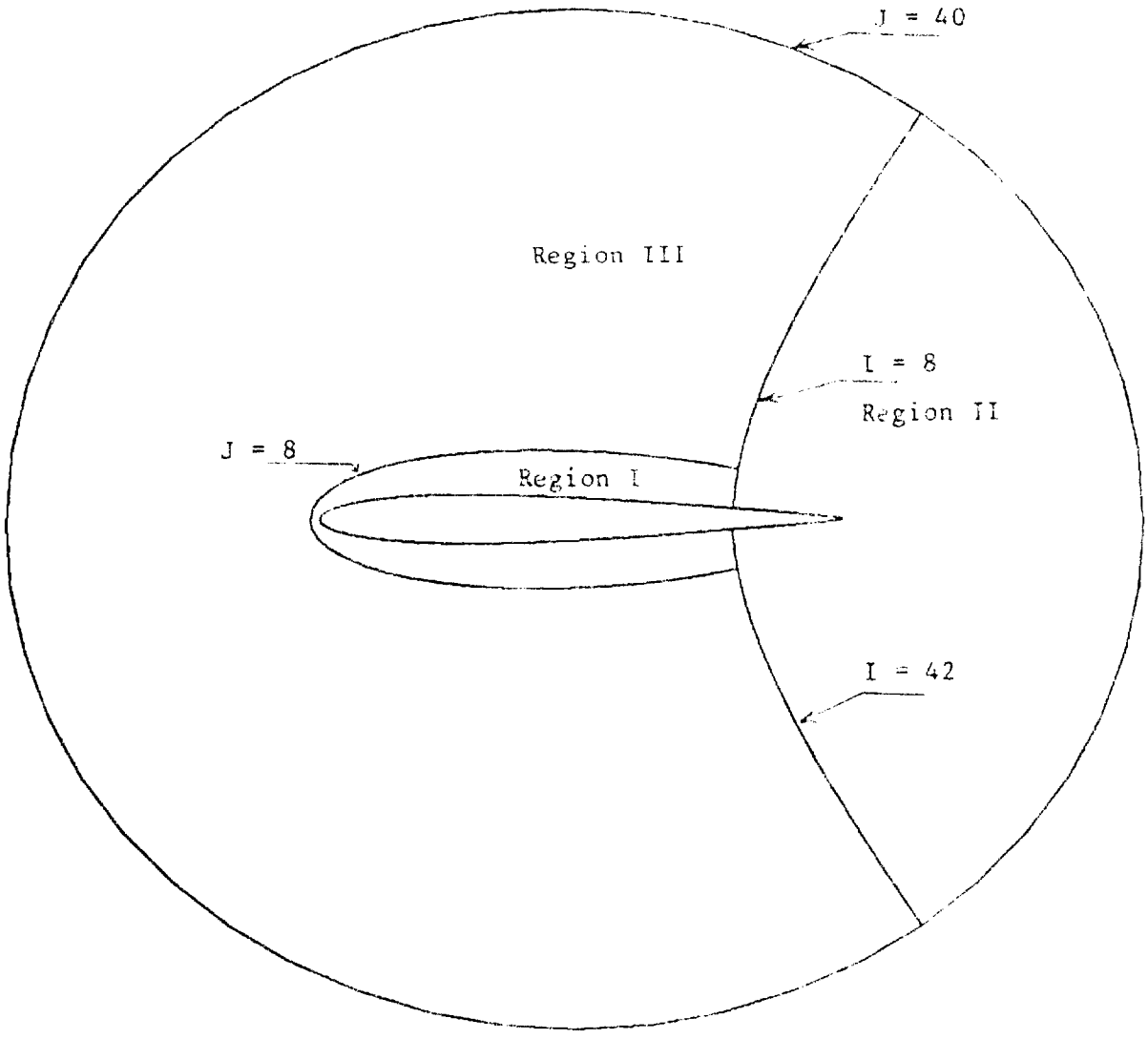

Region I The Integral Relation (3.30) is used to Calculate V_θ

Region II The Integral Relation (3.30) is used to Calculate V_θ

Region III Finite-Difference Equation (3.34) is used to Calculate V_θ

FIGURE (6) SEGMENTATION OF KINEMATICS AT LATE TIME LEVELS

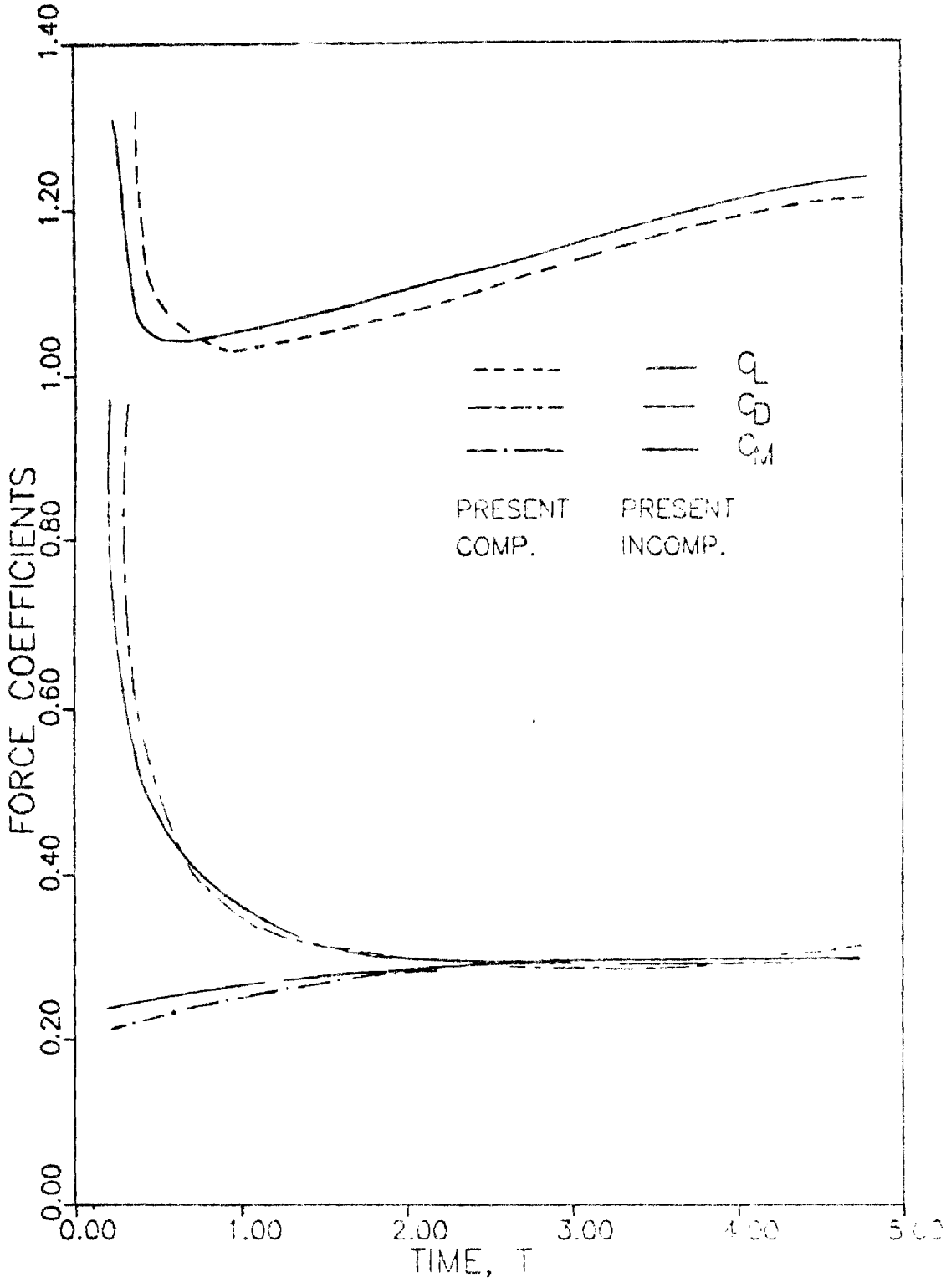

FIGURE(7) TIME HISTORIES OF LOADS , T=0. TO T=5.0

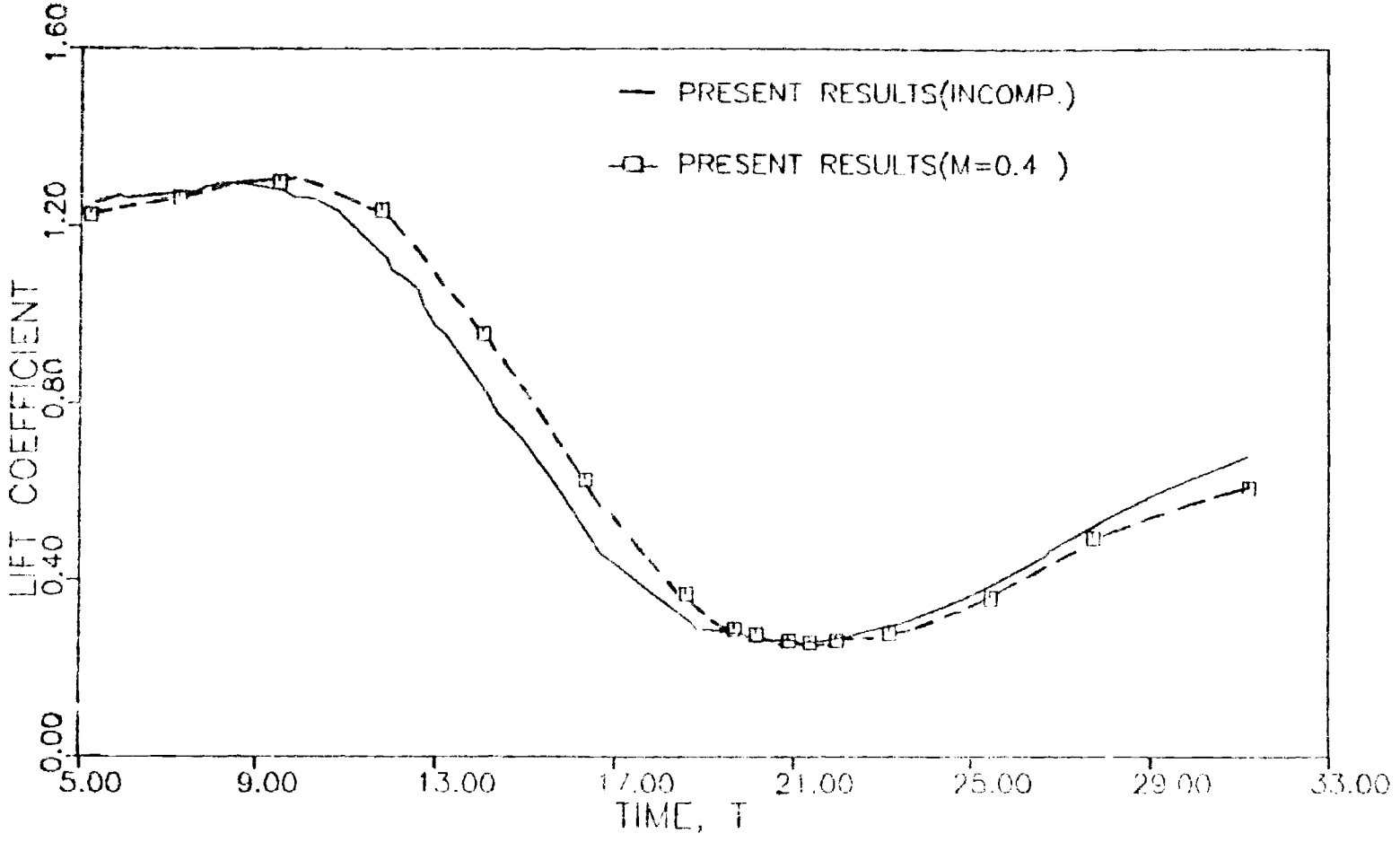

FIGURE(8) TIME HISTORIES OF LOADS

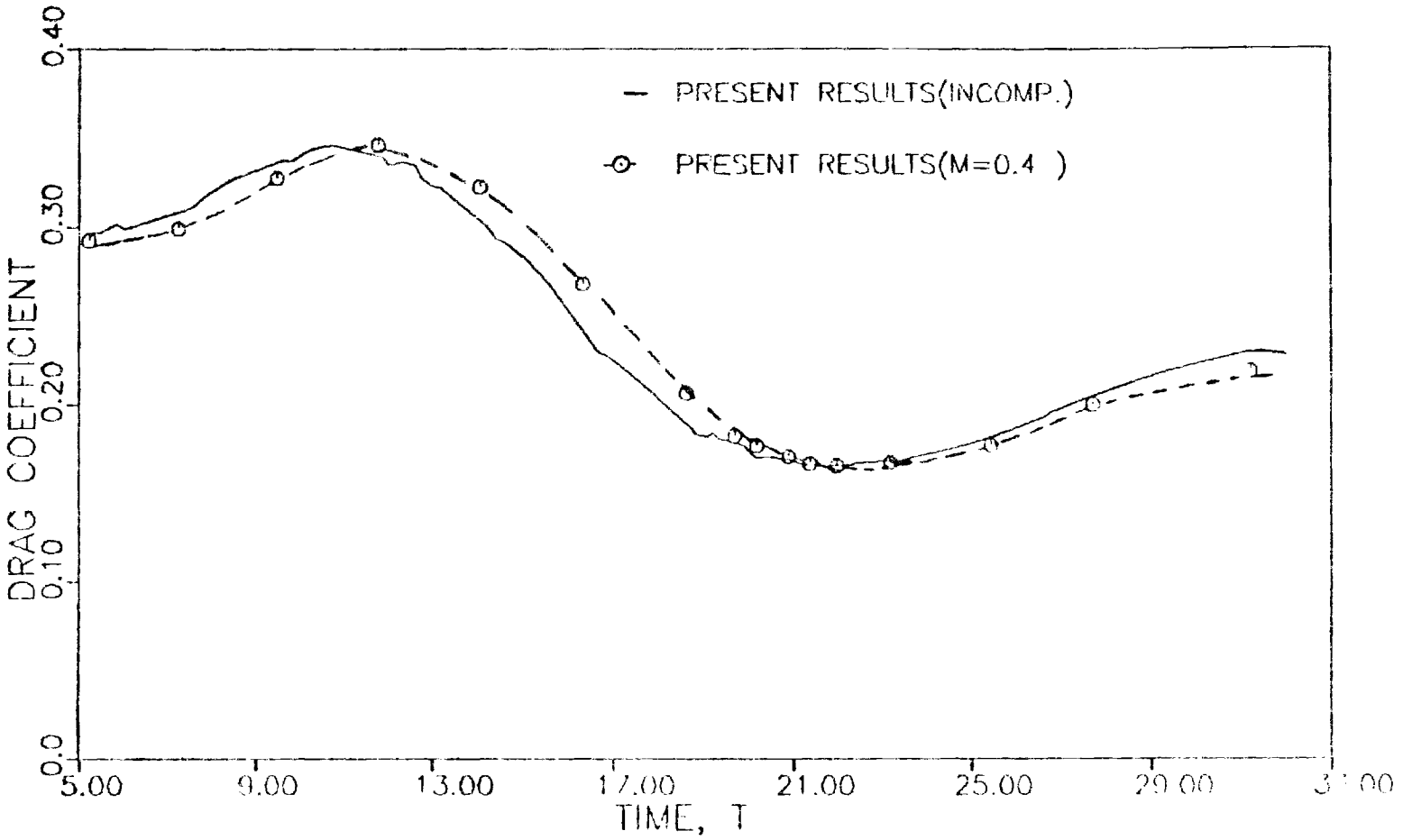

FIGURE(9). TIME HISTORIES OF LOADS

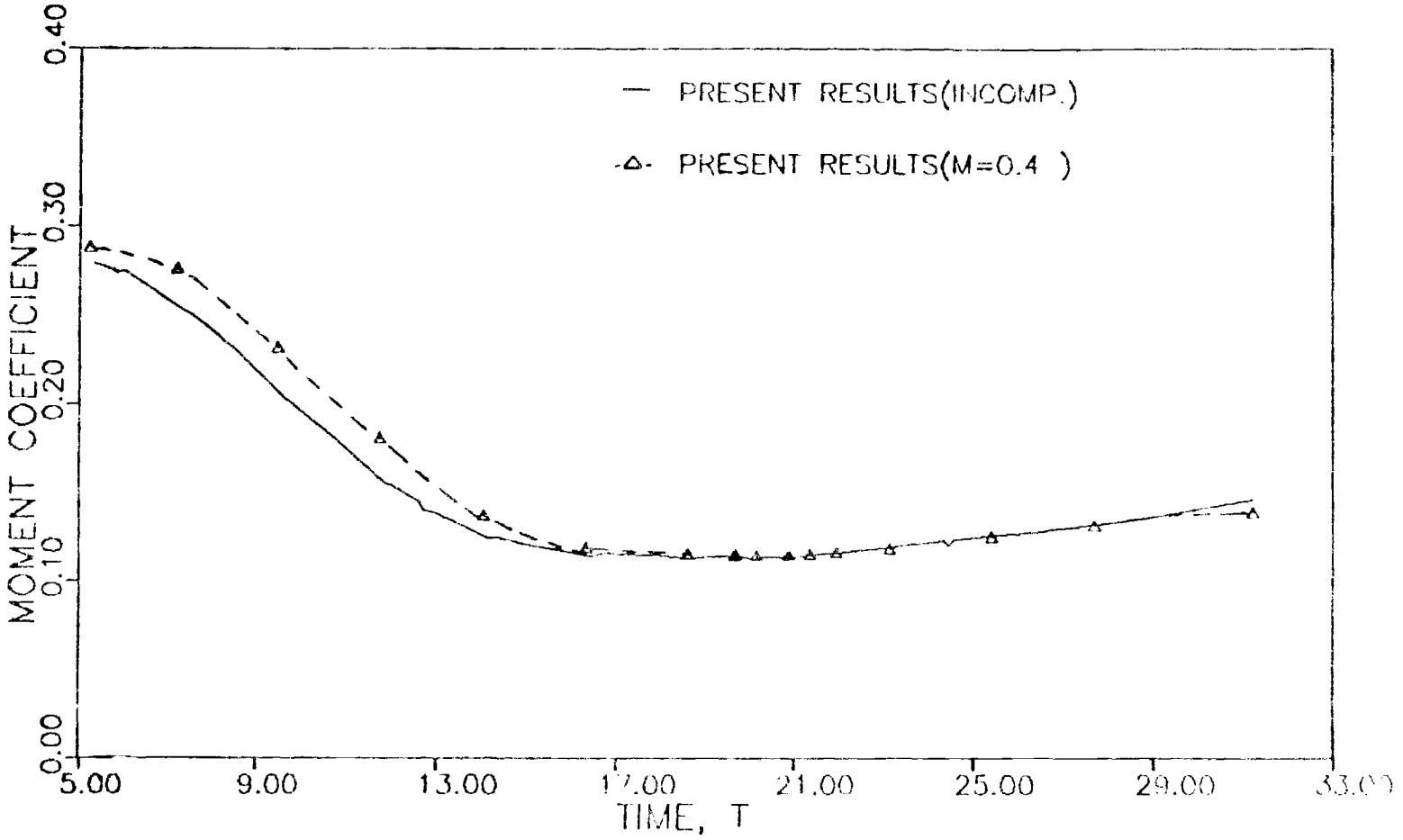

FIGURE(10) TIME HISTORIES OF LOADS

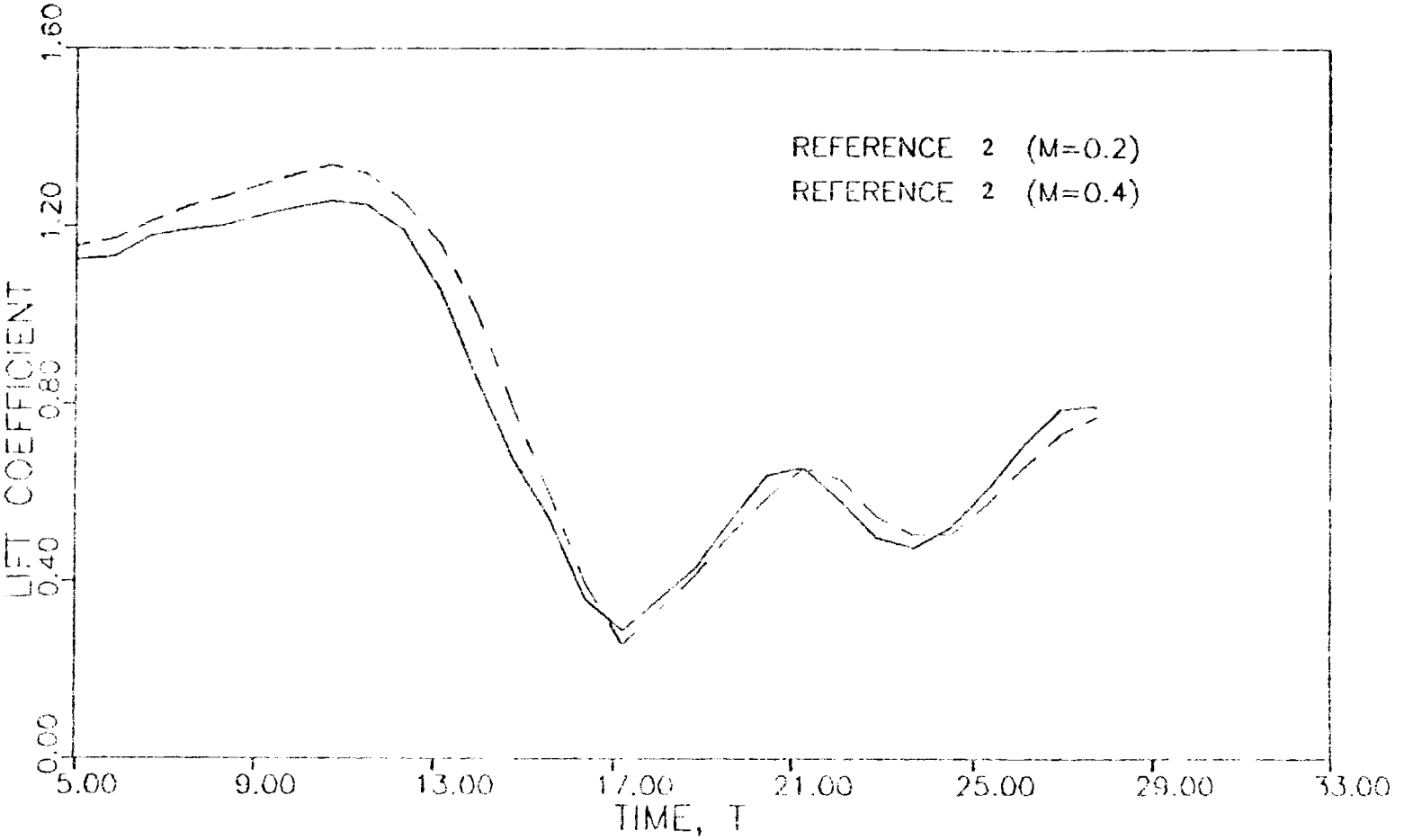

FIGURE(11) TIME HISTORIES OF LOADS

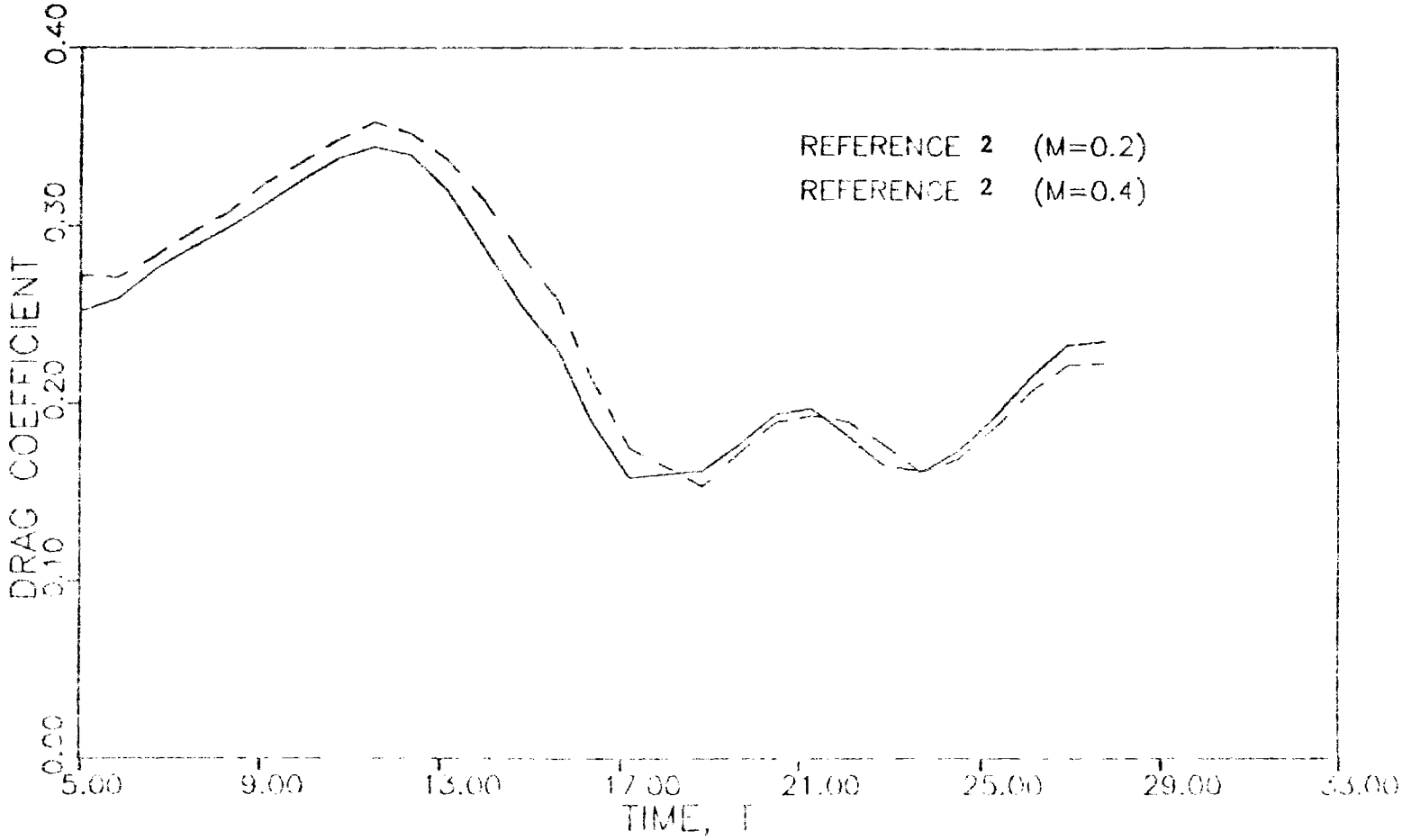

FIGURE(12) TIME HISTORIES OF LOADS

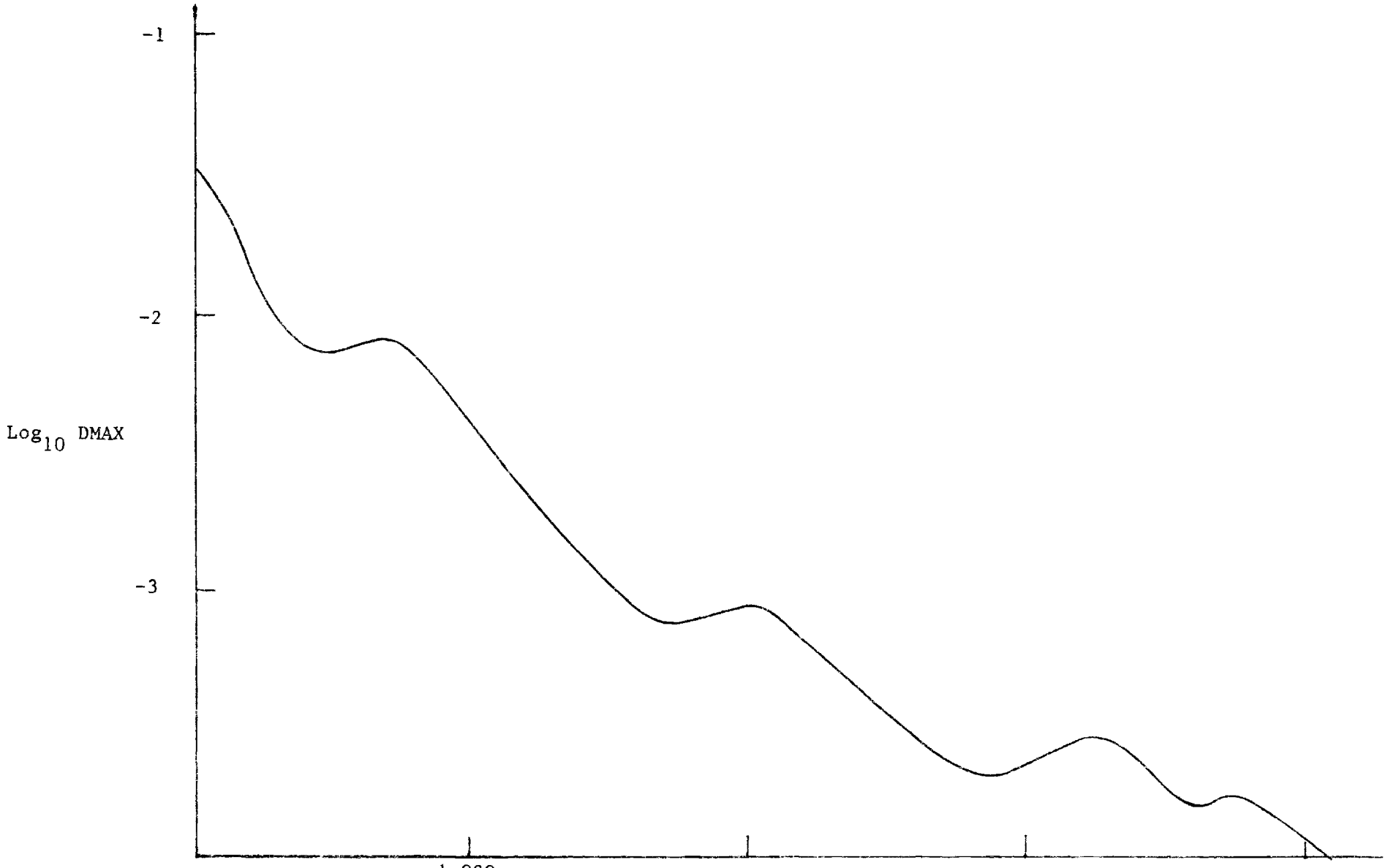

Figure 13

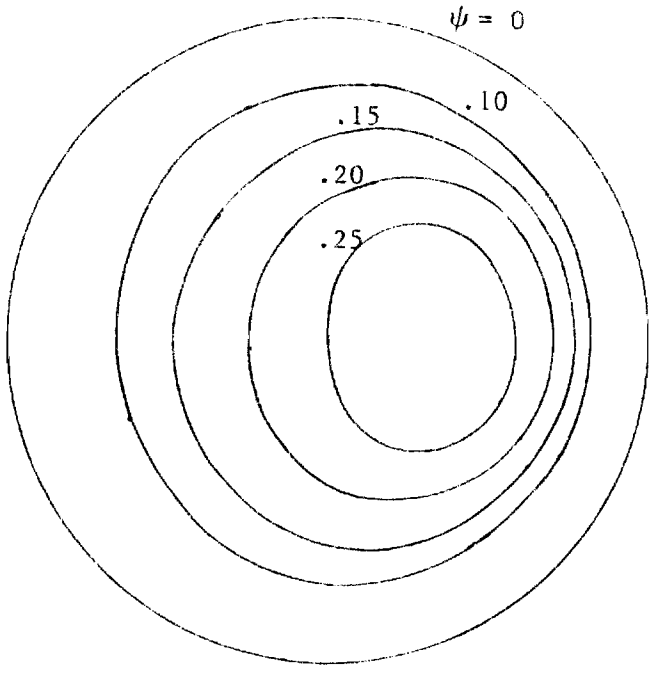

$R_e \longrightarrow 0$

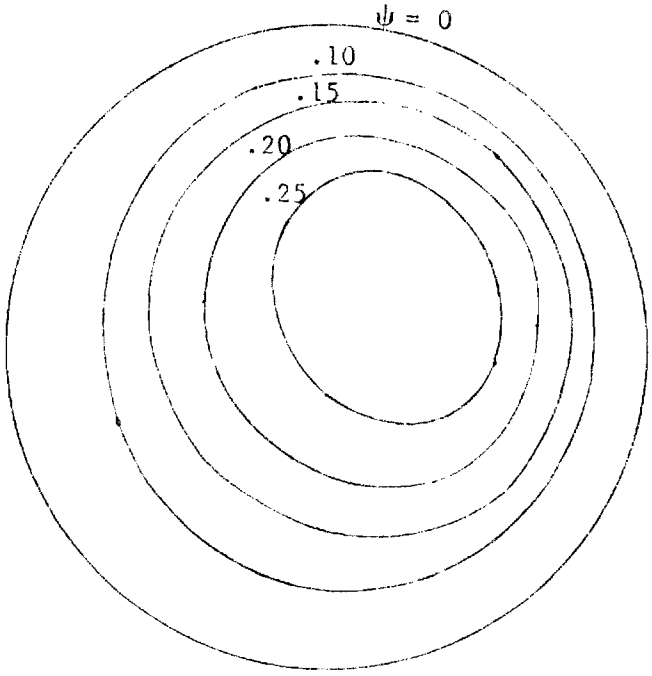

$R_e = 50$

Figure 14A

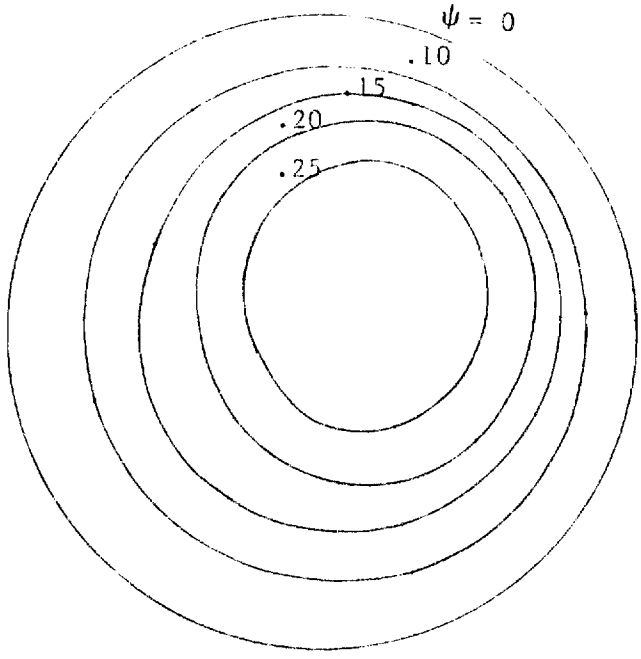

$R_e = 300$

Figure 14B

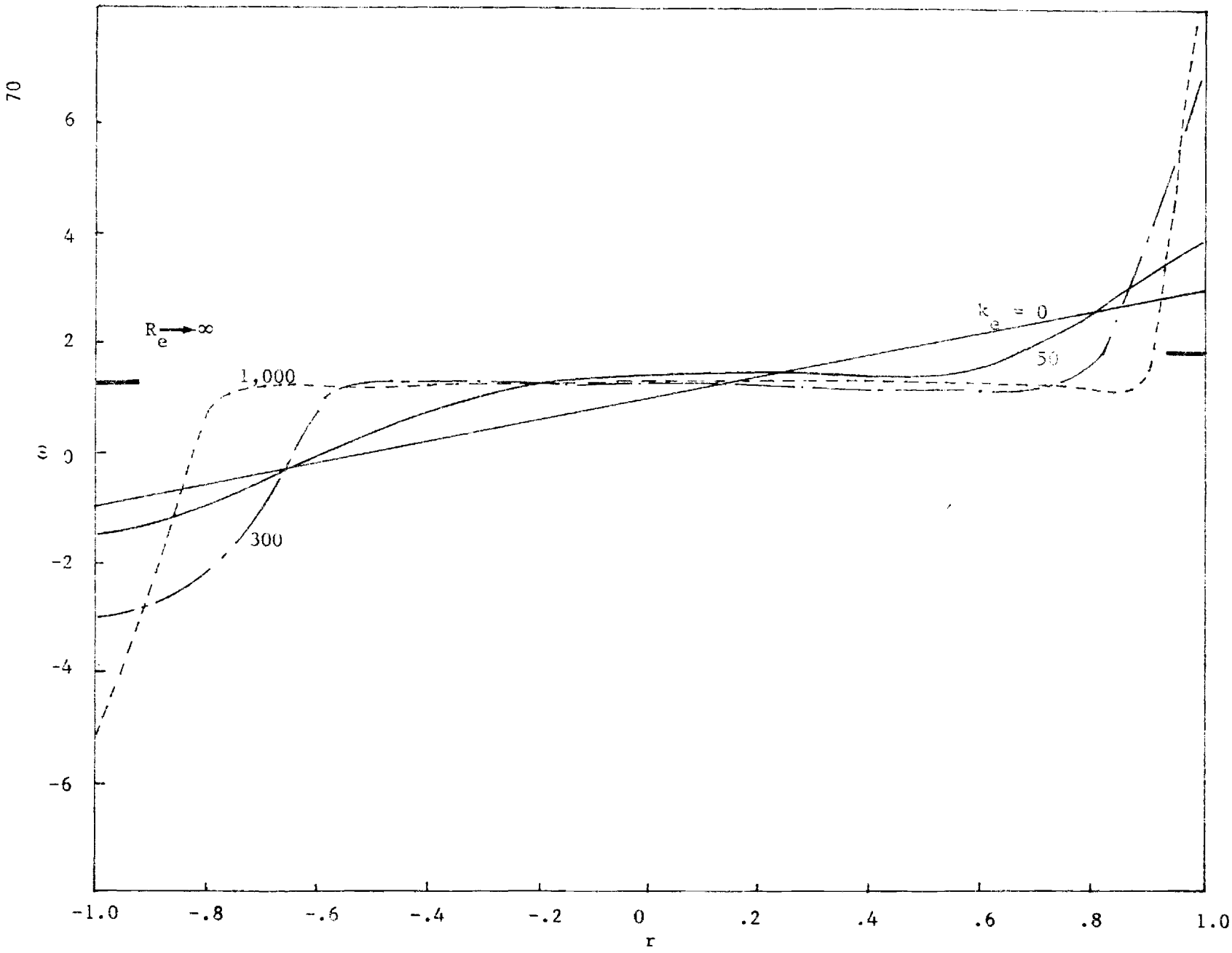

Figure 15

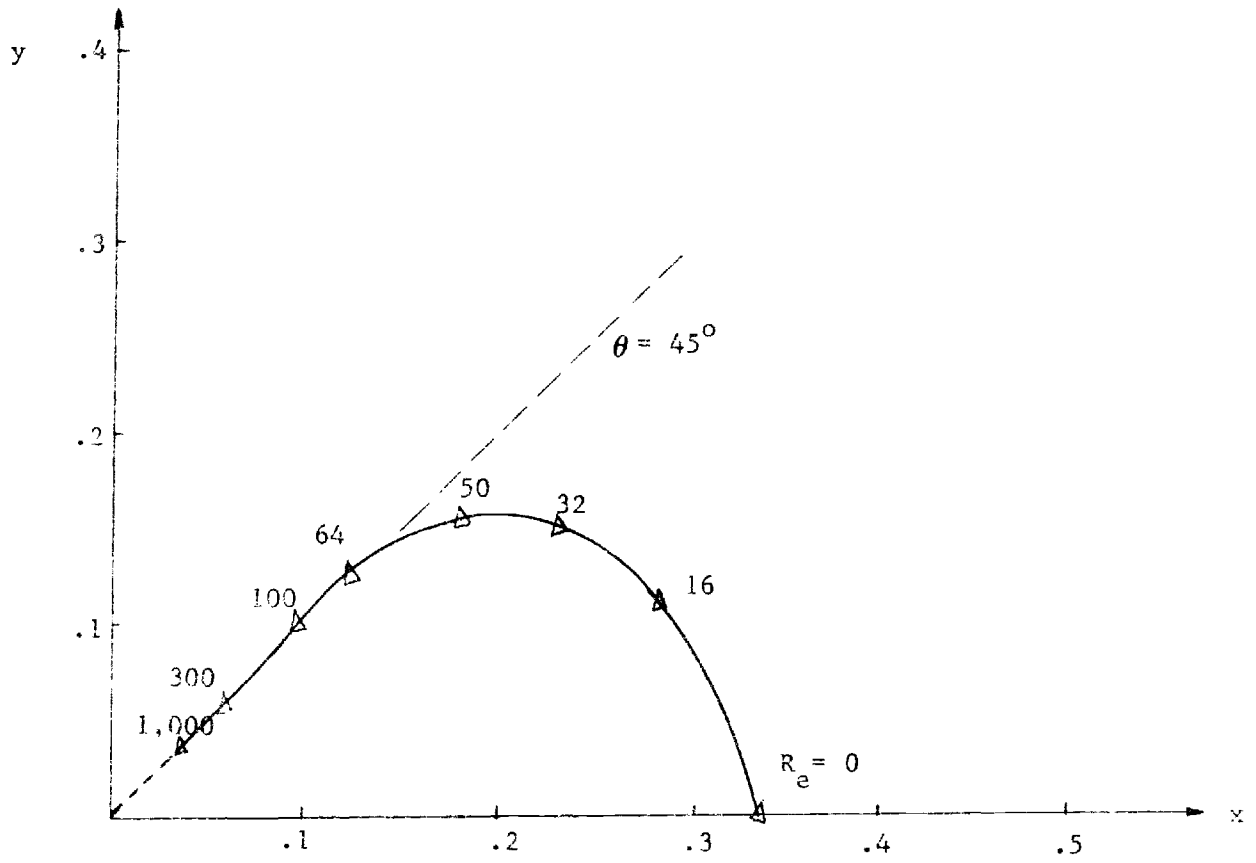

Figure 16

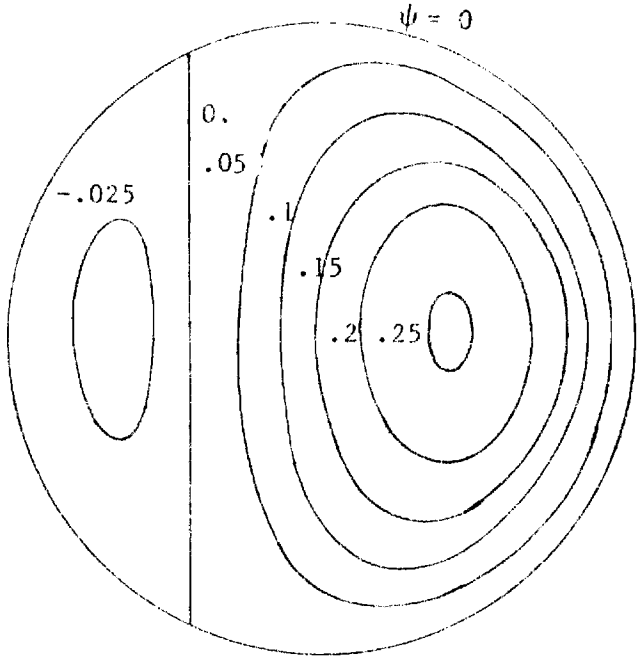

$R_e = 0$

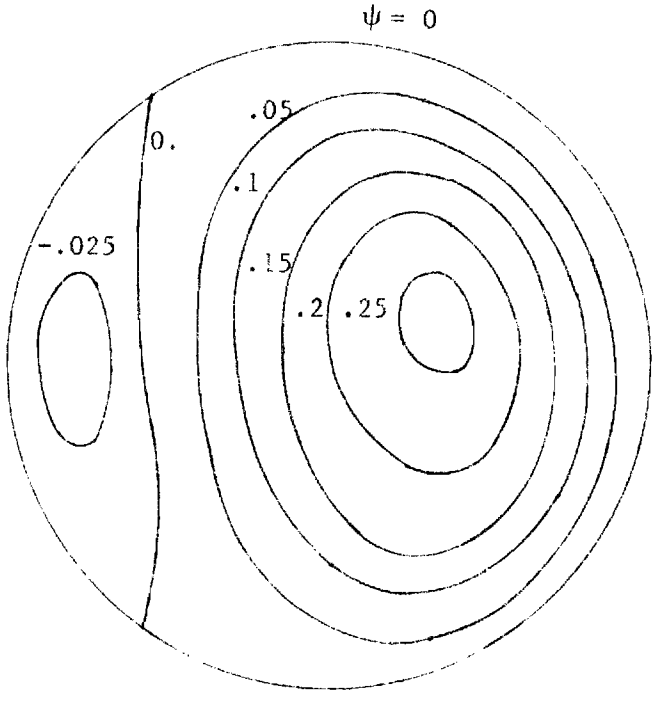

$R_e = 32$

Figure 17A

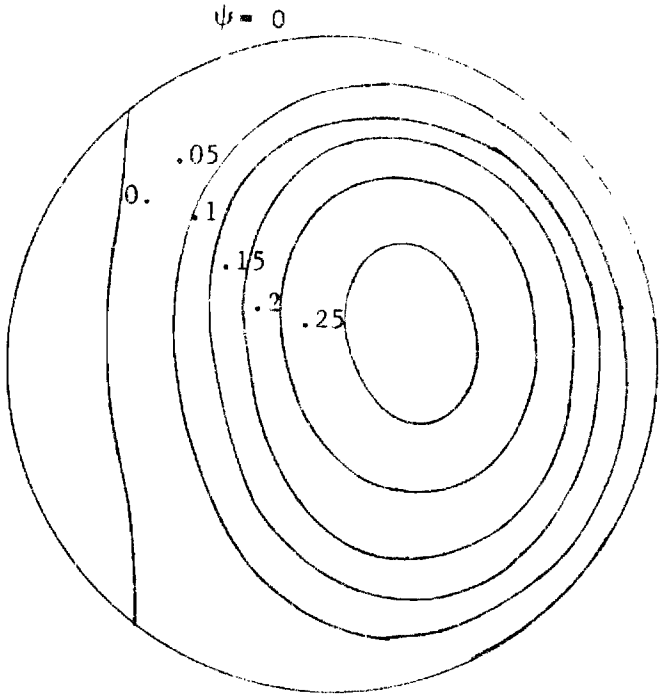

$R_e = 200$

Figure 17B

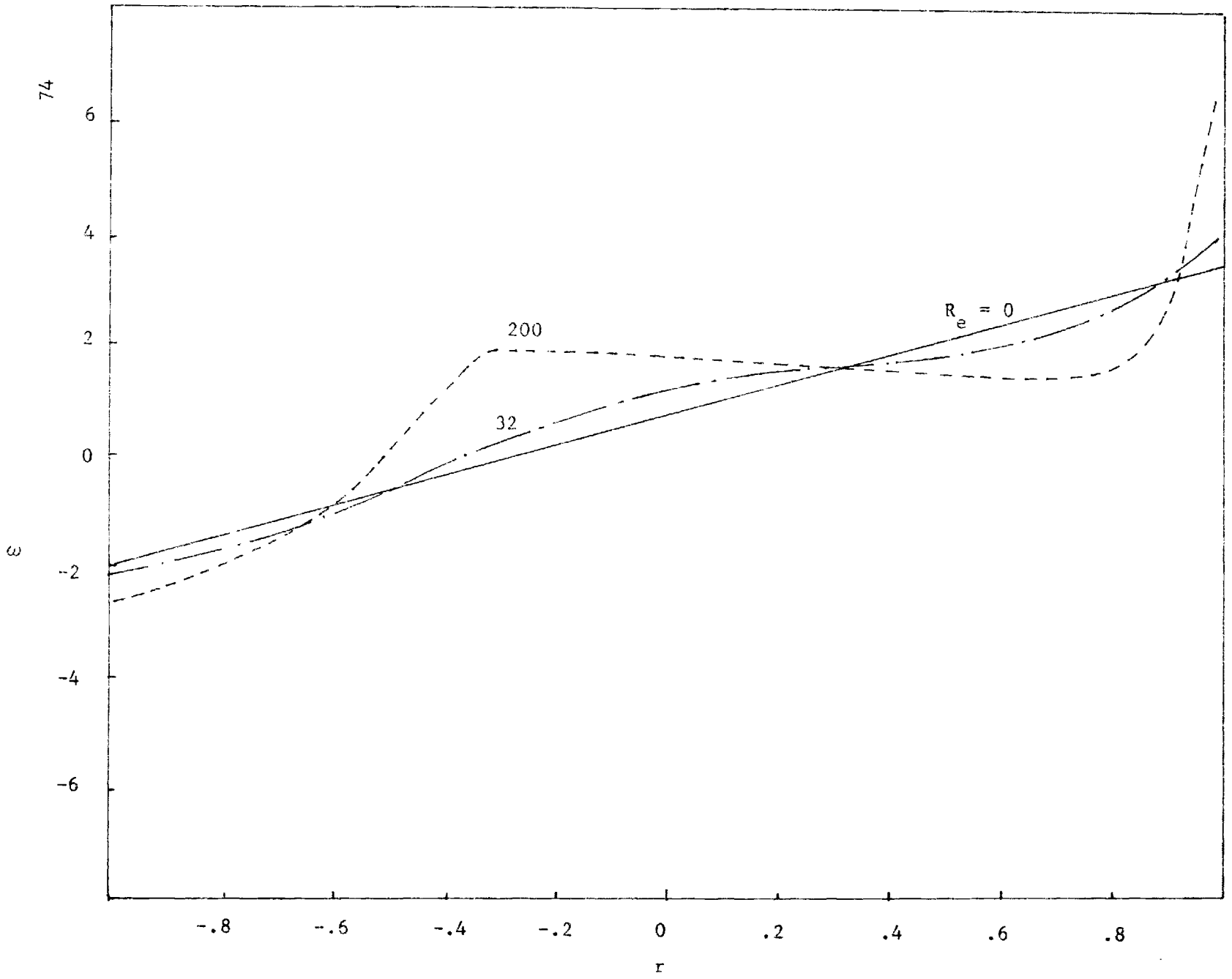

Figure 18

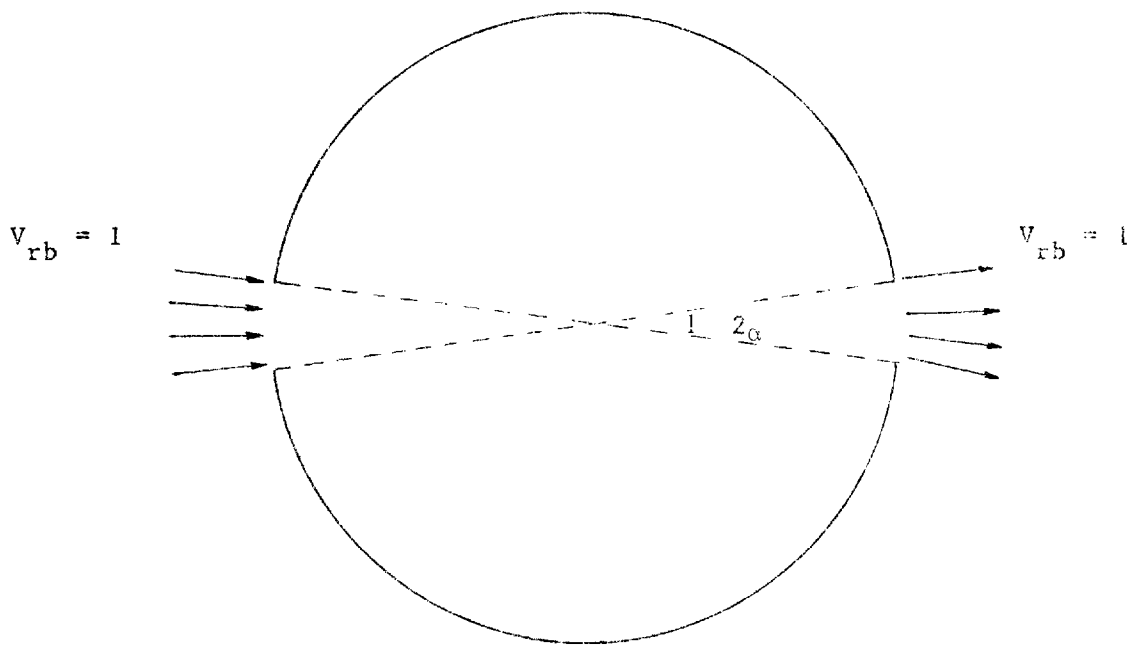

$$\alpha = 6^{\circ}$$

$$V_{\theta b} = 0$$

$$V_{rb} = \sum_{n=1}^{N} S_n(1) \cos\theta$$

$$S_n(1) = \frac{4}{n\pi} \sin n\alpha \qquad n=1,3,5\ldots$$

$$S_n(1) = 0 \qquad n=0,2,4,\ldots$$

Figure 19

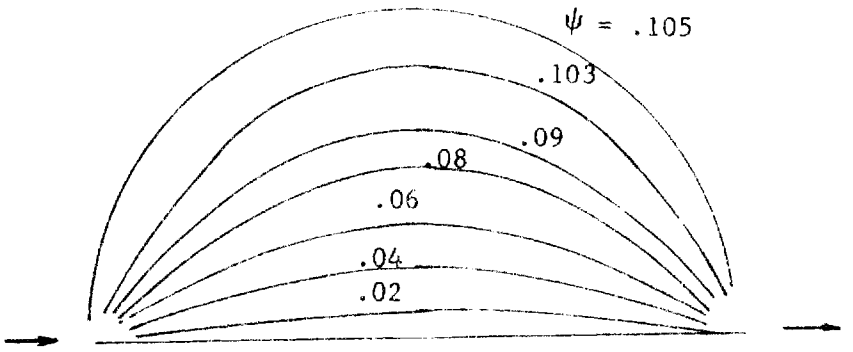

$R_e = 0$

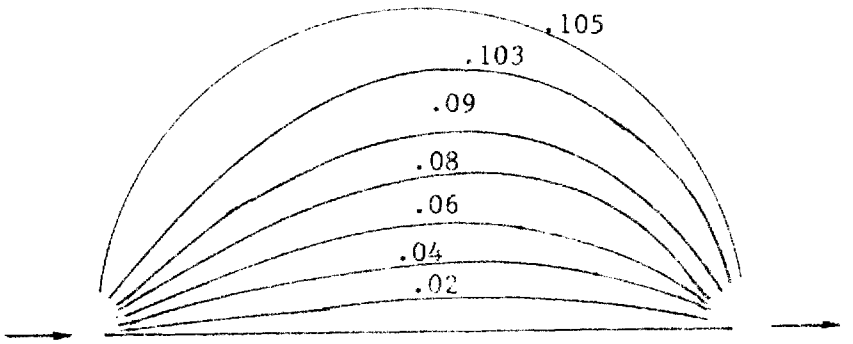

$R_e = 20$

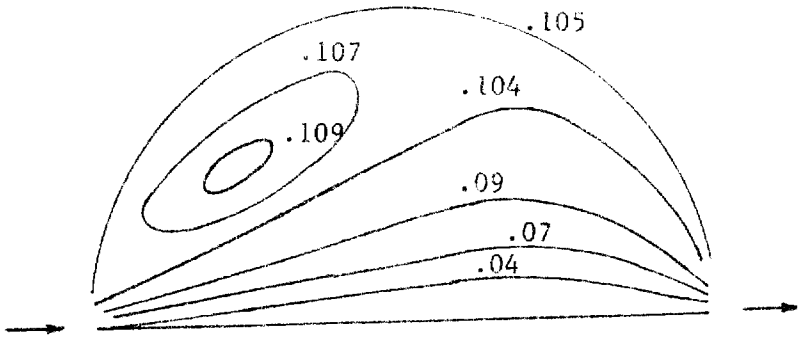

$R_e = 50$

Figure 20A

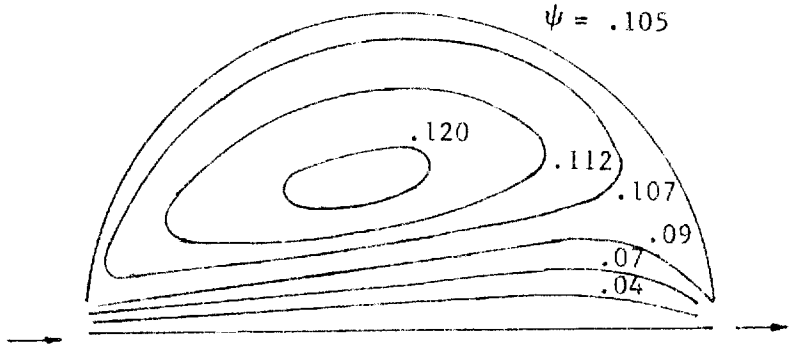

$R_e = 100$

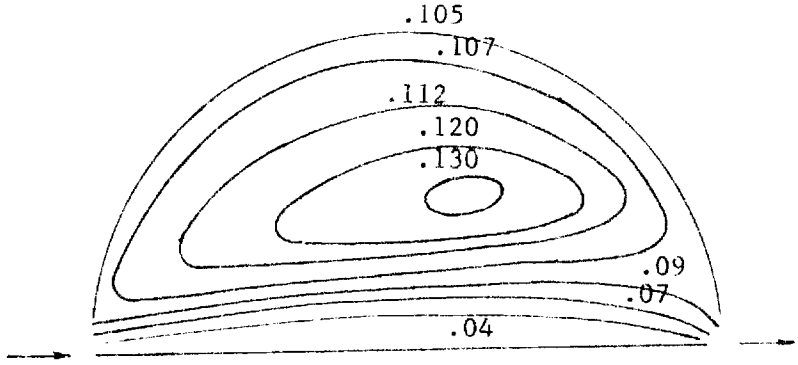

$R_e = 300$

Figure 20B

APPENDIX A

DERIVATION OF THE KINETIC TRANSPORT EQUATIONS

(1) The Vorticity Transport Equation

The vorticity transport equation (2.17) may be written as

$$\frac{\partial \omega}{\partial t} = \vec{\nabla} \times (\vec{v} \times \vec{\omega}) + \frac{(\gamma-1)}{\gamma} \vec{\nabla} \ln\rho \times \vec{\nabla} h + \frac{1}{Re} \vec{\nabla} \times (\frac{1}{\rho} \vec{\nabla} . \vec{\tau}) \qquad (A.1)$$

For two-dimensional flow, we have

$$\vec{\nabla} \times (\frac{1}{\rho} \vec{\nabla} . \vec{\tau}) = \frac{\partial}{\partial x} (\frac{1}{\rho} \frac{\partial}{\partial x} (\mu \frac{\partial u}{\partial y} + \mu \frac{\partial v}{\partial x}) + \frac{1}{\rho} \frac{\partial}{\partial y} (2\mu \frac{\partial v}{\partial y} - \frac{2}{3} \mu\beta)$$

$$- \frac{\partial}{\partial y} (\frac{1}{\rho} \frac{\partial}{\partial x} (2\mu \frac{\partial u}{\partial x} - \frac{2}{3} \mu\beta) + \frac{1}{\rho} \frac{\partial}{\partial y} (\mu \frac{\partial u}{\partial y} + \mu \frac{\partial v}{\partial x}) \qquad (A.2)$$

and

$$\vec{\nabla} \times (\vec{v} \times \vec{\omega}) = - (\vec{V} . \vec{\nabla} \vec{\omega} + \omega\beta) = - \vec{\nabla} . (\vec{V}\omega) \qquad (A.3)$$

Upon differentiating the terms in equation (A-2) it reduces to

$$\vec{\nabla} \times (\frac{1}{\rho} \vec{\nabla} . \vec{\tau}) = T_1 + T_2 \qquad (A.4)$$

where T_1 represents the summation of the free-viscosity change terms and T_2 represents the terms which include the change of viscosity.

$$T_1 = \frac{-1}{\rho^2}\frac{\partial\rho}{\partial x}\left(\mu\frac{\partial^2 u}{\partial x\partial y} + \mu\frac{\partial^2 v}{\partial x^2}\right) + \frac{1}{\rho^2}\frac{\partial\rho}{\partial y}\left(\mu\frac{\partial^2 u}{\partial y^2} + \mu\frac{\partial^2 v}{\partial x\partial y}\right) + \frac{\mu}{\rho}\nabla^2\omega$$

$$- \frac{1}{\rho^2}\frac{\partial\rho}{\partial x}\left(2\mu\frac{\partial^2 v}{\partial y^2} - \frac{2}{3}\mu\frac{\partial\beta}{\partial y}\right) + \frac{1}{\rho^2}\frac{\partial\rho}{\partial y}\left(2\mu\frac{\partial^2 u}{\partial x^2} - \frac{2}{3}\mu\frac{\partial\beta}{\partial x}\right) \qquad \text{(A.5)}$$

and

$$T_2 = \frac{1}{\rho}(u_y + v_x)(\mu_{xx} - \mu_{yy}) + \frac{2}{\rho}(v_y - u_x)\mu_{xy}$$

$$+ \mu_x\left(\frac{2}{\rho}\nabla^2 v + \frac{2}{\rho}u_{xy} - \frac{1}{\rho^2}(\rho_x u_y + v_x\rho_x - 2\rho_y u_x + \frac{2}{3}\rho_y\beta)\right)$$

$$+ \mu_y\left(-\frac{2}{\rho}\nabla^2 u + \frac{2}{\rho}v_{xy} - \frac{1}{\rho^2}(2\rho_x v_y - u_y\rho_y - v_x\rho_y - \frac{2}{3}\beta\rho_x)\right) \qquad \text{(A.6)}$$

For simplicity and convenience, the viscosity coefficients μ and $\lambda(\lambda = -\frac{2}{3}\mu)$, specific heat radio γ and the thermal conductivity k have been considered to be constant in the present subsonic study. In general, the incorporation of variable coefficients has no conceptual effect on the method. Several numerical experiments have been performed to verify the foregoing assumption and the results indicate a negligible contribution of the non-constant coefficient term T_2.

By using the above assumptions, equation (A.6) reduces to the following simple form:

$$\frac{\partial\omega}{\partial t} = -\vec{\nabla}.(\vec{V}\omega) + \left(\frac{\mu}{\rho.Re}\right)\nabla^2\omega + \phi(\omega,\beta,\rho,h) \qquad \text{(A.7)}$$

where,

$$\phi = \phi_1 + \phi_2$$

$$\phi_1 = \frac{\mu}{Re.\rho^2}\left(\frac{4}{3}\left(\vec{\nabla}\beta \times \vec{\nabla}\rho\right).\vec{k} - \vec{\nabla}\rho.\vec{\nabla}\omega\right)$$

$$\phi_2 = \frac{\gamma-1}{\gamma}\left(\vec{\nabla}\ln \times \vec{\nabla}h\right).\vec{k}$$

$\vec{k}$ is the unit vector normal to the plane of flow (x-y).

(2) The Dilatation Transport Equation

The dilatation transport equation (2-18) may be written as

$$\frac{\partial\beta}{\partial t} = -\vec{\nabla}.(\vec{V}.\vec{\nabla})\vec{V} - \frac{\gamma-1}{\gamma}\nabla^2 h - \frac{\gamma-1}{\gamma} h\,\nabla^2 \ln\rho - \frac{\gamma-1}{\gamma}\vec{\nabla}\ln\rho.\vec{\nabla}h$$

$$+ \frac{1}{Re}\vec{\nabla}.\left(\frac{1}{\rho}\vec{\nabla}.\vec{\tau}\right) \qquad \text{(A.8)}$$

Specializing this for two-dimensional flow and expanding the first and the last term in the right-hand side, one obtain:

$$-\vec{\nabla}.(\vec{V}.\vec{\nabla})\vec{V} = -\frac{\partial}{\partial x}\left(u\frac{\partial u}{\partial x} + v\frac{\partial u}{\partial y}\right) - \frac{\partial}{\partial y}\left(u\frac{\partial v}{\partial x} + v\frac{\partial v}{\partial y}\right)$$

$$-\left(u\frac{\partial^2 v}{\partial x\partial y} + \frac{\partial v}{\partial x}\cdot\frac{\partial u}{\partial y} + \left(\frac{\partial v}{\partial y}\right)^2 + v\frac{\partial^2 v}{\partial y^2}\right)$$

$$-\left(u\frac{\partial^2 u}{\partial x^2} + \frac{\partial v}{\partial x}\cdot\frac{\partial u}{\partial y} + \left(\frac{\partial u}{\partial x}\right)^2 + v\frac{\partial^2 v}{\partial x\partial y}\right) \qquad \text{(A.9)}$$

Further, noting that,

$$\beta = \frac{\partial u}{\partial x} + \frac{\partial v}{\partial y}$$

Equation (A.9) reduces to the following form

$$-\vec{\nabla}.(\vec{V}.\vec{\nabla})\vec{V} = -(u\frac{\partial \beta}{\partial x} + v\frac{\partial \beta}{\partial y} + u_x^2 + v_y^2 + 2v_x u_y) \qquad \text{(A.10)}$$

Equation (A.10) can be further reduced to

$$-\vec{\nabla}.(\vec{V}.\vec{\nabla})\vec{V} = -(u\frac{\partial \beta}{\partial x} + v\frac{\partial \beta}{\partial y} + \beta^2 + 2\vec{\nabla}vx\vec{\nabla}u.\vec{k})$$

$$= -(\vec{\nabla}.(\vec{V}\beta) + 2\vec{\nabla}vx\vec{\nabla}u.\vec{k}) \qquad \text{(A.11)}$$

Similarly,

$$\vec{\nabla}.(\frac{1}{\rho}\vec{\nabla}.\vec{\tau}) = \frac{\partial}{\partial x}(\frac{1}{\rho}(\frac{\partial}{\partial x}(2\mu\frac{\partial u}{\partial x} - \frac{2}{3}\mu\beta) + \frac{\partial}{\partial y}(\mu\frac{\partial u}{\partial y} + \mu\frac{\partial v}{\partial x})))$$

$$+ \frac{\partial}{\partial y}(\frac{1}{\rho}(\frac{\partial}{\partial x}(\mu\frac{\partial u}{\partial y} + \mu\frac{\partial v}{\partial x}) + \frac{\partial}{\partial y}(2\mu\frac{\partial v}{\partial y} - \frac{2}{3}\mu\beta))) \qquad \text{(A.12)}$$

By separating the right-hand side into two terms, similar to what has been done in the vorticity transport equation, one obtains

$$\vec{\nabla}.(\frac{1}{\rho}\vec{\nabla}.\vec{\tau}) = C_1 + C_2 \qquad \text{(A.13)}$$

where

$$C_1 = \frac{4}{3}\frac{\mu}{\rho}\nabla^2\beta - \left(\frac{4}{3}\frac{\mu}{\rho^2}\vec{\nabla}\rho.\vec{\nabla}\beta + \frac{\mu}{\rho^2}(\vec{\nabla}\rho x\vec{\nabla}\omega).\vec{k}\right) \tag{A.14}$$

$$C_2 = \left(\frac{8}{3}\rho\right)\vec{\nabla}\beta.\vec{\nabla}\mu + \frac{2}{3}(\vec{\nabla}\omega x\vec{\nabla}\mu).\vec{k} - \left(\frac{2}{3}\rho\right)\beta\nabla^2\mu$$

$$+ \left(\frac{2}{\rho}\right)(u_x\ _{xx} + v_y\ \mu_{yy}) + (v_x + u_y)\mu_{xy}$$

$$- \left(\frac{1}{\rho^2}\right)(v_x + u_y)\ (\rho_x.\mu_y + \rho_y\ .\mu_x) + \left(\frac{2}{3}\right)\frac{\beta}{\rho^2}\vec{\nabla}\rho.\vec{\nabla}\mu$$

$$- \left(\frac{2}{\rho^2}\right)(\rho_x.u_x.\mu_x + \rho_y\ .\ v_y.\ \mu_y) \tag{A.15}$$

Neglecting the term C_2, for the reasons mentioned before in (1), the dilatation transport equation is written as follows

$$\frac{\partial\beta}{\partial t} = -\vec{\nabla}.(\vec{\nabla}\beta) + \left(\frac{4.\mu}{3.\mathrm{Re}\rho}\right)\nabla^2\beta + \chi(\omega,\beta,\rho,h) \tag{A.16}$$

where

$$\chi = \chi_1 + \chi_2 + \chi_3$$

$$\chi_1 = -2\ (\vec{\nabla}v\ x\ \vec{\nabla}u).\vec{k}$$

$$\chi_2 = \frac{\mu}{\rho^2\mathrm{Re}}\left[-\frac{4}{3}\vec{\nabla}\rho.\vec{\nabla}\beta + (\vec{\nabla}\rho x\vec{\nabla}\omega).\vec{k}\right]$$

$$\chi_3 = -\left(\frac{\gamma-1}{\gamma}\right)(\nabla^2 h + h\nabla^2\ln\rho + \vec{\nabla}h.\vec{\nabla}\ln\rho)$$

(3) The Energy Transport Equation

Using the equation of state (2.4) in the energy equation (2.3), one obtains the following

$$\frac{\partial h}{\partial t} = -\vec{V}.\vec{\nabla}h - (\gamma-1)\beta h - \frac{\gamma}{\rho}\vec{\nabla}.\vec{q} + \frac{\gamma}{\rho}(\vec{\nabla}\vec{V}:\vec{\tau}) \qquad (A.17)$$

Equation (A.17) can be written in dimensionless form as follows

$$\frac{\partial h}{\partial t} = -\vec{V}.\vec{\nabla}h - (\gamma-1)\beta h - \frac{\gamma}{\rho}\frac{1}{Re.Pr}\vec{\nabla}.\vec{q} + \frac{\gamma}{\rho.Re}(\vec{\nabla}\vec{V}:\vec{\tau}) \qquad (A.18)$$

Expanding the conductive and dissapative terms in equation (A.18) one gets the following expressions

$$\frac{\gamma}{\rho Re.Pr}\vec{\nabla}.\vec{q} = \frac{\gamma}{\rho}\frac{1}{Re.Pr}\frac{\partial}{\partial x_j}\left(-k_j\frac{\partial h}{\partial x_j}\right) \qquad (A.19)$$

and

$$\frac{\gamma}{\rho}\frac{1}{Re}(\vec{\nabla}\vec{V}:\vec{\tau}) = \frac{\gamma}{\rho.Re}\left(\tau_{ij}\frac{\partial u_i}{\partial x_j}\right) \qquad (A.20)$$

Specializing these two equations for two-dimensional flow, they reduce to:

$$\frac{\gamma}{\rho Re.Pr}\vec{\nabla}.\vec{q} = \frac{\gamma}{\rho}\left(\frac{1}{Re.Pr}\right)(k\nabla^2 h + \vec{\nabla}h.\vec{\nabla}k) \qquad (A.21)$$

and

$$\frac{\gamma}{\rho}\frac{1}{Re}\vec{\nabla}\vec{V}:\vec{\tau} = \frac{\gamma\mu}{\rho.Re}\left(\frac{4}{3}\beta^2+\omega^2 + 4(\vec{\nabla}v \times \vec{\nabla}u).\vec{k}\right) \qquad (A.22)$$

Neglecting the thermal conductivity variation term and placing equation (A.21) and (A.22) into equation (A.18) one gets;

$$\frac{\partial h}{\partial t} = -\vec{\nabla}.(\vec{V}h) + \frac{\gamma k}{Re.Pr}\nabla^2 h + \Theta(\omega,\rho,\beta,h) \qquad (A.23)$$

where

$$\Theta = \Theta_1 + \Theta_2$$

$$\Theta_1 = (2-\gamma)\beta h$$

$$\Theta_2 = \frac{\gamma\mu}{\rho Re}\left\{\frac{4}{3}\beta^2 + \omega^2 + 4(\vec{\nabla}v \times \vec{\nabla}u).\vec{k}\right\}$$

(4) The Density Equation

The continuity equation (2.2) can be written as follows.

$$\frac{1}{\rho}\frac{\partial\rho}{\partial t} + \vec{\nabla}.\vec{V} + \frac{\vec{V}}{\rho}.\vec{\nabla}\rho = 0 \qquad (A.24)$$

Further, noting that

$$\beta = \vec{\nabla}.\vec{V}$$

thus equation (A.24) becomes,

$$\frac{\partial \ln\rho}{\partial t} = -\beta - \vec{V}.\vec{\nabla}\ln\rho \qquad \text{(A.25)}$$

In conservative form, equation (A.25) can be written as follows

$$\frac{\partial \ln\rho}{\partial t} = -\vec{\nabla}.(\vec{V}\ln\rho) + \Gamma \qquad \text{(A.26)}$$

where

$$\Gamma = \beta(\ln\rho - 1)$$

APPENDIX B

TRANSFORMATION RELATIONS

The transformation relations used in the derivation of the kinetic transport equations are given here. The following expressions relate the mathematical operations done in the physical plane, ph, with those that performed in the transformed plane, T.

$$(\vec{\nabla} f . \vec{\nabla} g)_{ph.} = \frac{1}{H^2} (\vec{\nabla} f . \vec{\nabla} g)_{T} \tag{B.1}$$

$$(\nabla f \times \nabla g)_{ph.} = \frac{1}{H^2} (\vec{\nabla} f \times \vec{\nabla} g)_{T} \tag{B.2}$$

$$(\nabla^2 f)_{ph.} = \frac{1}{H^2} (\nabla^2 f)_{T} \tag{B.3}$$

$$(\vec{\nabla} . (f\vec{V}))_{ph.} = \frac{1}{H^2} (\vec{\nabla} . (f\vec{V}))_{T} \tag{B.4}$$

where,

(i) H is the transformation scale factor

(ii) f and g are scalar functions which are invarient with the transformation.

(iii) $\vec{V}_{ph}$ is the velocity vector in the physical plane, while $\vec{V}_T$ is the apparent velocity vector in the transformed plane and its components (V_θ, V_r) are given by equations (2-27) and (2-28).

The components of the velocity vector V in the physical plane (u,v) are related to the velocity components (V_θ, V_r) as follows:

$$u = \frac{1}{H^2}\left(-V_\theta \frac{dy}{dr} + \frac{1}{r} V_r \frac{dy}{d\theta}\right) \tag{B.5}$$

$$v = \frac{1}{H^2}\left(V_r \frac{dy}{dr} + \frac{1}{r} V_\theta \frac{dy}{d\theta}\right) . \tag{B.6}$$

where y and x are the Cartesian coordinates in the physical plane. The transformed quantities can be expanded in polar coordinates (s-θ) as follows:

$$\left(\vec{\nabla} f \cdot \vec{\nabla} g\right)_T = \left[\left(\frac{1}{r-c}\right)^2 \frac{\partial f}{\partial s} \cdot \frac{\partial g}{\partial s} + \frac{1}{r^2} \frac{\partial f}{\partial \theta} \cdot \frac{\partial g}{\partial \theta}\right] \tag{B.7}$$

$$\left(\vec{\nabla} f \times \vec{\nabla} g\right)_T = \frac{1}{r(r-c)}\left(\frac{\partial f}{\partial s} \cdot \frac{\partial g}{\partial s} - \frac{\partial f}{\partial \theta} \cdot \frac{\partial g}{\partial \theta}\right) \tag{B.8}$$

$$\left(\nabla^2 f\right)_T = \left(\frac{1}{r-c}\right)^2 \frac{\partial^2 f}{\partial s^2} + \left(\frac{1}{r(r-c)} - \left(\frac{1}{r-c}\right)^2\right) \frac{\partial f}{\partial s} + \frac{1}{r} \frac{\partial^2 f}{\partial \theta^2} \tag{B.9}$$

where s is the stretched radial coordinate in the transformed polar plane and is given by;

$$r = e^s + c \tag{B.10}$$

APPENDIX C

EVALUATION OF INTEGRALS IN EQUATIONS (4.3) - (4.5)

The integrals that need to be evaluated are

$$I_m = r_o \int_o^{2\pi} \frac{\cos m\theta_o \left[r_o \cos(\theta_o-\theta)-r \right]}{r_o^2 + r^2-2r_o r \cos(\theta_o-\theta)} \, d\theta_o \tag{C.1}$$

$$J_m = r_o \int_o^{2\pi} \frac{\sin m\theta_o \left[r_o \cos(\theta_o-\theta)-r \right]}{r_o^2+r^2-2r_o r \cos(\theta_o-\theta)} \, d\theta_o \tag{C.2}$$

$$\tilde{I}_m = r_o^2 \int_o^{2\pi} \frac{\cos m\theta_o \sin(\theta_o-\theta)}{r_o^2+r^2-2r_o r \cos(\theta_o-\theta)} \, d\theta_o \tag{C.3}$$

$$\tilde{J}_m = r_o^2 \int_o^{2\pi} \frac{\sin m\theta_o \sin(\theta_o-\theta)}{r_o^2+r^2-2r_o r \cos(\theta_o-\theta)} \, d\theta_o \tag{C.4}$$

where $0 \leq m \leq N$. If the following complex variables are defined as

$$W_m = I_m + i J_m \tag{C.5}$$

$$\tilde{W}_m = I_m + i J_m \tag{C.6}$$

and

$$z_o = e^{i\theta_o} = \cos\theta_o + i \sin\theta_o \tag{C.7}$$

$$z = e^{i\theta} = \cos\theta + i \sin\theta \tag{C.8}$$

where $i = \sqrt{-1}$. The quantities W_m and $\tilde{W}_m$ could be reexpressed as follows after the variable transformation from θ, θ_o to z, z_o :

$$W_m = -\frac{1}{2ir}\oint \frac{z_o^{m-1}\left[r_o(z_o^2 + z^2) - 2rzz_o\right]}{(z_o - \frac{r}{r_o}z)(z_o - \frac{r_o}{r}z)}\,dz_o \tag{C.9}$$

$$\tilde{W}_m = \frac{r_o}{2r}\oint \frac{z_o^{m-1}(z_o^2 - z^2)}{(z_o - \frac{r}{r_o}z)(z_o - \frac{r_o}{r}z)}\,dz_o \tag{C.10}$$

By using of residue theorem, the integrals in equations (C.9) and (C.10) are evaluated explicitly and the results are

(1) for $r < r_o$:

$$W_o = 0 \tag{C.11}$$

$$W_m = \pi\left(\frac{r}{r_o}\right)^{m-1} z^m \tag{C.12}$$

$$\tilde{W}_o = 0 \tag{C.13}$$

$$\tilde{W}_m = i\pi\left(\frac{r}{r_o}\right)^{m-1} z^m \tag{C.14}$$

(2) for $r > r_o$:

$$W_o = -2\pi\left(\frac{r_o}{r}\right) \tag{C.15}$$

$$W_m = -\pi\left(\frac{r_o}{r}\right)^{m+1} z^m \tag{C.16}$$

$$\tilde{W}_o = 0 \tag{C.17}$$

$$\tilde{W}_m = i\pi\left(\frac{r_o}{r}\right)^{m+1} z^m \tag{C.18}$$

where $1 \leq m \leq N$. The values of I_m, J_m, $\tilde{I}_m$, $\tilde{J}_m$'s could be determined easily by equations (C.5) and (C.6). Thus

(1) for $r \leq r_o$:

$$I_o = 0 \tag{C.19}$$

$$I_m = \pi\left(\frac{r}{r_o}\right)^{m-1} \cos m\theta \tag{C.20}$$

$$J_o = 0 \tag{C.21}$$

$$J_m = \pi\left(\frac{r}{r_o}\right)^{m-1} \sin m\theta \tag{C.22}$$

$$\tilde{I}_o = 0 \tag{C.23}$$

$$\tilde{I}_m = -\pi\left(\frac{r}{r_o}\right)^{m-1} \sin m\theta \tag{C.24}$$

$$\tilde{J}_o = 0 \tag{C.25}$$

$$\tilde{J}_m = \pi\left(\frac{r}{r_o}\right)^{m-1} \cos m\theta \tag{C.26}$$

(2) for $r > r_o$:

$$I_o = -2\pi\left(\frac{r_o}{r}\right) \tag{C.27}$$

$$I_m = -\pi\left(\frac{r_o}{r}\right)^{m+1} \cos m\theta \tag{C.28}$$

$$J_o = 0 \tag{C.29}$$

$$J_m = -\pi\left(\frac{r_o}{r}\right)^{m+1} \sin m \tag{C.30}$$

$$\tilde{I}_o = 0 \tag{C.31}$$

$$\tilde{I}_m = -\pi\left(\frac{r_o}{r}\right)^{m+1} \sin m\theta \tag{C.32}$$

$$\tilde{J}_o = 0 \tag{C.33}$$

$$\tilde{J}_m = \pi\left(\frac{r_o}{r}\right)^{m+1} \cos m\theta \tag{C.34}$$

The integrals that need to be evaluated in kinetics are

$$I_m = r_o \int_o^{2\pi} \frac{\cos m\theta_o \left[r_o - r\cos(\theta_o - \theta)\right]}{r_o^2 + r^2 - 2r_o r\cos(\theta_o - \theta)} d\theta_o \tag{C.35}$$

$$J_m = r_o \int_o^{2\pi} \frac{\sin m\theta_o \left[r_o - r\cos(\theta_o - \theta)\right]}{r_o^2 + r^2 - 2r_o r\cos(\theta_o - \theta)} d\theta_o \tag{C.36}$$

$$\tilde{I}_m = r_o r \int_o^{2\pi} \frac{\cos m\theta_o \sin(\theta_o - \theta)}{r_o^2 + r^2 - 2r_o r\cos(\theta_o - \theta)} d\theta_o \tag{C.37}$$

$$\tilde{J}_m = r_o r \int_o^{2\pi} \frac{\sin m\theta_o \sin(\theta_o - \theta)}{r_o^2 + r^2 - 2r_o r\cos(\theta_o - \theta)} d\theta_o \tag{C.38}$$

also the complex quantities are

$$W_m = I_m + i J_m \tag{C.39}$$

$$\tilde{W}_m = \tilde{I}_m + i \tilde{J}_m \tag{C.40}$$

Following the same procedure as in kinematics, the following expressions are obtained

$$W_m = \frac{1}{2ir} \oint \frac{z_o^{m-1}\left[r(z_o^2 + z^2) - 2r_o z_o z\right]}{(z_o - \frac{r}{r_o} z)(z_o - \frac{r_o}{r} z)} dz_o \tag{C.41}$$

$$\tilde{W}_m = \frac{1}{2}\oint \frac{z_o^{m-1}\,(z_o^2 - z^2)}{(z_o - \frac{r}{r_o}\,z)(z_o - \frac{r_o}{r}\,z)}\,dz_o \qquad (C.42)$$

and the final results are

(1) for $r < r_o$:

$$I_o = 2\pi \qquad (C.43)$$

$$I_m = \pi(\frac{r}{r_o})^m \cos m\theta \qquad (C.44)$$

$$J_o = 0 \qquad (C.45)$$

$$J_m = \pi\,(\frac{r}{r_o})^m \sin m \qquad (C.46)$$

$$\tilde{I}_o = 0 \qquad (C.47)$$

$$\tilde{I}_m = -\,\pi(\frac{r}{r_o})^m \sin m\theta \qquad (C.48)$$

$$\tilde{J}_o = 0 \qquad (C.49)$$

$$\tilde{J}_m = \pi(\frac{r}{r_o})^m \sin m\theta \qquad (C.50)$$

(2) for $r > r_o$:

$$I_o = 0 \qquad (C.51)$$

$$I_m = -\,\pi(\frac{r_o}{r})^m \cos m\theta \qquad (C.52)$$

$$J_o = 0 \qquad (C.53)$$

$$J_m = -\pi\,(\frac{r_o}{r})^m \sin m\theta \qquad (C.54)$$

$$\tilde{I}_o = 0 \qquad (C.55)$$

$$\tilde{I}_m = -\pi\,(\frac{r_o}{r})^m \sin m\theta \qquad (C.56)$$

$$\tilde{J}_o = 0 \qquad (C.57)$$

$$\tilde{J}_m = \pi(\frac{r_o}{r})^m \cos m\theta \qquad (C.58)$$

where $1 \leq m \leq N$.

APPENDIX D

DERIVATION OF RELATIONSHIPS BETWEEN FOURIER COEFFICIENTS

The following expression for v_r is obtained after substituting equations (4.6, 4.8) into equation (4.3)

$$v_r = \frac{1}{2\pi}\int_o^1 \left[\alpha_o \tilde{I}_o + \sum_{n=1}^{N} (\alpha_n \tilde{I}_n + \beta_n \tilde{J}_n)\right] dr_o$$

$$+ \frac{1}{2\pi\rho}\left[s_o(1)\, I_o + \sum_{n=1}^{N} (s_n(1)\, I_n + t_n(1)\, J_n)\right]$$

$$- \frac{1}{2\pi}\left[p_o(1)\, \tilde{I}_o + \sum_{n=1}^{N} (p_n(1)\, \tilde{I}_n + q_n(1)\, \tilde{J}_n)\right] \quad (D.1)$$

where I, $\tilde{I}$, J, $\tilde{J}$ are those quantities defined in Section (i), Appendix E. From equations (C.11) - (C.34)

$$v_r = -\frac{1}{2}\int_o^r \sum_{n=1}^{N}\left[\alpha_n \left(\frac{r_o}{r}\right)^{n+1} \sin n\theta - \beta_n \left(\frac{r_o}{r}\right)^{n+1} \cos n\theta\right] dr_o$$

$$-\frac{1}{2}\int_r^1 \sum_{n=1}^{N}\left[\alpha_n \left(\frac{r}{r_o}\right)^{n-1} \sin n\theta - \beta_n \left(\frac{r}{r_o}\right)^{n-1} \cos n\theta\right] dr_o$$

$$+\frac{1}{2}\sum_{n=1}^{N}\left[s_n(1)\, r^{n-1} \cos n\theta + t_n(1)\, r^{n-1} \sin n\theta\right]$$

$$+\frac{1}{2}\sum_{n=1}^{N}\left[p_n(1)\, r^{n-1} \sin n\theta - q_n(1)\, r^{n-1} \cos n\theta\right] \quad (D.2)$$

If v_r is also expanded in Fourier series (as in equation 4.6), the corresponding Fourier coefficients are related by

$$s_o = 0 \tag{15}$$

$$s_n = \frac{1}{2} \int_o^r \beta_n \left(\frac{r_o}{r}\right)^{n+1} dr_o + \int_r^1 \beta_n \left(\frac{r}{r_o}\right)^{n-1} dr_o$$

$$+ \frac{1}{2} s_n(1)\, r^{n-1} - \frac{1}{2} q_n(1)\, r^{n-1} \tag{16}$$

$$t_n = -\frac{1}{2} \int_o^r \alpha_n \left(\frac{r_o}{r}\right)^{n+1} dr_o - \frac{1}{2} \int_r^1 \alpha_n \left(\frac{r}{r_o}\right)^{n-1} dr_o$$

$$+ \frac{1}{2} t_n(1)\, r^{n-1} + \frac{1}{2} p_n(1)\, r^{n-1} \tag{17}$$

where $1 \leq n \leq N$. Similarly, the expression for v_θ from equation (4.4)

$$v_\theta = \frac{1}{2} \int_o^1 \left[\alpha_o I_o + \sum_{n=1}^{N} (\alpha_n I_n + \beta_n J_n)\right] dr_o$$

$$+ \frac{1}{2\pi} \left[s_o(1)\, \tilde{I}_o + \sum_{n=1}^{N} (s_n(1)\, \tilde{I}_n + t_n(1)\, \tilde{J}_n)\right]$$

$$+ \frac{1}{2\pi} \left[p_o(1)\, I_o + \sum_{n=1}^{N} (p_n(1)\, I_n + q_n(1)\, J_n)\right] \tag{D.3}$$

which is

$$v_\theta = \frac{1}{2} \int_o^r \sum_{n=1}^{N} \left[\alpha_n \left(\frac{r_o}{r}\right)^{n+1} \cos n\theta + \beta_n \left(\frac{r_o}{r}\right)^{n+1} \sin n\theta\right] dr_o$$

$$- \frac{1}{2} \int_r^1 \sum_{n=1}^{N} \left[\alpha_n \left(\frac{r}{r_o}\right)^{n-1} \cos n\theta + \beta_n \left(\frac{r}{r_o}\right)^{n-1} \sin n\theta\right] dr_o$$

$$- \frac{1}{2} \sum_{n=1}^{N} \left[s_n(1)\, r^{n-1} \sin n\theta - t_n(1)\, r^{n-1} \cos n\theta\right]$$

$$+ \frac{1}{2} \sum_{n=1}^{N} \left[p_n(1)\, r^{n-1} \cos n\theta + q_n(1)\, r^{n-1} \sin n\theta\right] \tag{D.4}$$

Expanding v_θ in Fourier series as in equation (4.7) the corresponding coefficients are related by equations (4.12)-(4.14).

By expanding ωv_r, ωv_θ in equations (4.18) and (4.19) equation (4.5) could be expressed as

$$\omega = -\frac{Re}{2\pi}\int_o^1 \left[\xi_o I_o + \sum_{n=1}^{N}(\xi_n I_n + \eta_n J_n)\right] dr_o$$

$$-\frac{Re}{2\pi}\int_o^1 \left[\mu_o I_o + \sum_{n=1}^{N}\mu_n I_n + \zeta_n J_n)\right] dr_o$$

$$+\frac{Re}{2\pi}\left[f_o(1)\, I_o + \sum_{n=1}^{N}(f_n(1)I_n + g_n(1)J_n)\right]$$

$$+\frac{1}{2\pi}\left[\alpha_o(1)I_o + \sum_{n=1}^{N}(\alpha_n(1)I_n + \beta_n(1)J_n)\right] \qquad (D.5)$$

where I, I, J, J's are those quantities defined in Section (ii) Appendix C, and f_o, f_n, g_n's are the Fourier coefficients of the total pressure.

$$h = f_o + \sum_{n=1}^{N}(f_n \cos n\theta + g_n \sin n\theta) \qquad (D.6)$$

By the results of equations (C.43)-(C.58), equation (D.5) becomes

$$\omega = \frac{Re}{2}\int_o^r \sum_{n=1}^{N}\left(\frac{r_o}{r}\right)^n \left[(\xi_n - \zeta_n)\cos n\theta + (\eta_n + \mu_n)\sin n\theta\right] dr_o$$

$$-\frac{Re}{2}\int_r^1 \left\{2\xi_o + \sum_{n=1}^{N}\left(\frac{r}{r_o}\right)^n \left[(\xi_n + \zeta_n)\cos n\theta\right.\right.$$

$$\left.\left. + (\eta_n - \mu_n)\sin n\theta\right]\right\} dr_o$$

$$+\frac{Re}{2}\sum_{n=1}^{N}\left[-f_n(1)\, r^n \sin n\theta + g_n(1)\, r^n \cos n\theta\right]$$

$$+ \alpha_o(1) + \sum_{n=1}^{N} \alpha_n(1)\, r^n \cos n\theta + \beta_n(1)\, r^n \sin n\theta \qquad (D.7)$$

Thus, in using the Fourier series expansion for ω (equation 4.8), the corresponding coefficients are related by

$$\alpha_o = \alpha_o(1) - Re \int_r^1 \xi_o \, dr_o \qquad (21)$$

$$\alpha_n = \frac{Re}{2} \int_o^r (\xi_n - \zeta_n)\left(\frac{r_o}{r}\right)^n dr_o - \frac{Re}{2} \int_r^1 (\xi_n + \zeta_n)\left(\frac{r}{r_o}\right)^n dr_o$$

$$+ \frac{Re}{2}\, g_n(1)\, r^n + \frac{1}{2}\alpha_n(1)\, r^n \qquad (D.8)$$

$$\beta_n = \frac{Re}{2} \int_o^r (\eta_n + \mu)\left(\frac{r_o}{r}\right)^n dr_o + \frac{Re}{2} \int_r^1 (\mu_n - \eta_n)\left(\frac{r}{r_o}\right)^n dr_o$$

$$- \frac{Re}{2}\, f_n(1)\, r^n + \frac{1}{2}\beta_n(1)\, r^n \qquad (D.9)$$

where $1 \leq n \leq N$. Equations (D.8) and (D.9) are equivalent to equations (4.16) and (4.17) respectively, where the terms $g_n(1)$ and $f_n(1)$ are cancelled by applying the equations (D.8) and (D.9) on the boundary.

APPENDIX E

THE INTEGRAL REPRESENTATIONS FOR A DOUBLY-CONNECTED REGION

The boundary integrals in equations (4.3) and (4.4) consist of two parts, B_1 and B_2

$$\oint_B = \oint_{B_1} - \oint_{B_2} \tag{E.1}$$

At the interior boundary B_2, the velocity components are assumed to be known. The Fourier coefficients of the velocities at B_2 are zero except $p_o(R)$, which is the magnitude of the circumferential velocity at r=R due to the solid rotation.

The equations (D.1) for the velocity v_r needs to be rewritten to include the B_2 effect:

$$\begin{aligned} v_r = & \frac{1}{2\pi} \int_R^1 \left[\alpha_o I_o + \sum_{n=1}^{N} (\alpha_n \tilde{I}_n + \beta_n \tilde{J}_n)\right] dr_o \\ & + \frac{1}{2\pi} \left[s_o(1)\, I_o + \sum_{n=1}^{N} (s_n(1)\, I_n + t_n(1)\, J_n)\right] \\ & - \frac{1}{2\pi} \left[s_o(R)\, I_o + \sum_{n=1}^{N} (s_n(R)\, I_n + t_n(R)\, J_n)\right] \\ & - \frac{1}{2\pi} \left[p_o(1)\, \tilde{I}_o + \sum_{n=1}^{N} (p_n(1)\, \tilde{I}_n + q_n(1)\, \tilde{J}_n)\right] \\ & + \frac{1}{2\pi} \left[p_o(R)\, \tilde{I}_o + \sum_{n=1}^{N} (p_n(R)\, \tilde{I}_n + q_n(R)\, \tilde{J}_n)\right] \end{aligned} \tag{E.2}$$

where $s_o(R)$, $p_o(R)$, $s_n(R)$, $t_n(R)$, $p_n(R)$, $q_n(R)$ are the Fourier coefficients

of the velocities at r=R. Thus

$$s_o = 0 \tag{15}$$

$$s_n = \frac{1}{2}\int_R^r \beta_n \left(\frac{r_o}{r}\right)^{n+1} dr_o + \int_r^1 \beta_n \left(\frac{r}{r_o}\right)^{n-1} dr_o + \frac{1}{2} s_n(1)\, r^{n-1} - \frac{1}{2} q_n(1)\, r^{n-1} \tag{E.3}$$

$$t_n = -\frac{1}{2}\int_R^r \alpha_n \left(\frac{r_o}{r}\right)^{n+1} dr_o - \frac{1}{2}\int_r^1 \alpha_n \left(\frac{r}{r_o}\right)^{n-1} dr_o + \frac{1}{2} t_n(1)\, r^{n-1} + \frac{1}{2} p_n(1)\, r^{n-1} \tag{E.4}$$

where $1 \leq n \leq N$. Similarly, the velocity v_θ is reexpressed as:

$$\begin{aligned} v_\theta = {} & \frac{1}{2\pi}\int_R^1 \left[\alpha_o I_o + \sum_{n=1}^{N} (\alpha_n I_n + \beta_n J_n)\right] dr_o \\ & + \frac{1}{2\pi}\left[s_o(1)\,\tilde{I}_o + \sum_{n=1}^{N} (s_n(1)\,\tilde{I}_n + t_n(1)\,\tilde{J}_n)\right] \\ & - \frac{1}{2\pi}\left[s_o(R)\, I_o + \sum_{n=1}^{N} (s_n(R)\, I_n + t_n(R)\, J_n)\right] \\ & + \frac{1}{2\pi}\left[p_o(1)\,\tilde{I}_o + \sum_{n=1}^{N} (p_n(1)\,\tilde{I}_n + q_n(1)\,\tilde{J}_n)\right] \\ & - \frac{1}{2\pi}\left[p_o(R)\,\tilde{I}_o + \sum_{n=1}^{N} (p_n(R)\,\tilde{I}_n + q_n(R)\,\tilde{J}_n)\right] \end{aligned} \tag{E.5}$$

By using equations (A.7) and (C.17) the following relations are obtained

$$p_o = \int_R^r \alpha_o\left(\frac{r_o}{r}\right) dr_o + \frac{R}{r}\, p_o(R) \tag{E.6}$$

$$p_n = \frac{1}{2}\int_R^r \alpha_n \left(\frac{r_o}{r}\right)^{n+1} dr_o - \frac{1}{2}\int_r^1 \alpha_n \left(\frac{r}{r_o}\right)^{n-1} dr_o$$

$$+ \frac{1}{2}\, t_n(1)\, r^{n-1} + \frac{1}{2}\, p_n(1)\, r^{n-1} \tag{E.7}$$

$$q_n = \frac{1}{2}\int_R^r \beta_n \left(\frac{r_o}{r}\right)^{n+1} dr_o - \frac{1}{2}\int_r^1 \beta_n \left(\frac{r}{r_o}\right)^{n-1} dr_o$$

$$- \frac{1}{2}\, s_n(1)\, r^{n-1} + \frac{1}{2}\, q_n(1)\, r^{n-1} \tag{E.8}$$

where $1 \leq n \leq N$.

The equation (p.5) becomes

$$\omega = -\frac{Re}{2\pi}\int_R^1 \left[\xi_o I_o + \sum_{n=1}^{N} (\xi_n I_n + \eta_n J_n)\right] dr_o$$

$$- \frac{Re}{2}\int_R^1 \left[\mu_o \tilde{I}_o + \sum_{n=1}^{N} (\mu_n \tilde{I}_n + \zeta_n \tilde{J}_n)\right] dr_o$$

$$+ \frac{Re}{2\pi}\left[f_o(1)\, \tilde{I}_o + \sum_{n=1}^{N} (f_n(1)\, \tilde{I}_n + g_n(1)\, \tilde{J}_n)\right]$$

$$- \frac{Re}{2\pi}\left[f_o(R)\, \tilde{I}_o + \sum_{n=1}^{N} (f_n(R)\, \tilde{I}_n + g_n(R)\, \tilde{J}_n)\right]$$

$$+ \frac{1}{2\pi}\left[\alpha_o(1)\, I_o + \sum_{n=1}^{N} (\alpha_n(1)\, I_n + \beta_n(1)\, J_n)\right]$$

$$- \frac{1}{2\pi}\left[\alpha_o(R)\, I_o + \sum_{n=1}^{N} (\alpha_n(R)\, I_n + \beta_n(R)\, J_n)\right] \tag{E.9}$$

where $f_o(R)$, $f_n(R)$ and $g_n(R)$ are the Fourier coefficients of the total pressure at r=R. By using the equations (C.43)-(C.58):

$$\omega = \frac{Re}{2}\int_R^r \sum_{n=1}^{N} \left(\frac{r_o}{r}\right)^n \left[(\xi_n - \zeta_n)\cos n\theta + (\eta_n + \mu_n)\sin n\theta\right]dr_o$$

$$- \frac{Re}{2}\int_r^1 \left\{2\xi_o + \sum_{n=1}^{N}\left(\frac{r}{r_o}\right)^n \left[(\xi_n+\zeta_n)\cos n\theta + (\eta_n-\mu_n)\sin n\theta\right]\right\}dr_o$$

$$+ \frac{Re}{2}\sum_{n=1}^{N}\left[- f_n(1)r^n \sin n\theta + g_n(1)\, r^n \cos n\theta\right]$$

$$- \frac{Re}{2}\sum_{n=1}^{N}\left[- f_n(R)\left(\frac{R}{r}\right)^n \sin n\theta + g_n(R)\left(\frac{R}{r}\right)^n \cos n\theta\right] \qquad \text{(E.10)}$$

REFERENCES

1. J.C. Wu, "Integral Representation of Field Variables for the Finite Element Solution of Viscous Flow Problems," Proceedings of the 1974 Conference on Finite Element Methods in Engineering, pp. 27-840, Clarendon Press, 1974.

2. Sankar, N.L. and Tassa, Y., "Reynolds Number and Compressibility Effects on Dynamic Stall of a NACA 0012 Airfoil," AIAA Paper 80-0010.

3. Sampath, S., "A Numerical Study of Incompressible Viscous Flow around Airfoils," Ph.D. Thesis, Georgia Institute of Technology, Atlanta, Georgia, September, 1977.

4. Sankar, N.L., "Numerical Study of Unsteady Flow over Airfoils," Ph.D. Thesis, Georgia Institute of Technology, Atlanta, Georgia November 1977.

5. Rizk, Y., "An Integral-Representation Approach for Time Dependent Viscous Flows," Ph.D. Thesis, Georgia Institute of Technology, Atlanta, Georgia, 1980.

6. Gulcat, U., "Separate Numerical Treatment of Attached and Detached Flow Regions in General Viscous Flows," Ph.D. Thesis, Georgia Institute of Technology, Atlanta, Georgia, 1981.

7. Mehta, U.B., "Starting Vortex, Separation Bubbles and Stall -A Numerical Study of Laminar Unsteady Flow around an Airfoil," Ph.D. Thesis, Illinois Inst. of Technology, Chicago, Illinois, 1972.

8. Ames, W.F., Numerical Methods for Partial Differential Equations, Academic Press, pp. 73-82, 1977.

9. Desideri, J.A., Steger, J.L., and Tannehill, J.C., "On Improving The Iterative Convergence Properties of an Implicit Approximate Factorization Finite Difference Algorithm," NASA TM 73495, June, 1978.

10. Ballhaus, W.F., Jameson, A. and Albert, J., "Implicit Approximate Factorization Scheme for Steady Transonic Flow Problems," AIAA Journal, Vol. 16, No. 6, June, 1978.

11. ElRefaee M.M., "A Numerical Study of Laminar Unsteady Compressible Flows over Airfoils," Ph.D. Thesis, Georgia Institute of Technology, Atlanta, Georgia, May 1981.

12. Burggraf, O.R., "Analytical and Numerical Studies of the Structure of Steady Separated Flows," J. Fluid Mechanics, Vol. 24, pp. 113-151, 1966.

13. Batchelor, G.K., "On Steady Laminar Flow with Closed Streamlines at Large Reynolds Number," J. Fluid Mechanics, Vol. 1, pp. 177-190, 1956.

14. Kuwahara, K., Imai I., "Steady Viscous Flow within a Circular Boundary," The Physics of Fluids, Supplement II, pp. 94-101, 1969.

15. Wood, W.W., "Boundary Layers Whose Streamlines are Closed," J. Fluid Mechanics, Vol. 2, pp. 77-87, 1957.

16. Gottlieb, D. and Orszag S.A., Numerical Analysis of Spectral Methods: Theory and Applications, SIAM Publications, 1977.